ENERGY MANAGEMENT SYSTEM FOR UNDERGROUND MINE ELECTRIC VEHICLES

Fengxian He

Submitted in fulfilment of the requirements for the degree of

Doctor of Philosophy

Faculty of Science, Engineering and Technology

Swinburne University of Technology

2016

ABSTRACT

In most current underground mining operations, personnel carrier vehicles are driven by diesel engines. The exhaust from the engine vehicles spreads in the air in the mine with waste heat and noxious substances. Ventilation and filters are required to comply with the occupational health and safety rules for working in underground mines. Regular replacement of exhaust filters increases operating costs. Electric vehicles (EVs) provide the significant advantages of low noise and zero emissions over diesel engine vehicles and potentially reduce operating costs when EVs are adopted in underground mines. Lithium iron phosphate (LiFePO4) batteries have been selected as power sources for underground mine electric vehicles (UMEVs) due to their better safety than other lithium ion batteries. To meet the power and energy requirements of UMEVs, battery systems must be built with hundreds or thousands of cells connected in series and parallel. The development of battery management systems (BMSs) is crucial to ensure the safe and efficient operation of EV battery systems. This thesis focuses on three aspects of BMSs: the selection of battery systems for UMEVs from many types of LiFePO4 batteries and battery packs, the classification of cells for constructing consistent battery packs, and the estimation of state of charge (SOC) for battery packs.

The selection of the battery system for UMEVs is explored first. Two lithium iron phosphate ($LiFePO_4$) batteries and their corresponding battery packs with different capacities were chosen to make four battery systems for UMEVs. Experiments were conducted to identify the internal resistances, capacities, open circuit voltages and states of charge during charging/discharging periods at different ambient temperatures. A hybrid simulation is proposed to compare these four battery systems by integrating the experimental results of these batteries and battery packs into an UMEV model. Then,

the simulation of the UMEV was conducted at a specifically designed underground mine driving cycle with variable rolling resistance coefficients and variable uphill/downhill gradients. The results indicate the best option for the UMEV of the four battery systems is the A123 20Ah $LiFePO_4$ battery.

In order to reduce the cell inconsistence in the battery pack, a self-organizing map (SOM) based classification of LiFePO4 cells for a battery pack was then investigated. Experimental data on the cells were obtained to train the SOM. The temperature variation, internal resistance and available capacity of the cells were used as the inputs of the SOM, and the output of the SOM classified the cells into three groups with similar characteristics in terms of the input parameters. The cells in the same group were connected in series to build a sorted battery pack, whereas randomly chosen cells were connected in series to build an unsorted battery pack. The comparison of the consistency between the sorted battery pack and the unsorted battery pack under different discharging conditions demonstrated the effectiveness of the proposed classification method.

The SOC estimation based on H infinity observer is proposed for the battery packs in UMEVs by adopting the concept of an average virtual cell (AVC) model. The terminal voltage of the AVC was used to estimate the pack SOC in the estimation process. The difference of the terminal voltage of each cell in the pack and the AVC was set as the terminal voltage difference (TVD). In this study, the LiFePO4 cells were classified to build the pack with the series-connected cells so that the TVDs of each cell in the pack were within the pre-set value. Experiments were conducted on the battery pack to verify the effectiveness of the proposed SOC estimation for the battery packs in UMEVs.

DECLARATION

I declare that this thesis represents my own work and contains no material which has been accepted for the award of any other degree or diploma. To the best of my knowledge and belief, this thesis contains no material previously published or written by another person except where due reference is made in the text of the examinable outcome.

Fengxian He

August 2016

ACKNOWLEDGEMENTS

This work would not have been successfully completed without the support of many people. First of all, I would like to express my deep gratitude to my supervisor, Associate Professor Weixiang Shen, for his patient guidance, enthusiastic encouragement and great support throughout my PhD research journey. He has spent so much time in guiding me in my research. Without his encouragement and guidance, I would never have completed this amazing and tough journey. I would also like to thank my associate supervisor, Professor Ajay Kapoor, for his support in my research.

I would like to thank all the staff of the Faculty of Science, Engineering and Technology and Swinburne Research who helped me in my research during the past four years. My PhD work was financed by a Swinburne SUPRA scholarship, and I greatly appreciate the contribution of Swinburne University which made the award and provided me with a comfortable and conducive working environment. I would like to thank Professor Damon Hennery and Dr. Daya Dayawansa from Monash University for their support and help in the ARC linkage project "From diesel to electric: a new era in personnel transport for underground coal mines". Dr Alex McKnight assisted by proofreading the final draft for stylistic and grammatical errors.

I would like to thank my colleagues Xiudong Cui and Xiaopeng Chen, who helped me in conducting the battery experiment. Thanks are due to all my friends in Melbourne and China for their friendship and help and encouraging me to pursue my life's dream. I owe special thanks to Dr. Qiang Song and Dr. Rui Xiong from the Beijing Institute of Technology for their help and encouragement.

Finally, I would like to offer my deep and sincere thanks to my parents for their utmost support and encouragement for my study. I thank them for their understanding of my decision to remove myself from their lives in the past four years. I thank my brother for caring for and accompanying my parents for these years. I owe a great deal to my beloved husband, Shiqin Li, for his sacrifice for and understanding of my PhD career. Without his love and encouragement, this thesis would not have been successfully completed. I send a special greeting to the wonderful little life in my womb, my unborn baby, who gives me so much to look forward to in my future!

Dedicated to:

My beloved parents,
cherished husband & wonderful unborn baby

TABLE OF CONTENTS

LIST OF FIGURES

LIST OF TABLES

CHAPTER 1 INTRODUCTION

Due to the growing concerns over the shortage of fossil fuel and the progressively increasing cost of fuel and tightened emission controls, researchers have identified electric vehicles (EVs) as possible alternative modes of transportation in the future. The electrification of transportation will have a significant impact on the vehicle industry in relation to energy use, environmental issues and transportation. EVs are clean and sustainable if the electricity which is used to charge the EV batteries is generated from renewable energy resources. Since batteries have become the main power sources to drive EVs, the development of reliable and safe battery management systems (BMSs) is crucial for the commercialisation of EVs [1, 2]. The BMS can prevent EV batteries from overcharging and under-discharge, optimize the driving range and enable EVs to be driven safely.

The development of EVs has a long history dating back 150 years. From simple non-rechargeable batteries to modern controlled battery packs, the power system of EVs has experienced several alterations and innovations [1-3]. Recently, lithium-ion batteries have been adopted as primary power sources in EVs due to the merits of high power and energy densities, high operating voltage, long cycle life and low self-discharge rate. Therefore, the development of BMSs for lithium-ion batteries is very important, as they can ensure the safe and efficient operation of the battery systems in EVs [4, 5].

1.1 History of Electric Vehicles (EVs)

The first electric vehicle dates back to the 1830s. Between 1832 and 1839, Robert Anderson invented the first crude electric carriage, powered by non-rechargeable primary cells [6]. Later, more practical and more successful electric road vehicles were invented by the middle 19th century and the newly-invented non-rechargeable electric cells and batteries were first used by the inventors in that era [7].

In spite of their slow speed, EVs had many advantages in their early stage compared to other vehicles. They were more stable, clean and quiet. As a result the early electric cars became very popular as city cars, and they were also very popular due to their ease of operation. The first commercial EV application came to the market as a taxi in New York City, and was built by the Electric Carriage and Wagon Company of Philadelphia in 1897. Figure 1-1 shows an early 1900s electric vehicle. At the end of the 19th century and in the early 20th century, research on battery technology significantly affected the capacity improvement of batteries. In the later 19th century, the capacity of batteries was around 10Wh/kg, by the early 20th century the capacity had been improved to 18Wh/kg and by 1911 the capacity reached 25Wh/kg. EVs became widely used with the mass production of secondary rechargeable batteries, and soon the commercial electric automobiles had the majority of the market. For most of the 20th century, the UK was the world's largest user of electric road vehicles [8].

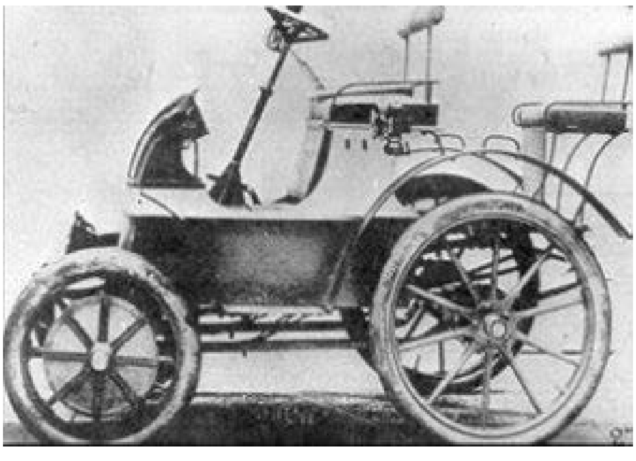

Fig. 1-1 Early 1900s electric car [6]

However, by the 1930s the number of EVs decreased to nearly zero due to the introduction of internal combustion engine vehicles (ICEVs). Compared with ICEVs, EVs were slower and more expensive. Therefore, the leadership of EVs was overtaken by ICEVs. In addition, the cheap price of petrol in the 1930s enabled ICEVs to travel a long distance by carrying a petrol tank.

In the 1960s, due to the decreased air quality the U.S. government started to address several air pollution control regulatory standards for automobiles. The energy crisis in the 1970s and 1980s caused EVs to attract new attention from the U.S. government. The U.S. government funded universities and laboratories to devote more time and resources to EV research. However, because of the limited performance of EVs at this stage and the lack of broad infrastructure support and the participation of corporations, the development of EVs slowed rapidly during the 1960s to the late 1980s [9].

The increasing concerns with energy conservation, cost and independence as well as environmental issues significantly stimulated the revival of EVs after the 1990s and have encouraged people to consider the EV as an alternative mode of transportation. From the 1990s until the present, major automobile companies have launched aggressive strategies to develop EVs for commercialisation. Governments, academic institutions and related industries are actively participating in the R&D of EVs. Table 1-1 shows the currently popular EVs on the commercial market around the world and their manufacturers, battery types and battery energy and travelling distances.

TABLE 1-1 CURRENT ELECTRIC VEHICLES

EV Name and Company	**Battery manufacturer**	**Battery type**	**Battery energy**	**Approx. range**
Nissan Leaf	AESC	LiMn2O4	24kWh	105 **miles**
BYD-e6	BYD	LiFePO4	57kWh	249 **miles**
BMW Mini E	LG-Chem	LiNiMnCoO2	35kWh	150 **miles**
Ford Focus	LG-Chem	LiMn2O4	23kWh	76 **miles**
Mitsubishi iMEV	Toshiba	Li2TiO3	20kWh	100 **miles**
Chevrolet Volt	A123	LiFePO4	20kWh	82 **miles**
Diamler Benz Smart EV	Tesla	LiCoO2	16.5kWh	84 **miles**
Tesla Model S	Panasonic	LiNiCoAlO2	60kWh	208 **miles**

1.2 Underground Mine Electric Vehicles

Currently, in most underground mining operations, personnel carrier vehicles are driven by diesel engines which have the power and mobility for high productivity [10]. However, due to the vehicle emissions and mine ventilation, the use of diesel engine vehicles in underground mines is very problematic. Exhaust from diesel engines is discharged to the mine air with waste heat and noxious substances. With the increasing cost of ventilation apparatus, strict emissions and health regulations, EV technologies are being adopted at an increasing rate in underground mines [11]. By replacing diesel vehicles with emission-free electric drive vehicles, mining companies can offer better working conditions for their underground employees and reduce operating expenses.

Of the several types of batteries for UMEVs, lead-acid batteries have been the main power sources for electric underground mine cruisers and personnel carriers for the past decades [12]. With the development of new battery technologies, lithium iron phosphate ($LiFePO_4$) batteries are currently the most acceptable batteries in underground mining personnel carriers [13] due to their relatively safe and reliable characteristics compared with other lithium ion batteries. UMEVs can be grouped into two categories: rail locomotives and electric load-haul-dump (LHD) vehicles which are used to handle ore, and personnel carriers.

1.2.1 Rail locomotives and LHDs in underground mines

Before the popularity of the battery technologies, fuel cells were used to power underground vehicle in the mine locomotive [10]. The fuel cells used in underground mine rail vehicles have many benefits, including zero emissions, low noise, low temperature, high power density and long life. They provide with the safety, compactness and simplicity in working environment [14]. Anglo American Platinum Ltd developed a 10 ton fuel cell locomotive which demonstrated well in the South Africa Tumela mine [15]. Figure 1-2 shows the fuel cell mine locomotive.

This locomotive is much heavier than other vehicles. Most locomotives in underground mines are rail vehicles, which confines the movement of the vehicles. This kind of vehicle carries equipment to handle ore or rocks.

Fig. 1-2 10 t fuel cell mine locomotive of Anglo American Platinum Ltd [15]

GE Mining is bringing forward its battery-powered vehicle in coal mining to the hard rock industry through battery powered load-haul-dump vehicles, as shown in Fig. 1-3. This vehicle is powered by GE's advanced Durathon battery, which is a sodium metal halide battery (NaMx) with improved performance and increased reliability. This new technology will make underground mining industries safe, cost-efficient and clean.

Fig. 1-3 GE mining battery powered LHD [16]

1.2.2 Electric personnel carriers in underground mines

To provide miners with better working conditions, an electric personnel carrier is essential for them to travel to the workface and to the workshop. Based on an investigation and survey of current electric personnel carrier vehicles, batteries are the most used power sources in electric underground mine personnel carriers and cruisers. There are several types of batteries in use. The most popular batteries are the lead acid battery and the lithium-ion battery. In 1989, Damascus Corporation designed their first three- or four-wheel battery-operated personnel carrier (shown in Fig.1-4), which became very popular for moving personnel, tools and parts in underground coal seams. This personnel carrier was powered by lead acid batteries.

Fig. 1-4 Damascus underground mine electric personnel carrier [17]

With the development of the lithium-ion battery technology, this type of battery is accepted as a promising candidate for underground mining personnel carriers [13] due to its safety characteristics. Of all the lithium-ion batteries, the $LiFePO_4$ (LFP) battery is the most popular in underground mine personnel carriers. The Canadian company Papabravo launched its underground mine electric personnel carrier vehicle (see Fig.1-5) propelled by an LFP battery pack with the energy of 40kWh. The vehicles can travel

120 km on a single charge and can re-charge for more than an hour during the crew change. By using this green and friendly vehicle in the underground mining industry, the air quality in underground mines and miners' working conditions can be improved. Table 1-2 summarizes the underground mine electric personnel carriers currently available around the world.

Fig. 1-5 Papabrovo underground mine electric personnel carrier [13]

TABLE 1-2 UNDERGROUND MINE ELECTRIC PERSONNEL CARRIERS

Name of Carriers	**Company**	**Battery type**	**Battery energy**
MAC-12 Electric transporter	Damascus	Lead acid	7.2 kWh
672 Inspector's friend	John B. Long Co	Lead acid	16.9 kWh
7200 Personnel carrier	A.L.LEE Corporation	Lead acid	8.6 kWh
GE Locomotive	GE	Durathon battery	24.8 kWh
Personnel carrier	Papabravo	LiFePO4	48 kWh
Rubber tyred car	CALB	Lithium ion	64 kWh

1.3 Batteries for EVs

The overall objective of EV development is to make it commercial, which means EVs must have a range, performance, safety, comfort and reliability comparable to ICEVs. In this context, developing a high performance, low-cost, reliable and safe alternative energy source is essential [1]. The alternative energy sources for EVs include batteries, fuel cells, capacitors and flywheels. Fuel cells generate energy by chemical reaction, while batteries, capacitors and flywheels are energy storage systems using charging and discharging processes. Currently and in the near future, batteries are considered to be the dominant EV energy source because of their increased energy capacity and reasonable price. The basic task of the battery is to store energy obtained from an external power source by charging the battery and releasing the energy which is transferred into kinetic energy by discharging. Table 1-3 shows the typical characteristics of batteries commonly used in EVs.

TABLE 1-3. BASIC TECHNICAL PERFORMANCE OF BATTERY TYPES USED IN EVS [18]

Battery type	Lead-acid	Ni-Cd	Ni-MH	Lithium-ion
Energy density (W/kg)	30-50	45-60	70-95	80-120
Nominal voltage	2V	1.25V	1.25V	3.6V
Overcharge tolerance	High	Moderate	Low	Very low
Self-discharge	Low	Moderate	High	Very low
Operating Temperature	-20~60 °C	-40~60°C	-20~60°C	-30~60°C
Cycle life	500~1000	800	750~1200	1500~3000
Energy efficiency	>80%	75%	70%	85%~95%

1.3.1 Lead acid battery

The lead acid battery has been successfully used as a commercial EV power resource for a long time since it was invented by the French physician Gaston Planté in 1859 [19]. It was the first rechargeable battery for commercial use. It uses lead dioxide for the anode, metallic lead for the cathode and sulphuric acid solution for the electrolyte.

The lead acid battery has a relatively low cost with a broad capacity range. It can work under different temperature ranges [20]. A typical lead acid battery has a self-discharge between 2% to 5% per month at room temperature [21, 22]. Lead acid batteries have undergone steady improvements in efficiency, durability, and lifetime, and are now widely used in many fields due to their relatively stable characteristics. The above advantages have led to their use as the power supply for golf cars, forklifts and some simple underground mine carriers.

The lead acid battery has a relatively short life cycle and is heavy compared with other battery types. The lifetime of a lead acid battery is reduced with the increase of the depth of discharge [23]. A lead acid battery cannot be fast charged, and a full charge cycle takes 14 to16 hours. When the lead acid battery is stored, it must be in the fully charged state to avoid sulfation. The main disadvantage of the lead acid battery is that lead is toxic, and environmentalists would like to replace the lead acid battery with other chemicals.

1.3.2 Ni-Cd and Nickel- Metal Hydride batteries

The nickel-cadmium battery, invented by Waldmar Jungner in 1899 [19], offered several advantages over lead acid batteries, but the materials were expensive at the time when it first came to commercialization. The nickel-cadmium (Ni-Cd) battery uses nickel oxide hydroxide and metallic cadmium as electrodes. For many years, the Ni-Cd battery was the preferred battery choice for radios, emergency medical equipment, professional video cameras and power tools. Compared with other types of rechargeable cells, the Ni-Cd battery offers relative short cycle life and capacity. Typically, the best performance for Ni-based batteries is obtained at temperatures between 0 and 40 °C, while it can work under an extremely low temperature of around minus 40°C [24]. The nickel-based battery can accept fast charging, and the charge time can vary from 14 hours at 0.1C charge to 1C charge for 1 hour. However, cadmium has the potential for carcinogenicity and is an environmental hazard. Despite these severe drawbacks, the Ni-Cd batteries were accepted to propel EVs before the advent of the nickel-metal hydride (Ni-MH) battery [25].

Research on nickel-metal-hydride batteries started in 1967. The Ni-MH battery is very similar to the Ni-Cd battery, and uses nickel oxy hydroxide for the anode like the Ni-Cd battery and adopts metal hydride as the cathode. Compared with the Ni-Cd battery, the Ni-MH battery offers relatively higher specific energy, an extended life span and is environmentally friendly. After the emergence of the Ni-MH battery, it soon replaced the Ni-Cd in HEV applications. The Ni-MH battery has a lower price and safer operation than the lithium-ion battery, but has the significant disadvantage of a high self-discharge rate. It can lose 20% of its capacity within the first 24 hours after being fully charged and 10 % per month thereafter. Therefore, it is important to store the battery under low-voltage conditions [24, 26].

1.3.3 Lithium-ion battery

Of the existing batteries used in EVs, the most promising candidate is the lithium-ion battery. The lithium-ion battery is superior to other type of batteries in terms of energy density and power density, which allows it to be designed to be lighter in weight and smaller in size. The lithium-ion battery also has the advantage of a wide temperature range of operation, rapid charge capability, no memory effects, long cycle life and low self-discharge rate, as shown in Table 1-2. Compared with other types of batteries, the charging time of the lithium ion battery is very fast, from 2.5 hours to 0.5 hours with the varying charge current [27]. Its self-discharge rate is around 1% to 2% per month at room temperature [28]. These appealing features also explain why they are already dominant in consumer electronics such as cell phones, laptop computers, digital cameras, video cameras, power tools and other portable devices [29].

There are many types of lithium-ion batteries, depending on the cathode materials. The most popular lithium-ion batteries include lithium cobalt oxide (LCO), lithium manganese oxide (LMO), lithium iron phosphate (LFP) and lithium nickel manganese cobalt oxide (NMC). Table 1-4 shows the performance of different lithium-ion batteries. It can be seen that the LFP-based lithium-ion batteries are the most promising batteries of the four types when considering all the aspects. The pivotal benefits of the LFP batteries are enhanced safety, good thermal stability, tolerance of abuse, high current rating and long cycle life [30].

TABLE 1-4. BASIC TECHNICAL PERFORMANCE OF LITHIUM-ION BATTERIES

Specifications	$LiCoO_2$ (LCO)	$LiMn_2O_4$ (LMO)	$LiFePO_4$ (LFP)	$LiNiMnCoO_2$ (NMC)
Nominal voltage (V)	3.6	3.8	3.3	3.6
Operating voltage range (V)	2.5~4.2	2.5~4.2	2~3.6	2.5~4.2
Specific energy (Wh/kg)	150-190	100-135	120-160	140-180
Cycle life (100%DOD to 80% capacity)	500+	500+	1000+	500+
Operating temperature during discharge (°C)	-20~60*	-30~60*	-30~50	-20~60*
Operating temperature during charge (°C)	0~45	0~45	0~45	0~45
Discharge rate (continuous)	2-3C	10C	10-125C	2-3C

*[19]

1.4 Battery Management System

Generally, the capacity and voltage of a single battery cell is relatively low if it is used in EVs. To meet the requirements of energy and power for EVs, hundreds and thousands of single cells are required to be connected in series and parallel to build a battery pack. The series connection of cells yields a higher total battery voltage at the same capacity and the parallel connection of cells yields a higher total battery capacity at the same battery voltage [31]. Usually, the battery system in EVs contains many battery packs. To manage the battery packs, a battery management system (BMS) is essential.

The main task of the BMS is to ensure the optimum use of the energy in the battery system and prevent the battery system from being damaged. The BMS is able to monitor and protect the battery cells in the battery pack, estimate the state of charge, control the battery cells' balance and report the status of the battery cells to the electronic control unit (ECU) in the EV.

The BMS in the vehicle is required to interface with other vehicle control systems. It also deals with the real-time rapidly changing charge and discharge conditions. With the acceleration and braking of the EV, the BMS works in a harsh environment. The hardware of the BMS in EVs is integrated with many sensors, actuators, controllers and signal wires. The main tasks of the BMS in EVs are as follows [5, 32]:

- Protect the cells and battery pack from damage,
- Prolong the life of the battery system through the control of the cell and battery pack to operate within the appropriate voltage, current and temperature range.
- Control and maintain the battery system in an optimum state in which the EV can operate at its best.

The BMS has many function modules, and the basic framework of the BMS functions is shown in Fig. 1-6.

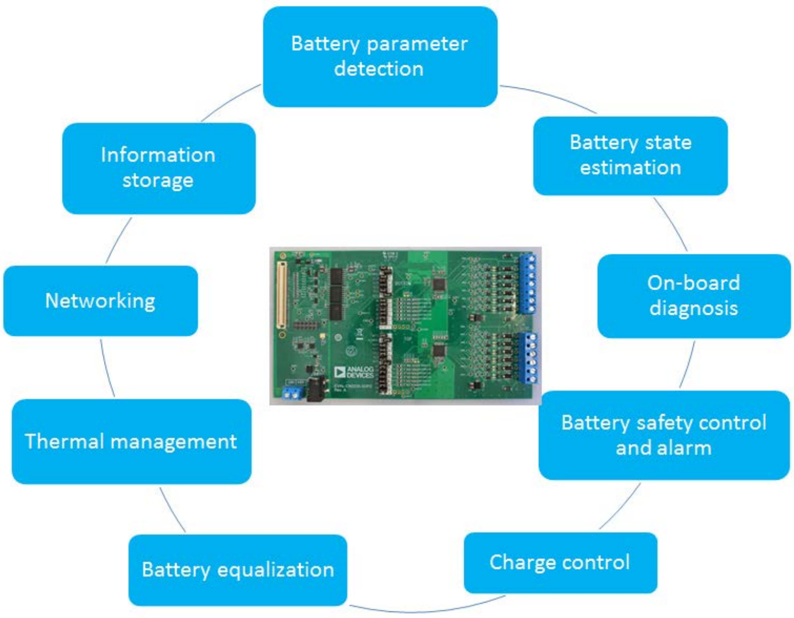

Fig. 1-6 Basic framework of BMS function

The main function modules of the BMS can be summarised as follows:

- Measurement module. This module usually detects the voltage and temperature of each cell and pack， as well as the total current of the battery pack.
- Management module. This module includes the protection of the battery system from damage by monitoring the condition of the cells and battery pack, the balancing of the battery cells to maximize the pack’s capacity and the control of the temperature of the system to make sure it works in a safe temperature range.
- Evaluation module. This module estimates the state of the battery pack, which includes the state of charge (SOC), state of health (SOH), pack capacity and pack resistance by analysing the measured data
- Communication module. This module exchanges the battery system information with the ECU and other external systems in the EV.
- Information storage module. This module stores the key data of the voltage, current, SOC and resistance for the battery pack and the maximum and minimum voltage and temperature of each cell as well as providing warnings and error messages.

Although the BMS has many modules, the present research focuses on the following parts of the BMS:

- Based on an analysis of characteristics of UMEVs, the comparison of different battery systems was conducted through simulation to choose the best battery system for UMEVs.
- To make a consistent battery pack, a battery sorting method based on a self-organization map (SOM) is proposed to classify the cells into groups with

similar characteristics and the cells in the same group are used to build the battery pack.

- The H-infinite observer is used to estimate the SOC for the sorted battery pack and the SOC of each cell.

1.5 Objectives and Major Contribution of the Thesis

This thesis focuses on three aspects of the BMS: the selection of battery systems for UMEVs among many types of LiFePO4 batteries and battery packs, the classification of cells for constructing battery packs, and the estimation of state of charge (SOC) for the battery pack.

The major contributions of the thesis are as follows:

- A modified UMEV model is developed based on the current EV model in ADVISOR.
- An underground mine driving cycle with variable rolling resistance coefficients and variable uphill/downhill gradients is designed.
- A hybrid simulation approach based on the modified Advanced Vehicle Simulator is proposed to integrate the experimental results of battery packs into the UMEV model.
- A SOM sorting approach is proposed to select cells of similar characteristics to alleviate the problems of non-uniformity and imbalance of cells in battery packs.
- An average virtual cell model-based H infinity observer method is proposed to estimate the state of charge (SOC) for a series-connected battery pack and cells.

In summary, the work of the thesis has the potential to significantly enhance the battery performance of UMEVs to achieve the desired driving experience in underground working conditions.

1.6 Organization of the Thesis

The structure of the thesis reflects the discussion about the current research and research gaps in three aspects of the BMSs for UMEVs. The thesis is organized as follows:

Chapter 2 presents a survey of EVs and underground mine EVs as well as the current batteries and BMSs. The main tasks of the BMS are discussed in detail, including battery types for UMEVs, cell inconsistency in the battery pack and SOC methods for battery packs and each cell in the pack.

Chapter 3 explores the selection of battery systems for UMEVs. The parameters of the batteries are identified based on battery experiments under various temperatures. A UMEV dynamic model is developed and implemented in ADVISOR. To compare the battery systems by integrating the experimental results of these batteries and battery packs into a UMEV model, a hybrid simulation is proposed and conducted for a specifically designed underground mine driving cycle with variable rolling resistance coefficients and variable uphill/downhill gradients.

Chapter 4 investigates a self-organizing map (SOM)-based classification of LiFePO4 cells for a battery pack so that the cells can be as consistent as possible before these cells form a battery pack. The parameters of cell temperature variation, internal resistance and available capacity obtained from the experiments are used as the inputs of the SOM to classify the cells. Next, the output of the SOM is used to classify cells into three groups with similar characteristics according to the input parameters. Cells in the same group are built in series for a sorted battery pack, whereas randomly chosen cells are connected in series to form an unsorted battery pack. The comparison of the consistency between the sorted battery pack and the unsorted battery pack under different discharging conditions verifies the effectiveness of the proposed classification method and the consistency of the cells in the battery pack.

Chapter 5 presents an H infinity observer-based method to estimate the SOC for a series-connected battery pack. An average virtual cell (AVC) model is defined and the SOC of the AVC model is estimated to represent the pack SOC when the terminal voltage differences (TVDs) between each individual cell in the pack and the AVC are all less than the pre-set value. When the TVD of one cell is larger than the pre-set value, the SOC of the cell is estimated together with the pack SOC. The $LiFePO_4$ battery pack is utilized to conduct the experiments to verify the effectiveness of the proposed method.

Chapter 6 provides the conclusions and recommendations for future work.

CHAPTER 2 LITERATURE REVIEW

This chapter provides a broad review of $LiFePO_4$ batteries, the sorting methods to build battery packs and the SOC estimation method used in cells and battery packs for UMEVs.

2.1. Battery Selection and Simulation for UMEVs

Currently, most underground mine vehicles are powered by diesel engines [10]. Due to the exhaust and ventilation problems in underground mines, electric powered vehicles are attracting much attention in underground mine industries [33]. As discussed in Section 1.3 above, batteries are the main power source for electric powered vehicles. Compared with most commercial rechargeable batteries, lithium ion batteries are the most acceptable batteries in EVs due to their high energy and power density, long cycle life, low self-discharge rate and wide operating temperature range [5]. To enable the selection of the best battery options for UMEVs, Table 2-1 summarizes battery companies around the world, their typical commercial lithium-ion batteries and the cost per kWh. Table 2-2 summarizes the typical characteristics of the above batteries. The $LiFePO_4$ battery is selected as the power source for UMEVs due to its safety and reliability [13]. Four $LiFePO_4$ batteries are listed in Table 2-2: the A123-AMP20, Saft-VL 10V Fe, BYD NS 60 and Guoxuan IFP1865140A. Of these four batteries, the A123 battery has the lowest kWh. After detailed comparison of these batteries, two types of A123 battery were investigated in this research project.

As the capacity of energy storage of a single cell cannot provide sufficient power and energy for UMEVs, it is crucial to compare and optimize the size and weight of battery packs in many aspects including performance, cost and life. Simulation approaches to evaluate and compare the batteries are generally chosen by researchers to optimize battery systems for EVs [34-36]. There are currently many simulation platforms for EVs, and the most popular simulation platforms are summarized in the following section.

TABLE 2-1 CURRENT COMMERCIAL LIFEPO4 BATTERIES

Manufacturer	**Country**	**Existing Customer(s)**	**Battery Type**	**Price US $/kWh**
Kokam	South Korea	No data	SLPB80460330H	600-800
LG-Chem	South Korea	GM, Hyundai		350-400
A123 system	USA	Chrysler LLC, GM	AMP20 Lithium	400-500
Sanyo	Japan	VW, Toyota	NCR18650 Series	350-500
GS Yuasa	Japan	Mitsubishi Motors,	LEV50	No Data
Saft	France	Daimler, Ford, BMW	Super-Phosphate	No Data
BYD	China	BYDAuto, SAIC	ET-Power	550-800
BAK	China	No data	BAK 18650	550-600
Guoxuan	China	JAC Motor	IFP1865140A	500-550

The advanced vehicle simulator (ADVISOR2002) is a simulation tool developed by the U.S. National Renewable Energy Laboratory. It is based on the MATLAB/Simulink platform. ADVISOR is designed for users to analyse and simulate both conventional and advanced EV configurations quickly and accurately [37]. Its model provides detailed vehicle system data including the power requirement of each block in EVs, particularly the power required to overcome rolling resistance, aerodynamic drag, and inertia [38]. This package evaluates the performance of the vehicle in a combined backward-forward approach.

TABLE 2-2 TYPICAL LITHIUM-ION BATTERIES OF DIFFERENT BATTERY COMPANIES

Battery Type	Nominal Voltage	Energy Density (Wh/Kg)	Capacity (Ah)	Dimension (mm)	Mass (g)
Kokam-SLPB 80460330H	3.7V	50-80	100	8*455*325	2700
LG-Chem ICR18650S3	3.7V	No data	2.2	Φ 18.5×65	48
A123-AMP20	3.3V	2400	20	7.2×160×227	496
Sanyo-NCR18650	3.6V	183	3.1	Φ 18.6×65.2	45.5
GS Yuasa-LEV50	3.7V	109	50	171×44×115	1700
Saft-VL 10V Fe	3.3V	55	10	Φ 47×173	600
BYD-NS60/55D23R	3.3V	No data	60	260×170×228	12000
BAK-18650	3.6V	No data	1.5	Φ 18.4 ×65	45.0
Guoxuan-IFP1865140A	3.3V	185	10	65×18×140	330

Figure 2-1 shows the structure of the module of the EV. The EV module consists of several subsystems. Each subsystem has its own MATLAB file, which defines the related parameters of this particular subsystem. Users can modify the subsystem SIMULINK model as well as the M-file to fit new modelling requirements. For example, in the energy storage subsystem, different battery models can substitute the existing battery model. The user can change the M-file related to the battery block diagram and choose different batteries from different companies. In this research project, the A123 2.3Ah and 20Ah batteries were chosen to replace the Saft 6Ah lithium ion battery. It is very easy to build your own EV model using ADVISOR.

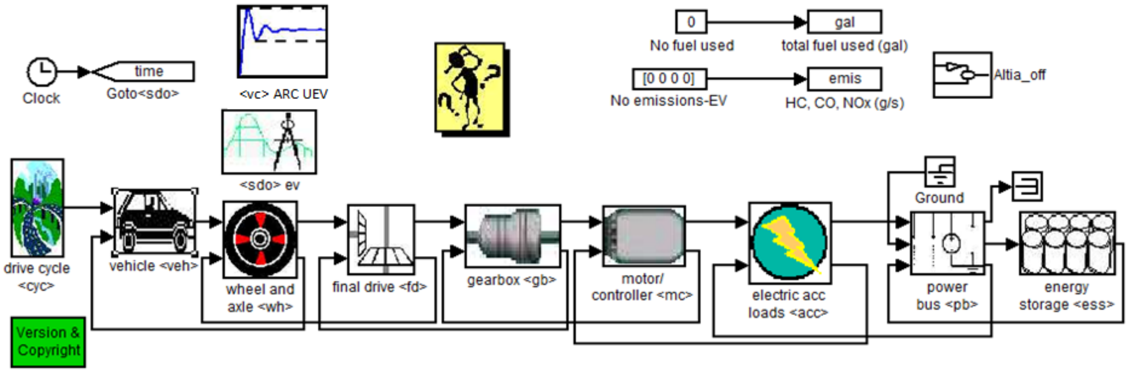

Fig. 2-1 Top module of EV

The Powertrain System Analysis Toolkit (PSAT) is a simulation toolbox for electric power system analysis and control software, developed by the Argonne National Laboratory and sponsored by the U.S. Department of Energy (DOE) [39]. PSAT is developed in a MATLAB/SIMULINK environment and with graphical user interfaces (GUIs) based on the SIMULINK-based library, which makes PSAT a user friendly Toolbox. As a forward-looking model, PSAT provides users more than 200 predefined configurations, which include conventional vehicles, pure EVs, fuel cell vehicles, and hybrid EVs. PSAT's core is the power flow routine, which also takes care of state variable initialization. PSAT includes power flow, continuation power flow, optimal power flow, small signal stability analysis and time domain simulation. PSAT supports a variety of static and dynamic component models [40, 41]. Figure 2-2 shows a typical GUI of the PSAT vehicle model.

AVL CRUISE is a simulation package that supports tasks in vehicle system and drivetrain analysis throughout all development phases, from concept planning to final design. Its application range covers all conventional vehicle powertrain systems to advanced EV & HEV systems. The program provides the flexibility to develop a single system model to meet the requirements of diverse applications in the development of powertrains and drivelines. CRUISE offers a streamlined workflow for all parameter optimization and component matching. It is usually used in powertrain and engine development to optimize vehicle systems, including cars, buses, trucks and hybrid vehicles.

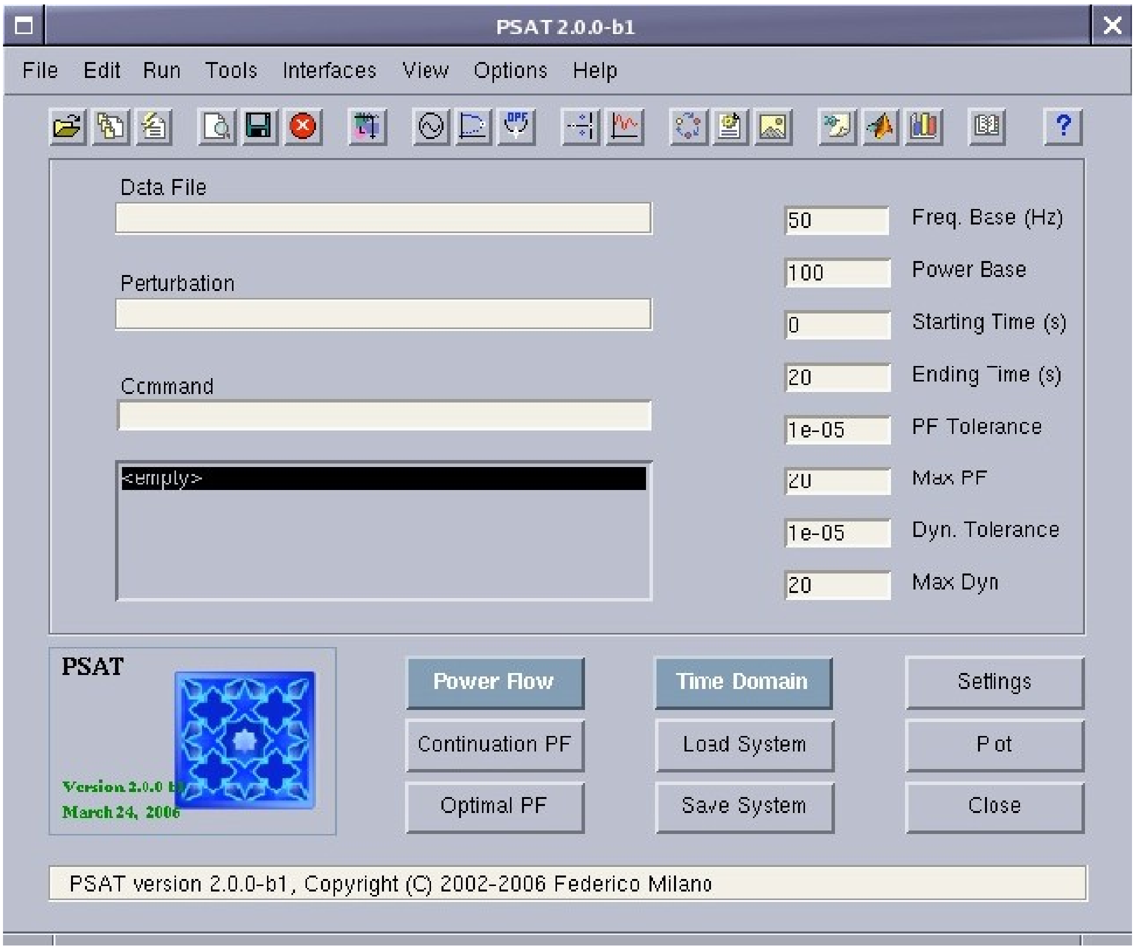

Fig.2-2 PSAT GUI and initial windows

EVSIM is an EV simulation module developed by Hong Kong University based on MATLAB for Windows. EVSIM has a modular programming structure and is programmed as M-files. It includes four hierarchical menus, namely the Main Menu, Input Menu, Specific Data Input Menu and Output Menu. The main menu consists of various sub-systems which are graphically presented [42]. Users can start the simulation with the default values. On the other hand, users can alter the vehicle parameters to perform the simulation.

Table 2-3 summarizes the above four simulation tools. Of these software packages, ADVISOR has more users and it is easy to modify the existing vehicle parameters. It provides a secondary development platform and has a backward and forward development environment, which is more flexible for users to build their own vehicle models. In addition, the software provides users with the open source code to develop their own models. Therefore, the ADVISOR was the best option for our research to perform the simulation for UMEVs.

Table 2-3 Current EV simulation software

Software Name	**Developer**	**Application**	**GUI and versatility**	**Development platform**
ADVISOR	U.S. National Renewable Energy Laboratory (NREL)	EVs, HEVs, PHEVs, normal vehicles, fuel-cell vehicles	GUI friendly and easy to use	MATLAB/Simulink Secondary development
PSAT	Argonne National Laboratory & U.S. Department of Energy (DOE)	EVs, HEVs, PHEVs, normal vehicles, fuel-cell vehicles	GUI friendly and easy to use	MATLAB/Simulink Secondary development
CRUISE	AVL	EVs, HEVs, PHEVs, normal vehicles, fuel-cell vehicles	GUI	C/Fortran
EVSIM	Hong Kong University	EVs	Graphic control and user friendly	MATLAB/Simulink Secondary development

The details of ADVISOR simulation approaches used in the UMEV are explained in detail in Chapter 3.

2.2. Battery Uniformity and Balancing

UMEVs require a battery system to supply sufficient power and energy. The battery system consists of a number of battery packs connected in series and parallel, and a battery pack consists of hundreds and thousands of battery cells which are connected in series and parallel. Due to differences in the parameters in each cell, there is the phenomenon of imbalance and non-uniformity among the cells in battery packs [43]. Figure 2-3 shows the key problems of the battery cells. The causes of the non-uniformity come from two aspects. On one hand, there are always slight differences in the process of manufacturing each single cell, leading to slightly different characteristics of the cells [44]. On the other hand, the cells operate in different conditions, such as different temperatures. Furthermore, the cells can have different capacities, internal resistances, voltages, and states of charge with the development of the ageing process.

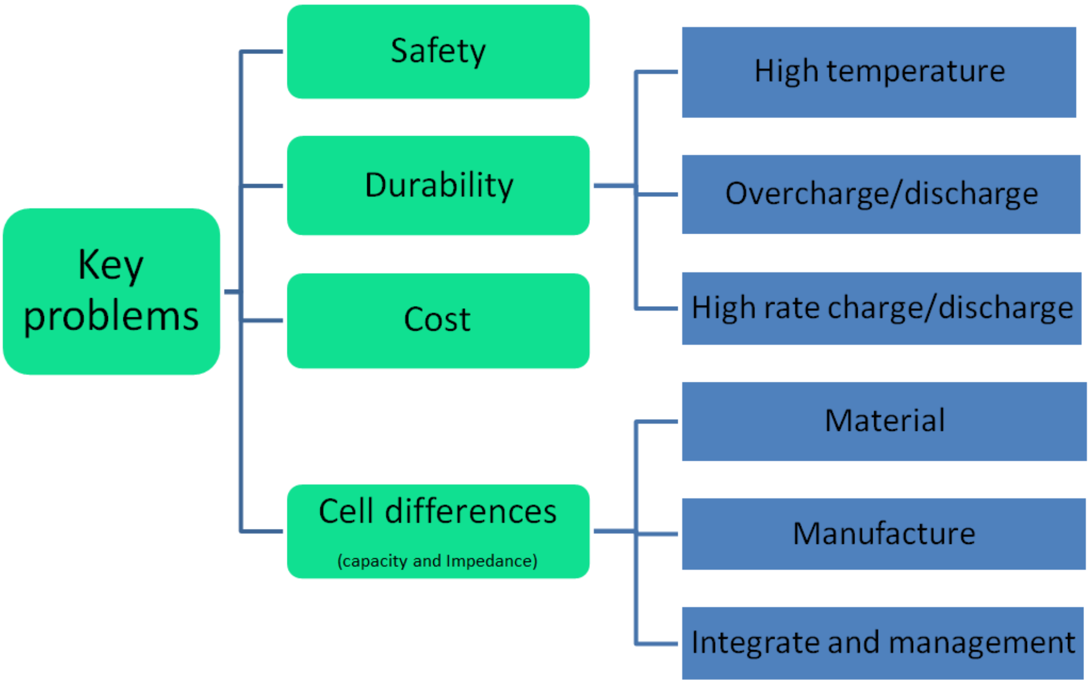

Fig. 2-3 Key problems of cell differences

Due to the differences in the cells, the cell voltage is not always equal to the pack voltage divided by the number of cells when the cells are connected in series. These differences will cause several problems which have drawn much attention. First, un-uniformity of cells causes incomplete charging of the battery pack. When charging the battery pack, the charging process stops when one cell’s voltage becomes close to unsafe condition while the other cells may not be fully charged, which means less available capacity of the battery pack. The second problem of imbalanced battery packs is incomplete use of the pack energy. When the battery pack discharges, the lowest voltage cell will decide the end of the discharge process to prevent over-discharge, while other cells still have relatively high voltage and energy left. This causes energy waste. As a result, non-uniformity can cause safety problems. These problems affect the on-board performance and cycle life of the battery packs in UMEVs. Therefore, it is important to analyse the uniformity and imbalance of batteries.

In order to alleviate the inconsistency of the cells in the battery pack, several methods have been reported in the literature to classify similar cells. There are two groups of clustering methods. One group of methods is based on observing the directly measured battery parameters. The other group is based on machine learning approaches.

2.2.1 Sorting methods based on observing direct measurement

Sorting methods based on observing the directly measured parameters from experiments are used to classify the cells into groups. They can be further divided into several classification methods, including the voltage classification method, the static capacity classification method, the resistance matching method and combinations of these methods.

Based on the above methods, a screening process has been introduced by Kim [45]. The screening process is a process to select cells which have similar electrochemical characteristics. Figure 2-4 shows a diagram of the screening process. In the first screening process, the cell's capacity within the capacity range is chosen and entered into the second screening step. In the second screening process, the measured internal resistance within the range is chosen as one group. Therefore, the cells in the selected group will have similar electrochemical characteristics in terms of capacity and resistances. However, the thermal variances of each cell in the battery pack during charging and discharging process are not considered.

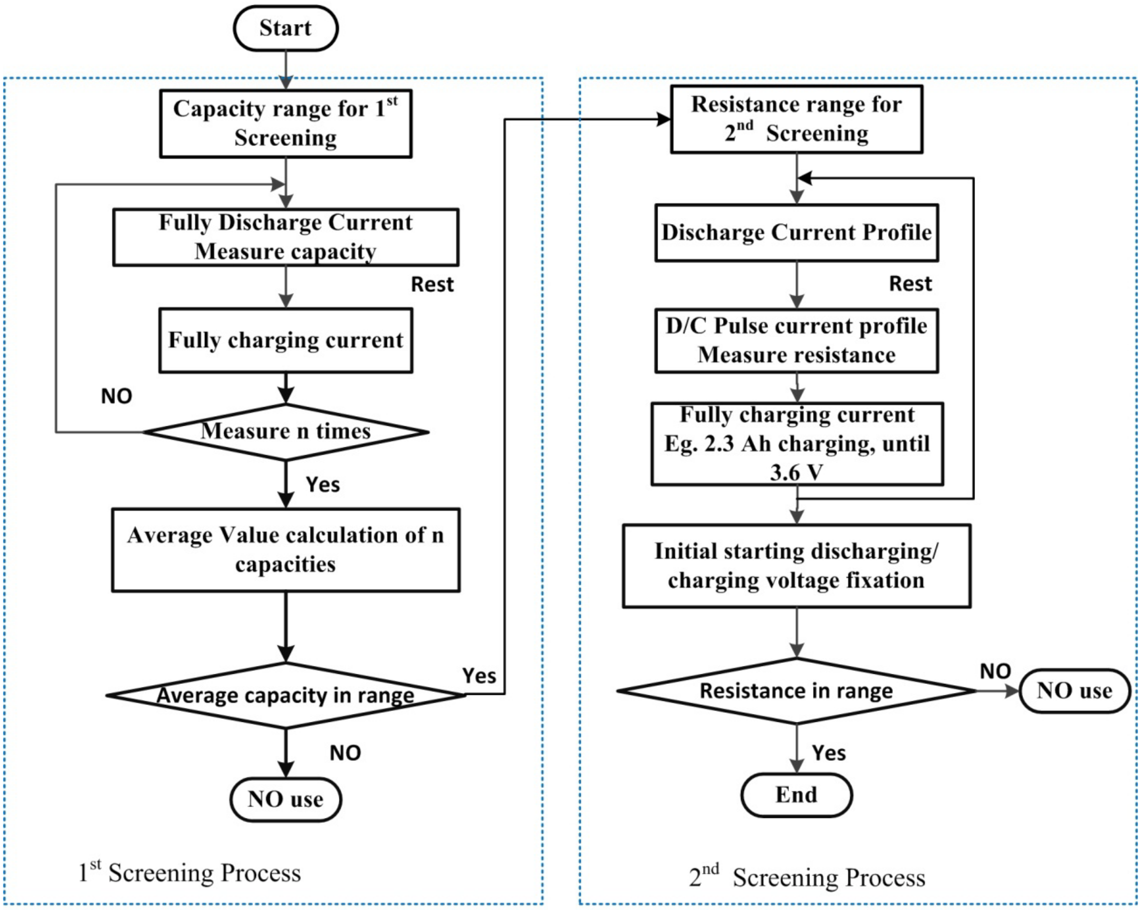

Fig. 2-4 Screening process sorting method [45]

2.2.2 Sorting methods based on machine learning

The fuzzy c-means (FCM) sorting method is a type of machine learning sorting approach. It is a data clustering technique in which a dataset is grouped into n clusters with every data point in the dataset belonging to every cluster to a certain degree [46]. This technique was originally introduced by Bezdek in 1973 as an improvement on earlier clustering methods. It provides a method that shows how to group data points that populate some multi-dimensional space into a specific number of different clusters.

Fuzzy C means uses the membership of each data point to determine which fuzzy group it belongs to. It divides n vectors $X_i(i = 1,2,3, \dots, n)$ into c fuzzy groups and its steps of clustering are shown in Table 2-4.

TABLE 2-4 FUZZY C-MEAN ALGORITHM AND STEPS

Initialization： dividing n vectors $X_i \left(i = 1,2,3,\dots,n\right)$ into c fuzzy groups $\sum_{i=1}^{c} u_{ij} = 1, \forall j = 1,\dots,n$ Then the value function of FCM will be $J\left(U, c_1, c_2 \dots c_n\right) = \sum_{i=1}^{c} J_i = \sum_{i=1}^{c}\sum_{j}^{n} u_{ij}^{m}\ d_{ij}{}^{2}$
Step 1：Use the random value between 0 and 1 to initialize the membership matrix U, and satisfy the constraint conditions of the following equations: $\bar{J}(U, c_1, \cdots c_n, \lambda_1 \cdots \lambda_n) = J(U, c_1, \cdots c_c) + \sum_{j=1}^{n} \lambda_j (\sum_{i=1}^{c} u_{ij} - 1)$
Step 2：Use following equation to calculate the clustering centres c_i, $(i = 1, \dots, c)$: $c_i = \frac{\sum_{j=1}^{n} u_{ij}^{m} x_j}{\sum_{j=1}^{n} u_{ij}^{m}}$
Step 3：If the value function calculated by the equation in step 2 or the value change

compared with the last time value is less than a certain threshold, the algorithm will stop working.

Step 4：Use the equation below to calculate a new U matrix. Then return to step 2

$$u_{ij} = (\sum_{k=1}^{c} \frac{d_{ij}}{d_{kj}})^{-2/(m-1)}$$

The other type of machine learning sorting approach is based on neural networks and is known as the Self-Organization Map (SOM) sorting method. SOM consists of a competitive layer which can classify a dataset of vectors with any number of dimensions into as many classes as the layer has neurons. The neurons are arranged in a 2-D topology, which allows the layer to form a representation of the distribution and a two-dimensional approximation of the topology of the dataset. SOMs operate in two modes: training and mapping. Figure 2-5 shows a SOM diagram in cell sorting. The input vectors of the SOM can be the capacity, internal resistance, temperature and other measureable parameters of the cells. The SOM Toolbox in MATLAB can then be used to cluster the cells into groups with the same electrochemical characteristics.

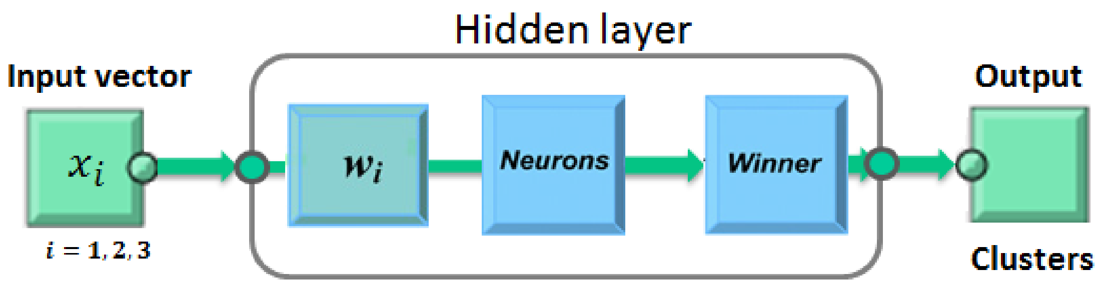

Figure 2-5 SOM model for cell sorting

2.3. SOC Estimation

The SOC means the percentage of the remaining charge of the battery capacity when the battery is fully charged under the specific standard conditions. The SOC uses the values between 100% and 0%, where 100% reflects a full battery and 0% reflects an empty battery. The SOC is one of the important parameters to ensure safe operation of the battery during charging and discharging. It can be defined as follows:

$$SoC_t = C_t / C_N \tag{2.1}$$

where C_t represents the capacity of the battery, and C_N represents the nominal capacity of the battery. For a parallel connected battery pack, the SOC can be calculated in the same way as for a single cell, while for cells connected in series, the battery pack SOC has to be considered for the non-uniformity of the cells in the pack.

Accurate estimation of SOC can be used to prevent a battery from being damaged or rapid ageing by avoiding overcharge and over-discharge. Precise estimation of the SOC is particularly important for large lithium battery packs. Control of the SOC is a major function of the BMS. Furthermore, for the EV industry, the large lithium battery packs used in EVs need very precise control of the SOC in order to manage the energy flow efficiently and safely [47].

There are many ways to estimate the SOC in an electric chemistry laboratory by physical measurement. However, it is quite challenging to estimate the SOC of commercial batteries without destroying the battery by disturbing the routine work of the battery power supply, especially the online estimation in UMEVs. With the precise estimation of the cell SOC in a sorted battery pack, the pack's SOC can be calculated. The literature documents a number of methods for SOC estimation summarized in Table 2-5.

TABLE 2-5. BASIC BATTERY SOC ESTIMATION METHODS OF LITHIUM-ION BATTERY

Approaches	Advantages	Disadvantages
Discharge test method	Accurate	Very hard to implement in online estimation
Open circuit voltage method	No algorithm needed to implement	Battery needs to rest for long time
Coulomb counting method	Easy to operate	Highly reliant on initial SOC value
Battery model-based method	Accurate	Complex battery model, needs signal collection. Needs long computing time and large computer memory, with complicated algorithm
Machine learning method	Details of the battery are not needed	Needs large training data set and long computation time

Details of the battery estimation methods are explained in the following sections.

2.3.1 Discharge test method

One of the most reliable methods to determine the SOC is the discharge test method. This method is to completely discharge a fully charged battery, record the discharge rate and ambient temperature, and determine the remaining capacity which can be used to calculate the precise SOC. However, it is time-consuming and can only be used in the laboratory.

2.3.2 Open-circuit voltage

The open-circuit voltage (OCV) is the battery voltage under equilibrium conditions, i.e. the voltage when no current is flowing in or out of the battery, and hence no reactions occur inside the battery. For the lithium ion battery, the OCV usually has a nonlinear relationship with the SOC [48]. The typical relationship of the OCV-SOC of lithium-ion batteries is shown in Fig.2-6. The OCV can be used to estimate the SOC [49] based on the relationship of the OCV-SOC curve. The greatest advantage of the OCV estimation method is that it has high precision. The disadvantage is that battery is required to rest for a long time to achieve equilibrium. This method is not suitable for dynamic SOC estimation. It can only be used when the UMEV is parked rather than being driven.

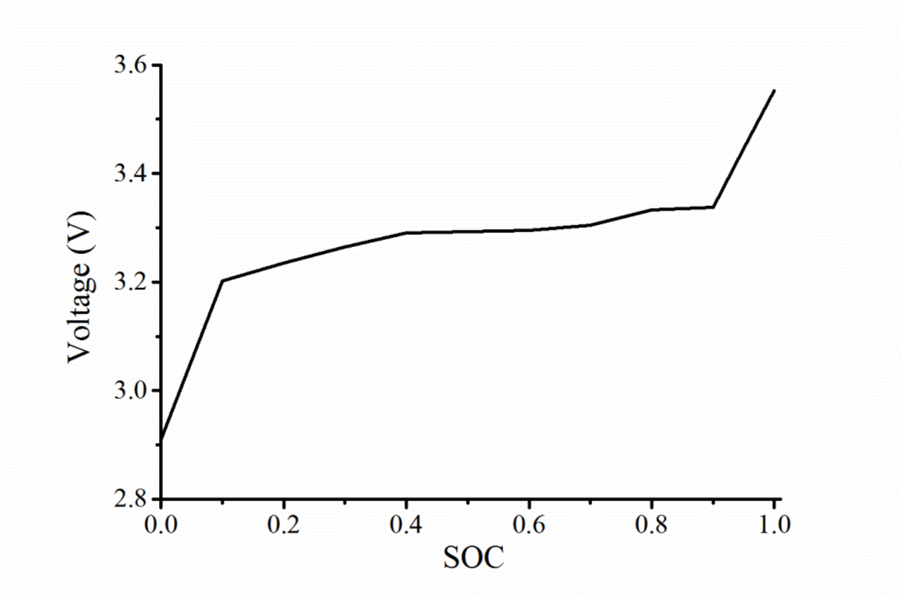

Fig.2-6 Relationship of OCV-SOC for the lithium-ion battery derived from experimental data of this study

2.3.3 Coulomb counting method

The Coulomb counting method is a simple and fundamental method to acquire the battery SOC, since it measures the discharge current directly and integrates the current of the battery over time. The Coulomb counting method for SOC estimation can be calculated using the following equation:

$$s_t = s_0 - \frac{1}{Q}\int_{t_0}^{t} \eta I(\tau)d\tau \tag{2.2}$$

where s_0 represents the initial SOC, Q denotes the battery nominal capacity, η is the Coulombic efficiency, and $I(\tau)$ is the instantaneous current.

This method has quite satisfactory accuracy with the known capacity and the accurate measurement of current. When the initial SOC is known, the SOC of a battery can be calculated by integrating the charging and discharging currents over the operating periods [50]. However, the precision of the battery's initial SOC and the Coulombic efficiency, which can be greatly influenced by the temperature and current, are difficult to obtain, which accumulates errors in SOC estimation over time [50]. Therefore, the Coulomb counting method used alone cannot meet the requirement of SOC accuracy.

2.3.4 Battery model-based SOC estimation

Based on the lithium-ion battery intrinsic relationship between the SOC and OCV, the battery equivalent circuit model (ECM) is adopted to estimate the SOC for overcoming the disadvantages of the OCV method. For the battery model-based SOC estimation method, the precision and complexity of the battery model are very important. Hu [44] and He [51] summarizes several equivalent circuit models, including the Rint model, the RC model and the nth order RC model. All these models can be used for dynamic estimation of the SOC, but their accuracy relies on the model's precision and the signal collection accuracy. Figure 2-7 and Table 2-6 summarize four typical ECM models which are widely used to estimate the SOC in lithium ion batteries [51]. In the following section, Thevenin ECM (Figure 2-7 (b)) is taken as an example to show how the SOC can be estimated. Based on Thevenin ECM model, the terminal voltage can be described by the equation

$$V_t = V_o - V_p - V_i \tag{2.3}$$

where V_t denotes the terminal voltage, V_o is the OCV of the battery, V_R is the resistance voltage drop and V_p is the voltage drop caused by internal polarization. It can be seen from the equation that the battery OCV can be estimated using observer techniques when the battery model parameters are known, and the battery parameters can be identified by the experimental results. With the OCV, the battery SOC can be easily obtained from the OCV-SOC look-up table.

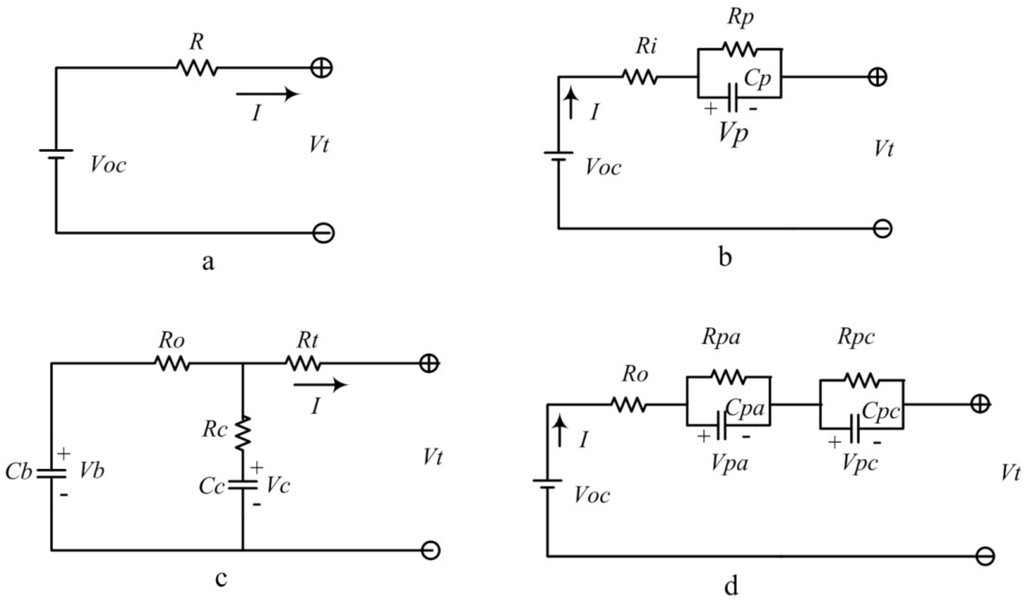

Fig.2-7 ECMs (a) Rint model (b). Thevenin model (c) RC model (d) DP model

TABLE 2-6 ECMS AND THEIR CHARACTERISTICS AND EQUATIONS

Battery model	**Characteristics**	**Equations**
Rint model	Simple; but does not suit dynamic operation	$V_t = V_{oc} - IR_0$
Thevinin model	Approximates the dynamic behaviour of lithium-ion batteries, dynamic characteristics cannot be represented very accurately	$V_t = V_{oc} - V_p - IR_i$ $\dot{V}_p = -\frac{1}{C_p R_p} V_p + \frac{I}{C_p}$
RC model	Simplifies the complex of the dynamic characteristics of batteries	$\begin{bmatrix} \dot{V}_b \\ \dot{V}_c \end{bmatrix} = \begin{bmatrix} \frac{-1}{C_b(R_0+R_c)} & \frac{1}{C_b(R_0+R_c)} \\ \frac{-1}{C_c(R_0+R_c)} & \frac{1}{C_c(R_0+R_c)} \end{bmatrix} \begin{bmatrix} V_b \\ V_c \end{bmatrix} + \begin{bmatrix} \frac{-R_c}{C_b(R_0+R_c)} \\ \frac{R_0}{C_c(R_0+R_c)} \end{bmatrix} [I_t]$ $[V_t] = \begin{bmatrix} \frac{R_c}{R_0+R_c} & \frac{R_0}{R_0+R_c} \end{bmatrix} \begin{bmatrix} V_b \\ V_c \end{bmatrix} + \begin{bmatrix} -R_t & -\frac{R_0 R_c}{R_0+R_c} \end{bmatrix} [I_t]$
DP model	Simulates the concentration polarization and the electrochemical polarization separately. Best dynamic performance and accuracy; does not rely on the initial SOC value	$\begin{bmatrix} \dot{V}_{pa} \\ \dot{V}_{pc} \end{bmatrix} = \begin{bmatrix} \frac{-1}{R_{pa}C_{pa}} & 0 \\ 0 & \frac{-1}{R_{pc}C_{pc}} \end{bmatrix} \begin{bmatrix} V_{pa} \\ V_{pc} \end{bmatrix} + \begin{bmatrix} \frac{1}{C_{pa}} \\ \frac{1}{C_{pc}} \end{bmatrix} I_t$ $V_t = V_{oc} - V_{pa} - V_{pc} - I_L R_0$

Model-based SOC estimation methods are usually applied with Kalman filter (KF), extended Kalman filter (EKF), sliding mode observer (SMO) and H infinity observer (HIO). The OCV (V_{oc}) is considered to be the internal state variables of the battery model. In the observer techniques, the output terminal voltage is usually estimated by an observer. The difference between the experimental voltage and the estimated voltage is applied to the observer as a feedback to adapt the state variables of the model. Once such difference is smaller than the pre-set value, the observer is converged. As a result, the terminal voltage from the observer matches the measured terminal voltage well, which indicates that the battery model states correspond well with the state of the measured battery, including the OCV. As mentioned earlier, the SOC can be obtained by checking the OCV-SOC look-up table. Figure 2-8 shows the basic theory of the observer topology.

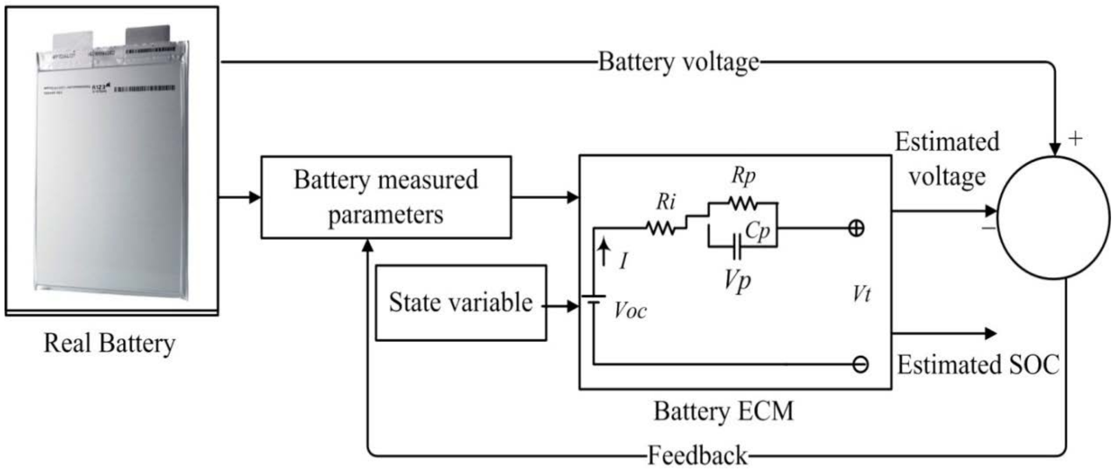

Figure 2-8 State observer for SOC estimation

KF is applied for dynamic system state estimation which is commonly used in many engineering fields. Plett introduced the KF and extended KF (EKF) for battery SOC estimation for cells and battery packs [52-62]. The system inputs usually consist of the current and temperature measured during the operation of the batteries, while the output is the battery terminal voltage. The state vectors include SOC, relaxation dynamics and hysteresis effects. The essential theory of the KF method for SOC estimation is to set up a reasonable battery model and build a group of state equations. Later, Plett also introduced the sigma-point KF. KF-based methods provide accurate battery SOC estimation. Table 2-7 demonstrates how to use the basic KF observer to estimate the battery SOC, and the Thevinin equivalent circuit model is chosen as the battery dynamic model.

TABLE 2-7 SUMMARY OF THE KALMAN FILTER USED TO ESTIMATE SOC [52, 63]

Step 1:Battery model equation $V_t = V_{oc} - V_p - IR_i$ $\dot{V}_p = -\frac{1}{C_p R_p} V_p + \frac{I}{C_p}$ $V_{oc} = K_0 + K_1 z + K_2 / z + K_3 \ln z + K_4 \ln(1-z)$ (z stands for the SOC)
Step 2: Parameter identification (1) Identify the parameter $K_0 \cdots K_4$ (2) Identify the parameter $R_i, R_p, C_p \cdots$
Step 3: Define the SOC $s_t = s_0 - \frac{1}{Q}\int_{t_0}^{t} \eta I(\tau) d\tau$ The discretization equation is : $SoC_k = SoC_{k-1} - \frac{\eta I_k \Delta t}{Q}$
Step 4 Kalman linear state-space equation: $x_{k+1} = Ax_k + Bu_k + \omega_k$ $y_k = Cx_k + Du_k + \upsilon_k$ ω_k and υ_k are independent, zero-mean, Gaussian noise processes of covariance matrices Here we define:

$$A=\begin{bmatrix}\exp(\frac{-\Delta t}{R_pC_p}) & o\\ 0 & 1\end{bmatrix}, B=\begin{bmatrix}R_p(1-\exp(\frac{-\Delta t}{R_pC_p})\\ \frac{\eta\Delta t}{Q}\end{bmatrix}, C_k=\frac{\partial V_t}{\partial x}\Big|_{x=\hat{X}_k{}^{-1}}=[-1 \quad \frac{dV_o(z)}{dz}\hat{z}_k^{-1}],$$

$$D=[-R_i]$$

Step 5: Transform the ECM equation to a discrete system

$$V_{t,k}=V_{oc}-I_kR_i-V_{p,k}$$
$$V_{p,k}=V_{p,k-1}\exp(-\Delta t/R_pC_p)+I_{k-1}R_p(1-\exp(-\Delta t/R_pC_p))$$

The state variable can be defined as

$$x_k=[V_{p,k},z_k)$$
$$y_k=V_{t,k}$$
$$u_k=I_k$$

Step 6: Initialization

For $k=0,$ set

$$\hat{x}_0^+=E[x_0]$$
$$\sum_{\hat{x}}^+=E[(x_0-\hat{x}_0^+)(x_0-\hat{x}_0^+)^T]$$

Step7: Computation

For $k=1,2,\cdots$

State estimate time update: $\hat{x}_k^-=A_{k-1}\hat{x}_{k-1}^++B_{k-1}u_{k-1}$

Error covariance time update: $\sum_{\hat{x},k}^-=\hat{A}_{k-1}\sum_{\hat{x},k-1}^+\hat{A}_{k-1}^T+\sum_\omega$

Kalman gain matrix: $G_k=\sum_{\hat{x},k}^-\hat{C}_k^T[\hat{C}_k\sum_{\hat{x},k}^-\hat{C}_k^T+\sum_\omega]^{-1}$

State estimate measurement update: $\hat{x}_k^+=\hat{x}_k^-+G_k[y_k-C_k\hat{x}_k^--D_ku_k]$

Error covariance measurement update: $\sum_{\hat{x},k}^+=(I-G_k\hat{C}_k)\sum_{\hat{x},k}^-$

SMO has been integrated in model-based SOC estimation in recent years [64-67]. The SMO technique is based on sliding mode control and can compensate for inaccuracies in battery models and variations noises to estimate the SOC. The state space model matrix of the system is always fully ranked, which means that all the state variables can be determined by observation of the battery terminal voltage. Therefore, the SMO aims to minimize the error between the battery model terminal voltage and the measured terminal voltage. Once the error has been converged to the pre-set value, the estimated OCV will be compared with the experimentally determined OCV-SOC look-up table to find the SOC of the battery.

The HIO is derived from the Kalman filter estimation method. In contrast with the Kalman filter-based estimation method, the HIO method does not need to know the exact system and measurement errors. The H infinity observer aims to design an observer to minimize the error between the output of the battery and its model so that the SOC estimation error is less than a given attenuation level. The attenuation level can be minimized by the optimization method LMI in the MATLAB Toolbox, which can also solve the feedback gain of the H infinity observer.

2.3.5 Machine learning method

Other algorithms such as fuzzy logic, neural network models, and the support vector machine method [64, 68-74] are also used to estimate the SOC by using large battery data sets to train the network model for SOC estimation. The machine learning method does not need to consider the details of the batteries. It is suitable for the SOC estimation of all kinds of batteries. However, a large training data set is needed to train the network model, and the accuracy of the model can be greatly influenced by the training data and methods. The drawback is that the training process in the machine learning method is very time-consuming.

The application of neural networks and fuzzy logic to SOC estimation for EV batteries provides a useful tool to solve the problems that exist in conventional methods. The key feature of a neural network is its learning capability. When the neural network is used for battery SOC estimation, the only problem is to select the parameters as inputs of the neural network. The relationship between the SOC and the related parameters can be modelled by the training data. Therefore, the neural network estimation method can ignore complicated battery models.

Figure 2-9 shows an example of a neural network SOC estimation diagram. The core of the neural network for SOC estimation is the relationship between the SOC and the input variables. The input variables, such as terminal voltage, discharge current, discharged capacity and temperature should be easy to measure. The neural network has three layers, namely the input layer, hidden layer and output layer. In Fig.2.9, the input neurons $X_i(t)$ from $X_1(t)$ to $X_6(t)$ are the discharged capacity, and $X_7(t)$ is the temperature. The input candidates are examined within the hidden layers with n neurons to perform the training and study. The output $p(t)$ represents the SOC at time t. The value of the SOC estimation can be expressed by $\widehat{p}(t)$.

$$\widehat{p}(t) = \sum_{i}^{n} W_i F(y_i) + b_1^0 \tag{2.4}$$

$$F(y_i) = \frac{1 - \exp(-2y_i)}{1 + \exp(-2y_i)} \tag{2.5}$$

where n is the number of neurons at the hidden layer, W_i are the weights between the hidden layer and the output layer. b_1^0 is the bias at the output layer, and

$y_i = \sum_{j=1}^{6} W_{ij} X_j(t) + b_i^h$ is the input to the i^{th} neurons at the hidden layer, W_{ij} are the weights between input layer and the hidden layer and b_i^h is the bias at the hidden layer.

The training algorithm of the neural network is a numerical process which determines the weights between layers and the bias in neurons. The learning process is ended when the error function trend begins to change.

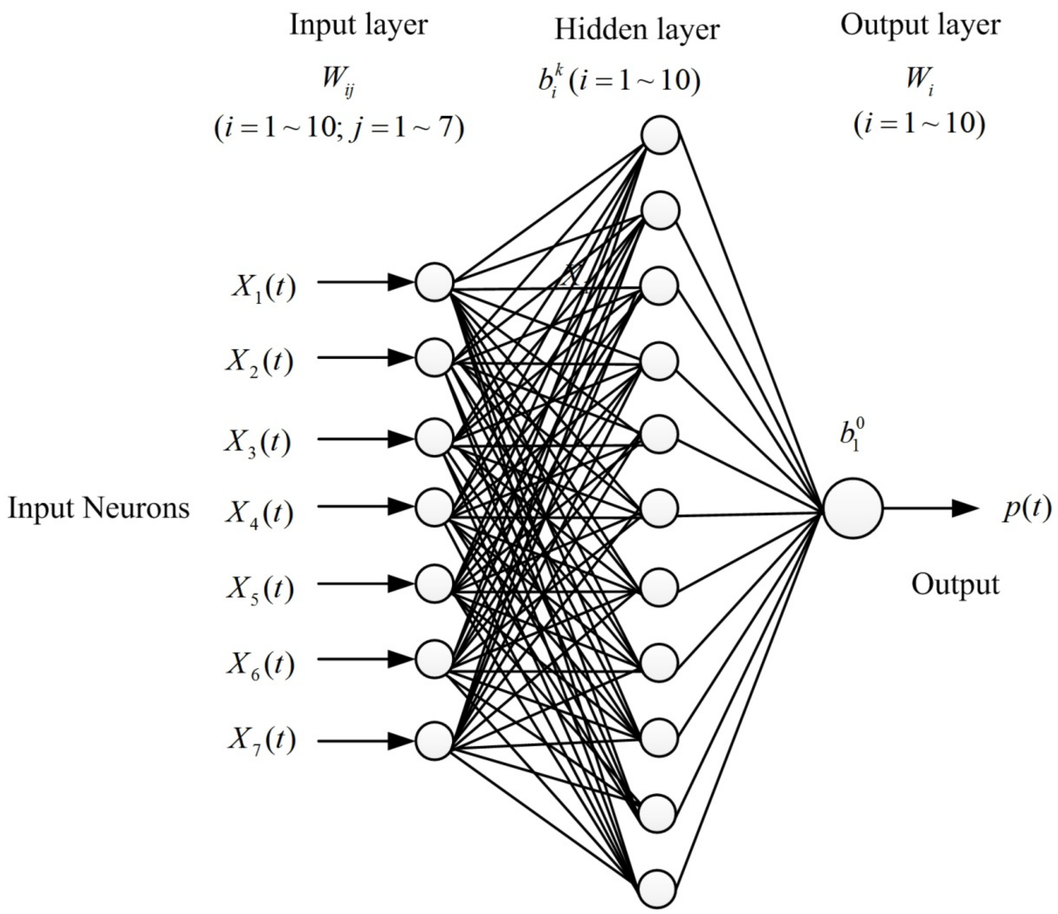

Fig. 2-9 Neural network for battery SOC estimation [75]

The support vector machine (SVM) learning approach has been adopted in various fields of pattern recognition. When applied to battery SOC estimation, SVM can be designed to integrate thousands of training data points and reduce all these data to one set of support vectors. The SOC estimation steps using the SVM training include: choose the training data, find the optimal SVM parameters, and choose and process the testing data. It is used as a nonlinear robust estimator because it is insensitive to small changes.

Battery pack and in-pack cell SOC estimation are discussed in detail in Chapter 5.

2.4. Summary

A review of underground mine electric vehicles (UMEVs), batteries and battery management systems has been presented in this chapter. First, the conventional UMEVs and the batteries used in UMEVs have been briefly reviewed. Then, the currently used UMEVs have been summarized and reviewed. Finally, three topics of the battery management system, including the selection of battery systems for UMEVs, cell clustering methods to alleviate the inconsistency of the cells in battery packs and battery SOC estimation methods, have been surveyed. These three topics are thoroughly discussed in the following chapters.

CHAPTER 3 COMPARISON OF DIFFERENT LITHIUM IRON PHOSPHATE BATTERY PACKS

In this chapter, the optimization of battery systems for EVs and the EV simulation approach are further reviewed. A four-wheel-drive (4WD) UMEV model is modified, based on the existing EV model in the ADVISOR. The experimental results on the charge and discharge characteristics of these batteries and battery packs at different ambient temperatures are reported. The extracted parameters of the experimental results for four batteries are integrated into the battery model in the ADVISOR. The UMEV model based on ADVISOR is then simulated to evaluate the performance of the UMEV for the selection of the most suitable battery system.

3.1 Introduction

In most current underground mining operations, personnel carrier vehicles are driven by diesel engines [10]. Exhaust from the diesel engines spreads into the mine air with waste heat and noxious substances. Ventilation and filters are required to comply with the occupational health and safety regulations on working conditions in underground mine. Regular replacement of exhaust filters increases operating costs. Electric vehicles (EVs) provide significant advantages of low noise and zero emissions over diesel engine vehicles and hence potentially reduce operating costs when EVs are adopted in underground mines [33]. Batteries are the main power sources for EVs. Of the existing commercial batteries, lithium ion batteries are the most acceptable batteries in EVs due to their high energy and power density, long cycle life, low self-discharge rate and wide operating temperature range [5] .

Since there is limited capacity for energy storage on board EVs, it is very important to optimize the size and weight of battery packs in terms of the required performance, driving distances and costs. Simulation approaches are generally used to optimize the size of battery systems in hybrid electric vehicles (HEVs) and plug-in hybrid electric vehicles (PHEVs) to reduce fuel consumption, costs and green-house gas emissions [34-36], and to compare different battery systems made from nickel-metal hydrate (NiMH) and lithium ion batteries in PHEVs for their suitability in terms of specific energy and power density, cycle life, operational temperature and cost [76]. Simulation approaches have also been used to evaluate hybrid energy storage systems of Li-ion batteries and ultra-capacitors for underground mine electric vehicles (UMEVs) [33, 77], and the simulation results show that such hybrid energy systems are suitable for the complex and poor road conditions in underground mines. For all the above simulations, specific software has been developed to include the models of each component of HEVs, PHEVs and UMEVs. There is a generic software package, Advanced Vehicle Simulator (ADVISOR), which can be used to analyses and simulate both conventional vehicles and EVs [78]. The modified ADVISOR can compare and simulate the hybrid energy source of the batteries and ultra-capacitors in HEVs [79, 80].

This chapter proposes a hybrid simulation approach to compare the four battery systems by integrating the experimental results into the battery models for a four-wheel-drive (4WD) UMEV. Since safety and reliability are particularly crucial for UMEVs, two lithium iron phosphate (LiFePO4) batteries and their corresponding packs were chosen. The charge and discharge characteristics of these batteries and battery packs were experimentally studied at different ambient temperatures. The experimental data were obtained to identify the model parameters for the batteries and battery packs. These models with the identified parameters were then used to evaluate the performance of the UMEV for the selection of the most suitable battery system.

The rest of the chapter is organized as follows. The model of the UMEV and the underground mine driving cycle (UMDC) are presented in Section 3.2, followed by an explanation of the experimental set-up, the test results and the identified model parameters for the batteries and battery packs. In Section 3.4, the simulation and validation results and discussion are demonstrated. Conclusions are given in Section3.5.

3.2 Model of UMEV

The ADVISOR is a comprehensive and generic software package. It includes the models of each component in conventional vehicles and EVs. The following section shows only the models particularly modified for the UMEV, and accordingly the blocks in the ADVISOR corresponding to the modified models were changed to facilitate the simulation of the UMEV.

3.2.1 UMEV vehicle dynamic model

UMEVs experience harsh and steep road conditions compared with conventional EVs driven on concrete pavement. To increase vehicle-road adhesion and improve performance and stability, a 4WD vehicle has been proposed for the UMEV and the 4WD vehicle model is used to describe the UMEV. Figure 3-1 shows all the forces acting on the 4WD UMEV in motion along a slope.

The total traction force F in the contact area between the tyres of the front and rear wheels and the road surface propels the vehicle forward. It is produced by the powertrain which is then transferred through the vehicle transmission system to the front and rear drive wheels. It can be calculated by [81-84]:

$$F = F_1 + F_2 = (W_1 + W_2) \times u_{rr} \tag{3.1}$$

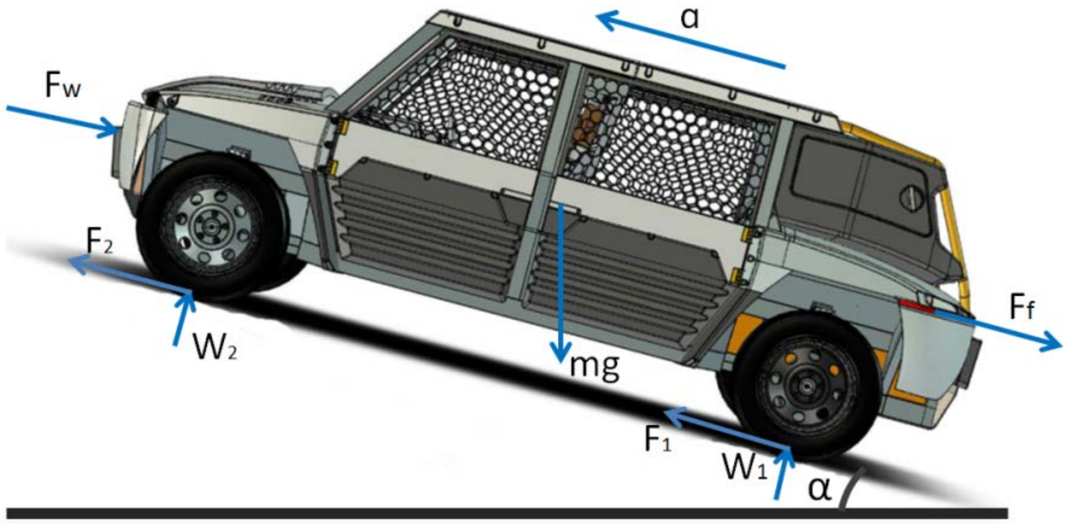

Fig. 3-1 Forces in action on UMEV

where u_{rr} is the adhesion coefficient, W_1 and W_2 represent the adhesion forces of the rear and front wheels, respectively. They are expressed as

$$W_1 = mg\frac{b}{L}\cos\alpha + \frac{h_g}{L}(mg\sin\alpha + m\frac{dv}{dt}) \tag{3.2}$$

$$W_2 = mg\frac{d}{L}\cos\alpha - \frac{h_g}{L}(mg\sin\alpha + m\frac{dv}{dt}) \tag{3.3}$$

where v is vehicle moving speed, m is vehicle mass, g is acceleration of gravity, α is the gradient of slope which varies along the road in underground mines. Along the slope, b is the distance between the front wheel axle and the vehicle's centre of gravity, d is the distance between the rear wheel axle and the vehicle's centre of gravity, L is the length of the wheelbase, and h_g is the height of the vehicle's centre of gravity. While the vehicle is moving, there are two resistance forces that impede its movement, namely rolling resistance and aerodynamic drag. The rolling resistance force mainly depends on the friction of the vehicle tyres on the road. It is proportional to the vehicle's weight and can be expressed as

$$F_f = mgC_{rr} \tag{3.4}$$

where C_{rr} is the rolling resistance coefficient which varies along the road in underground mines. The aerodynamic drag is caused by the friction of the vehicle body moving through the air and can be calculated by

$$F_w = 0.5 C_D A \rho v^2 \tag{3.5}$$

where C_D is the coefficient of aerodynamic drag, A is the front area of the vehicle, and ρ is the air density.

The uphill/downhill force F_i may oppose or assist the motion. It is the resolution of the gravity force due to the vehicle weight that acts along the slope

$$F_i = mg\sin\alpha \tag{3.6}$$

According to Newton's second law, vehicle acceleration a along the slope can be written as

$$F_a = F - F_w - F_f - F_i = ma = m\frac{dv}{dt} \tag{3.7}$$

where F_a is the acceleration force to drive the vehicle.

The energy flow chart for the electric vehicle is shown in Fig. 3-2

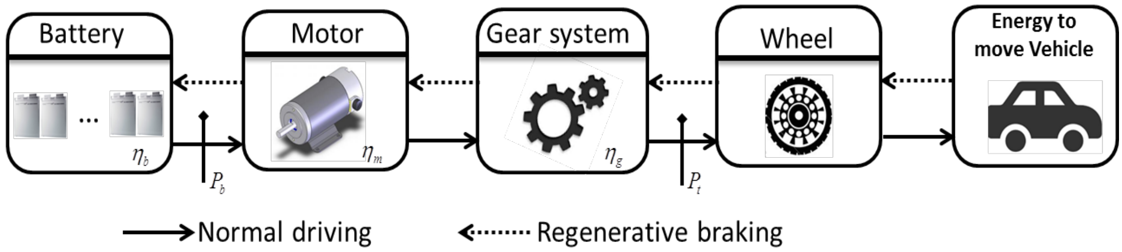

Fig. 3-2 Power flow chart for UMEVs

3.2.2 Motor model

A look-up table in two dimensions is used to model the motor in the UMEV. This look-up table includes the motor efficiencies indexed by the rotor speed and output torque, and the motor's maximum torques indexed by the rotor speed. The force required to turn the motor for angular acceleration a_ω is

$$F_\omega = I \frac{G^2}{r^2} a_\omega \tag{3.8}$$

where I is the moment of inertia of the motor rotor, G is the gear ratio of the vehicle system, and r is the radius of the tyre.

The output power of the motor to drive the UMEV through the wheels can be calculated as

$$P_m = \tau_m \times \omega_m \times \eta_m = \frac{1}{3600}(mg\sin\alpha + mg\cos\alpha \cdot C_{rr} + 0.5C_D A\rho v^2)\cdot v \tag{3.9}$$

where $\tau_m = F_\omega \cdot r / G$ and $\omega_m = v \cdot G / r$, η_m is the motor efficiency. To achieve high efficiency, the motor operates at high speed, and a transmission system with a gear ratio G (<1) is required to reduce the speed as UMEVs are driven at low speeds in underground mines.

3.2.3 Battery model

Many battery-equivalent circuit models have been developed to describe the characteristics of batteries. In [51], the internal resistance (Rint) model, the Thevenin model, the RC model, the PNGV model and the DP model are evaluated for the accurate estimation of battery SOC [85]. In [86], battery terminal voltages in EV operating conditions are compared in terms of accuracy and parameterization effort under different battery models, including the Rint model, the Thevenin model and the RC model. The Thevenin model offers the best trade-off. In this study, the simulation focuses on the performance of the UMEV under different LiFePO4 battery systems rather than the detailed comparison of battery terminal voltages and their transient behaviour. Therefore, the simple Rint model is preferable [87]. As shown in Fig. 3-3, the Rint model consists of a voltage source and an internal resistance R. The former represents the open circuit voltage (OCV) to provide power for the UMEV and the latter represents battery internal losses. The OCV and R vary with the battery's state of charge (SOC) and temperature [37]. The OCVs for both charge and discharge are obtained from the experimental data of a pulse current charge (PCC) test and a pulse current discharge (PCD) test. The detailed procedure to determine the OCVs and identify internal resistances is discussed in Section 3.3.

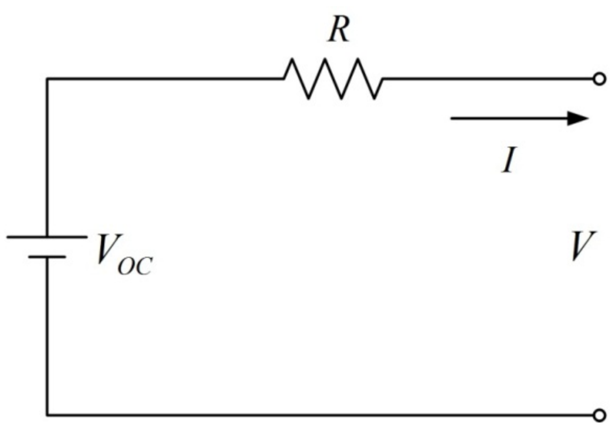

Fig. 3-3 Internal resistance battery model

The power provided by the battery system to drive the motor is

$$P_b = V \times I \times \eta_b \tag{3.10}$$

where V is battery terminal voltage, I is battery discharge current (positive) or regenerative current (negative), η_b is battery discharge efficiency.

3.2.4 Underground mine driving cycle

An underground mine road is much more complex than the normal pavement road, and has variable rolling resistance coefficients and variable uphill/downhill gradients. As a result, the driving cycle in underground mines is different from standard driving cycles. Based on data collected from Australian mines, a single trip of the UMEV to the mine workface is proposed, taking into account the most severe conditions of the pit and drift in Australian mines. This single trip is shown in Fig. 3-4, where there is a flat road and a slope with the constant rolling resistance coefficients, and a flat road at the bottom with variable rolling resistance coefficients due to the muddy surface. The underground mine driving cycle (UMDC) is constructed as a single return trip from the workshop to the workface and then return to the workshop. The speed of the UMEV, the road gradients and the rolling resistance coefficients for one UMDC are shown in Fig.3-5.

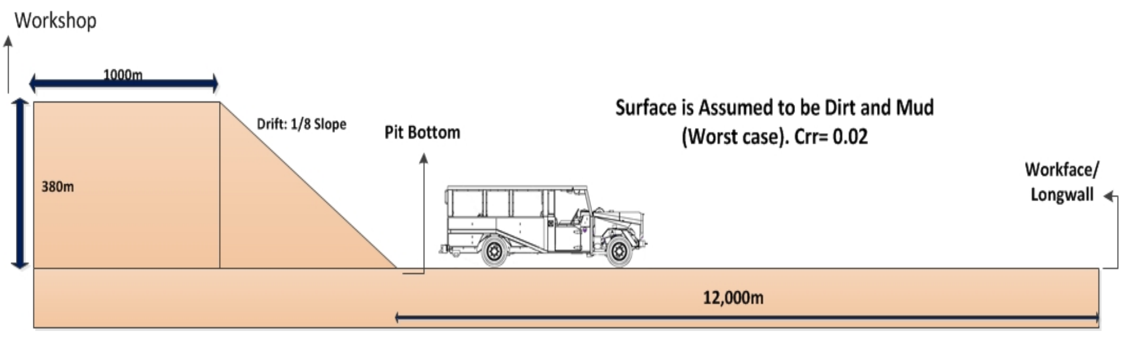

Fig. 3-4 Single trip to workface in underground mine

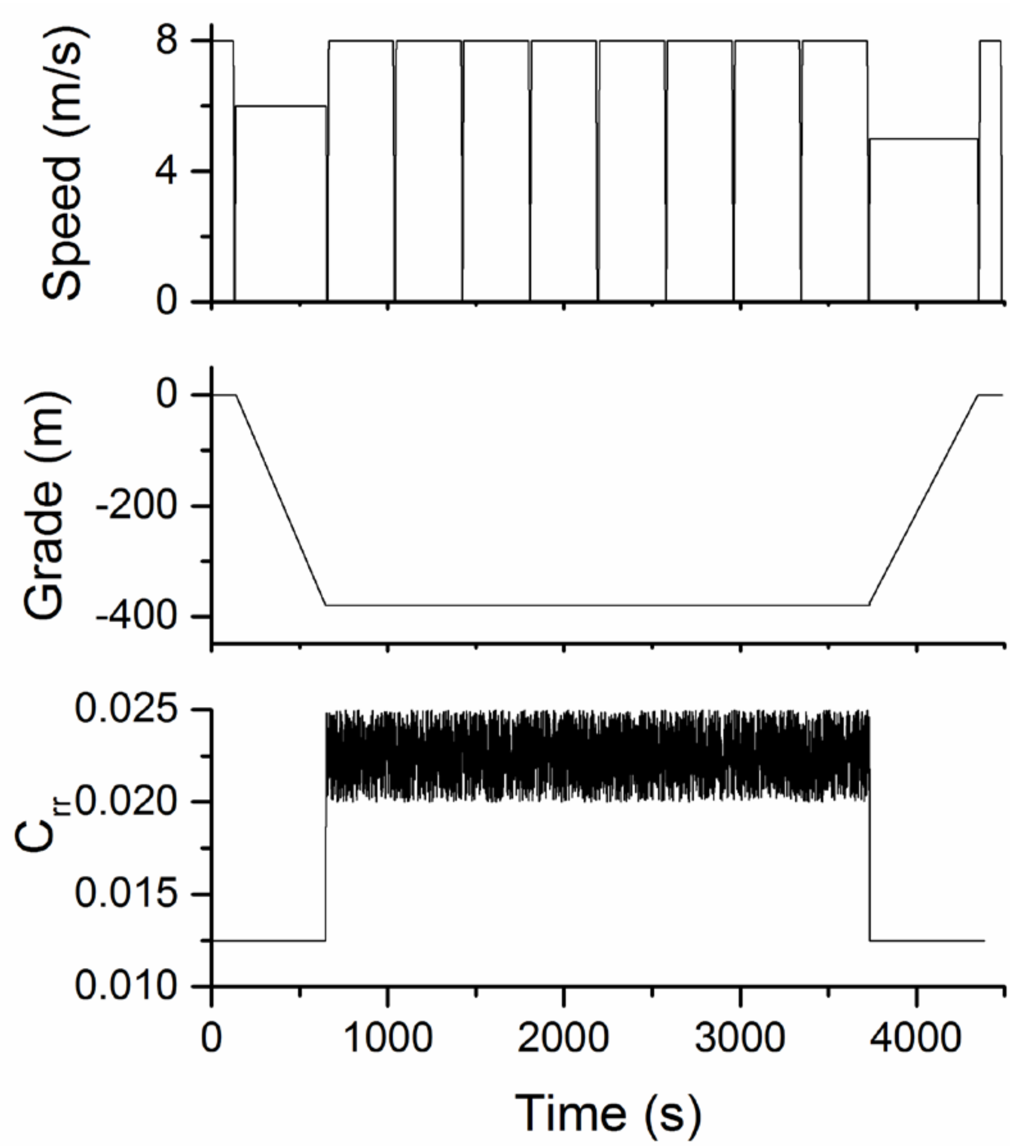

Fig. 3-5 Speed, grade and rolling resistances for one UMDC

3.3 Experimental Set-up and Results

3.3.1 Experimental set-up

An experimental bench was established to test two LiFePO4 batteries and their corresponding battery packs. The experimental data were then used to identify the parameters of the R and VOC of the Rint models and to determine the battery capacities at various temperatures. As shown in Fig. 3-6, this set-up consists of (1) the Arbin2000 battery test system with the four independent channels which can charge and discharge four batteries simultaneously using programmable currents (2) an ESPEC temperature chamber to create different ambient temperatures in which the batteries and battery packs can be placed (3) a PC with Arbin Mits Pro software installed to control and monitor battery charging and discharging.

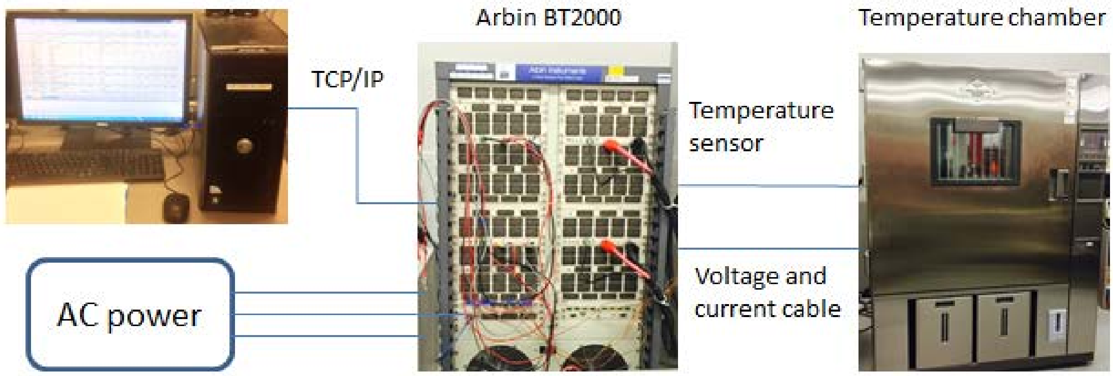

Fig. 3-6 Battery experiment set-up

In this study, there are batteries and battery packs. The following conventions are used to name the batteries and battery packs to avoid confusion. A single battery is the smallest unit. A number of batteries are paralleled to form a module. A number of modules are connected in series to form a battery pack. A battery system in the UMEV is defined as an assembly of battery packs either in series or parallel or their combination. Two LiFePO4 batteries and their corresponding packs were chosen: cylinder and prismatic batteries and battery packs, respectively. They include: a) a single 20Ah LiFePO4 prismatic battery, b) 40 Ah 4S2P battery pack consisting of eight 20Ah prismatic batteries with two in parallel as a module and four of these modules in series, where P represents the number of batteries or battery packs in parallel and S represents the number of batteries and battery packs in series in 4S2P. c) a single 2.3Ah cylinder battery, d) an 2.3Ah 4S1P battery pack consisting of four 2.3 Ah cylinder batteries in series. Table 3-1 shows the parameters of the selected batteries and battery packs.

TABLE 3-1 PARAMETERS OF SELECTED BATTERIES AND BATTERY PACKS

	a. A single 20Ah prismatic battery	b. 40Ah 4S2P battery pack	c. A single 2.3Ah cylinder battery	d. 2.3Ah 4S1P battery pack
Nominal Voltage	3.3V	13.2V	3.3V	13.2V
Capacity (Ah)	20	40	2.3	2.3
Cycle life (cycle)	2000-3000	2000	2000-3000	2000-2500
Operating temperature	-30~55°C	-20~50°C	-30~55°C	-30~50°C
Mass (g)	496	5420	76	350
Dimensions (mm)	7.25×160×227	165×135×250	Φ26×65	28×106×68
Price (AU $)	$22	$ 300	$8	$45
Picture				

Three types of tests were conducted on these batteries and battery packs at the ambient temperatures of 15°C, 25°C and 40°C, which cover the temperatures in the real working environment in Australian underground mines which are around 17~25°C. The tests were a capacity test, a PCC test and a PCD test. During these tests, the current, voltage and temperature of the batteries and battery packs were sampled at a sampling rate of 1 per second.

3.3.2 Capacity test

The capacity test is used to determine the battery capacities at various temperatures. To conduct this test, the batteries and battery packs are put into a temperature chamber and connected by a cable to the Arbin 2000. The constant current/constant voltage (CCCV) charging method was adopted to charge the batteries and battery packs with different constant current rate. According to driving distances and speeds of current EVs in the markets, the average driving time is 3 hours, for example, BYD Qin EV300 can drive 300 km with the speed of 100km/h. the average discharge current with respect to their battery packs is equivalent to about 0.3C [58, 88, 89]. Also, the underground mine EV driving cycle has an average discharge current of 0.3C. As a result, 0.3C is adopted to discharge the batteries in EVs, where 1C refers to the charging current in terms of the nominal capacity, namely the ratio of the nominal capacity to 1 hour [75]. The charging voltage was maintained at 3.6V per battery and the charging current was reduced exponentially. When the current reached a pre-set current (e.g. 0.01C), the charging process was terminated [90]. Since one hour rest time is sufficient for the terminal voltage of lithium ion batteries to reach the equilibrium state [65,91]. After one hour, the batteries and battery packs at the temperatures of 15℃, 25℃ and 40℃ were discharged at the constant current of 0.3C until the cut-off voltage of 2.0V per battery was reached, which was defined as the fully discharged state. Table 3-2 shows the available capacities for these batteries and battery packs at different temperatures.

TABLE 3-2 BATTERY CAPACITIES AT TEMPERATURES OF 15℃, 25℃ AND 40℃

	a. 20Ah prismatic battery	b. 40Ah 4S2P battery pack	c. 2.3Ah cylinder battery	d. 2.3Ah 4S1P battery pack
15℃ (Ah)	19.2	37.81	2.2	2.05
25℃ (Ah)	19.6	38.25	2.3	2.14
40℃ (Ah)	19.8	38.75	2.45	2.2

3.3.3 Pulse current discharge test

A pulse current discharge (PCD) test is used to obtain the OCV versus SOC at different temperatures during battery discharging [91]. In the PCD test, the fully charged batteries and battery packs were discharged at 1C for 6 minutes and rested for 1 hour to allow the terminal voltage to reach its equilibrium state, namely the OCV. This pulse current discharge equals approximately 10% of the nominal capacity, which is equivalent to a reduction in the SOC by 10%. This process was repeated until the terminal voltage reached the cut-off voltage. The PCD test was conducted on the two batteries and two battery packs at the temperatures of 15℃, 25℃ and 40℃. As an example, Fig. 3-7 shows the current profile of the PCD and the corresponding responses of the terminal voltage for the A123 20Ah prismatic battery at 15℃. The circled section is magnified in Figure 3-8 to demonstrate the details of the transient terminal voltage at the 4th pulse current discharge. It can be seen that when the battery begins to discharge the terminal voltage has a steep voltage drop across the internal resistance R. Therefore, the internal resistance can be calculated by

$$R = \Delta V_t / I \tag{3.11}$$

namely $R = (V_{t0} - V_{t1}) / I = \Delta V_t / I$ =0.0197Ω.

Using the same equation (3.11), the discharge resistances of the two batteries and two battery packs versus the SOCs at the temperatures of 15℃, 25℃ and 40℃ were calculated. The OCVs versus the SOCs at the temperatures of 15℃, 25℃ and 40℃ were also determined using this PCD test. The results are shown in Figs. 3-9 and 3-10, respectively. The SOCs in both cases were calculated by the ampere hour counting method:

$$SOC = (C_{\max} - C_{dis}) / C_{\max} \tag{3.12}$$

where $C_{\max}$ is the maximum capacity of the battery, and C_{dis} is the discharged capacity.

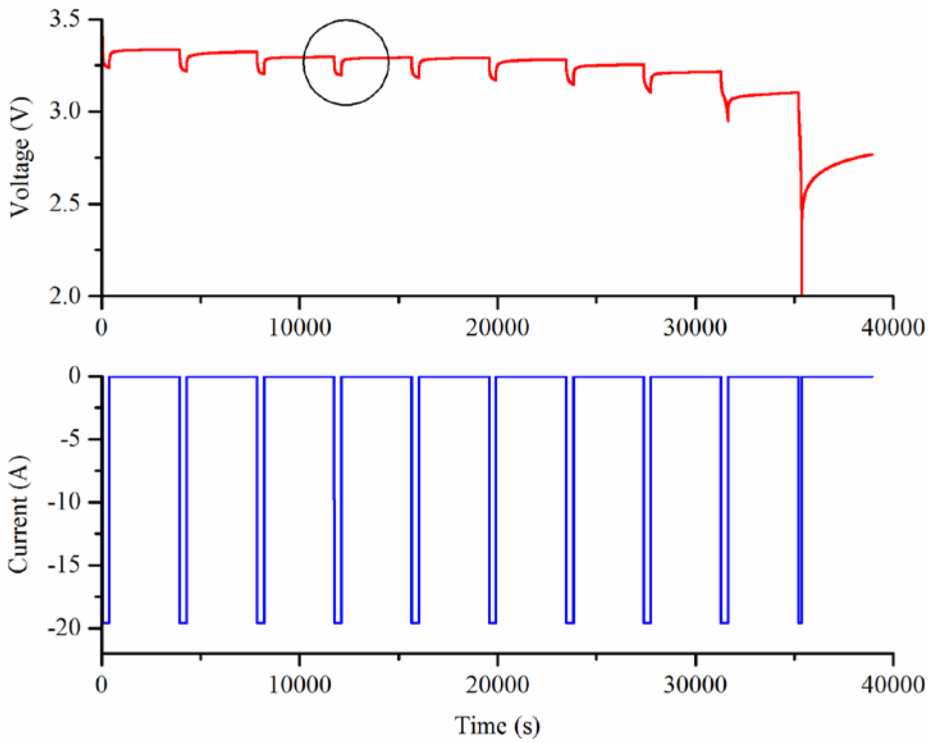

Fig. 3-7 Voltage responses of PCD test for a single 20Ah prismatic battery at 15℃

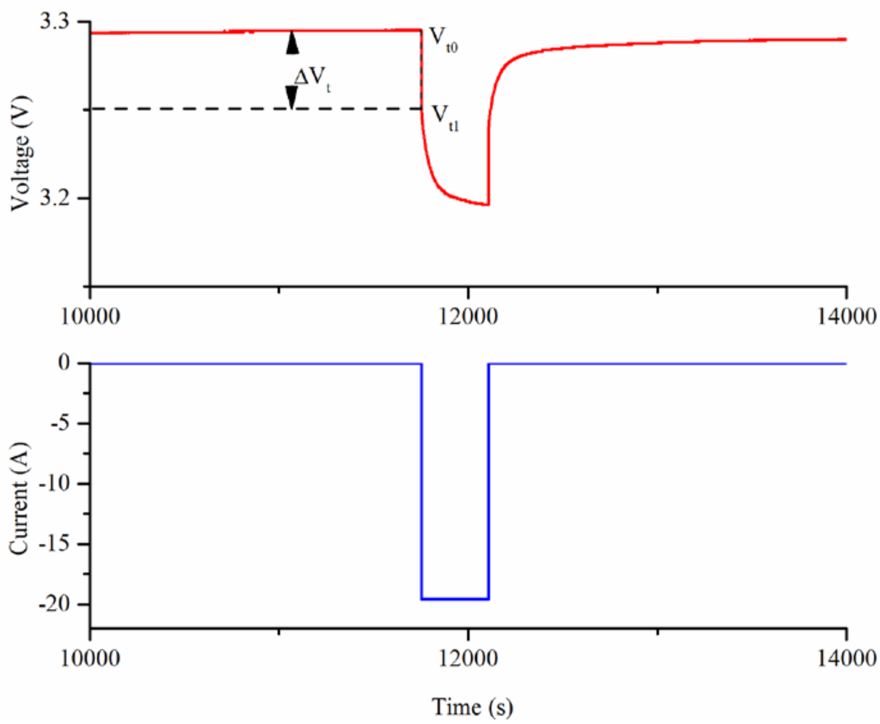

Fig. 3-8 Magnified transient response of voltage at the 4th pulse current discharge

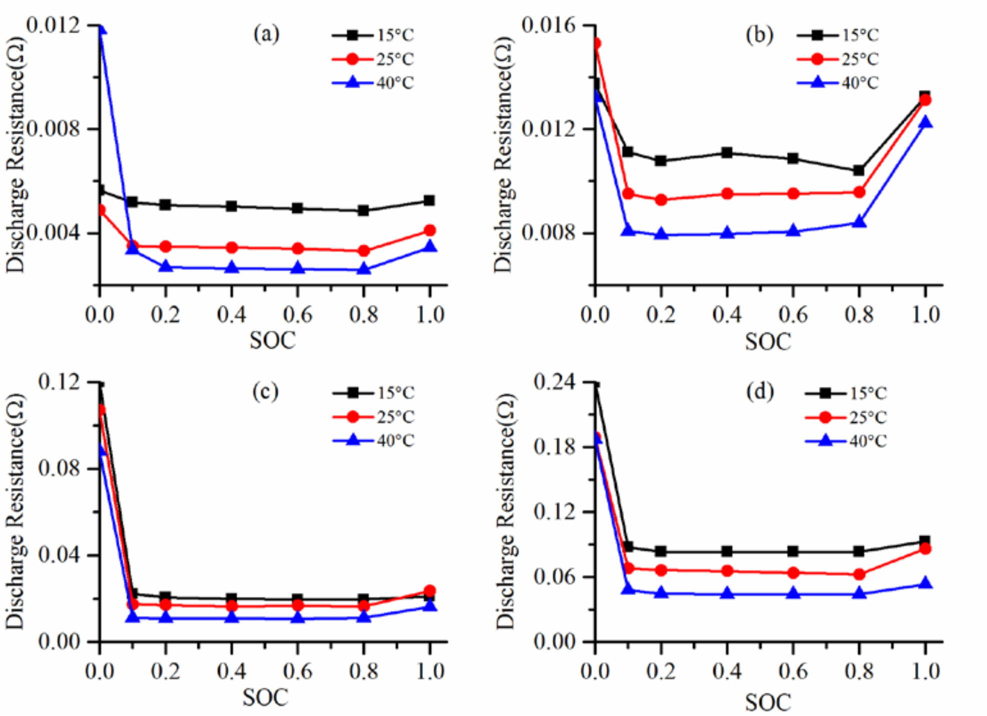

Fig.3-9 Internal resistances versus SOCs during battery discharging at temperatures of 15℃, 25℃ and 40℃: a) 20Ah prismatic cell, b) 40Ah 4S2P battery pack, c) 2.3Ah cylinder battery, d) 2.3Ah 4S battery pack

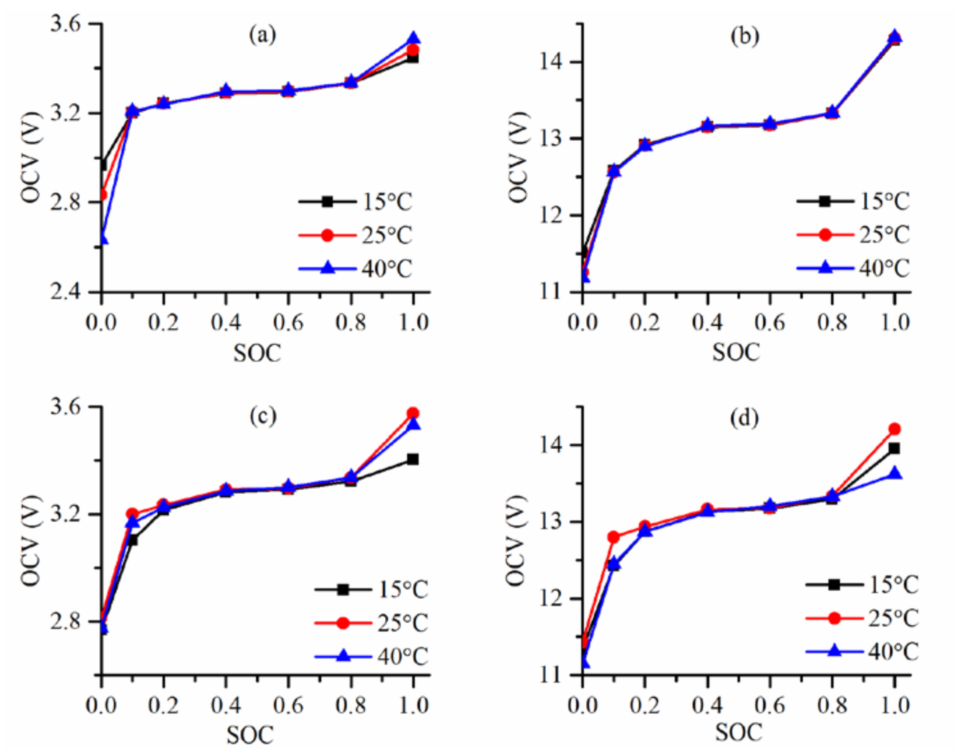

Fig.3-10 OCVs versus SOCs during battery discharging at the temperatures of 15℃, 25℃ and 40℃: a) 20Ah prismatic cell, b) 40Ah 4S2P battery pack, c) 2.3Ah cylinder battery, d) 2.3Ah 4S battery pack

3.3.4 Pulse current charge test

Similar to the PCD test, the pulse current charge (PCC) test was performed to calculate the internal resistances and to acquire the OCVs versus the SOCs during battery charging. In the PCC test, the fully discharged batteries and battery packs were charged at the charge current of 1C for 6 minutes followed by 1hour rest at the temperatures of 15℃, 25℃ and 40℃. This process was repeated until the voltage of the battery or battery pack reached the maximum allowable voltage. Figure 3-11 shows the current profile of the PCC and the corresponding terminal voltage for the A123 20Ah prismatic cell at 15℃. From Fig. 3-11, the internal resistances and the OCVs during battery charging at different SOCs were calculated. Their results are shown in Figs. 3-12 and 3-13, respectively. The internal resistance during battery charging was used in the estimation of energy losses during the regenerative braking process.

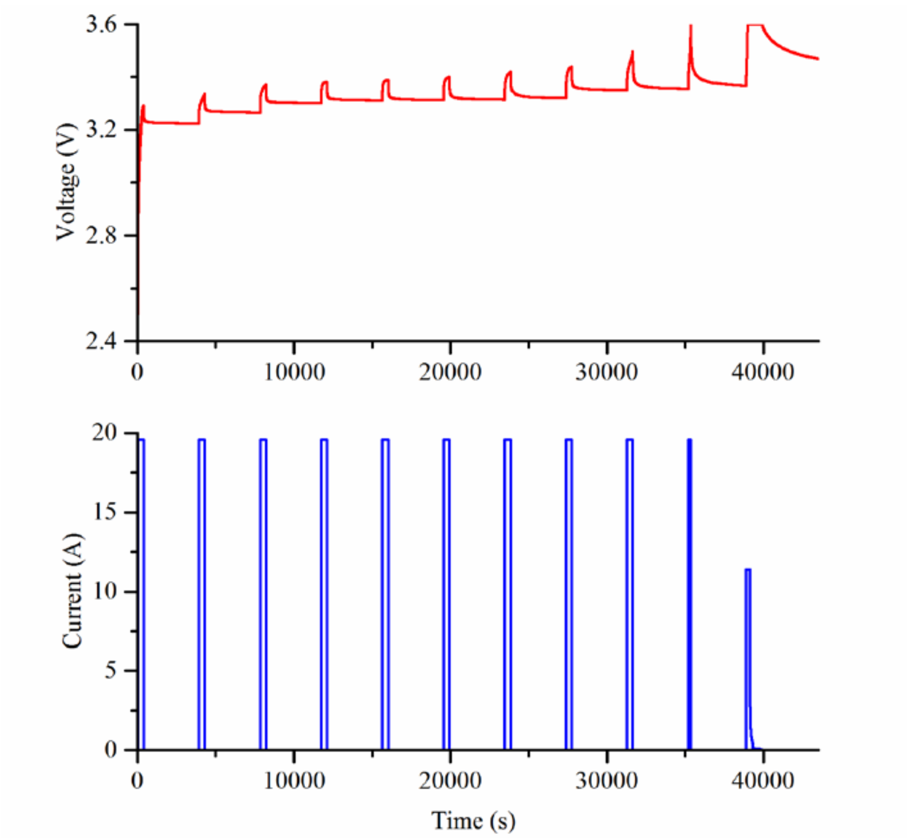

Fig. 3-11 Voltage responses of PCC test for a single 20Ah prismatic battery at 15℃

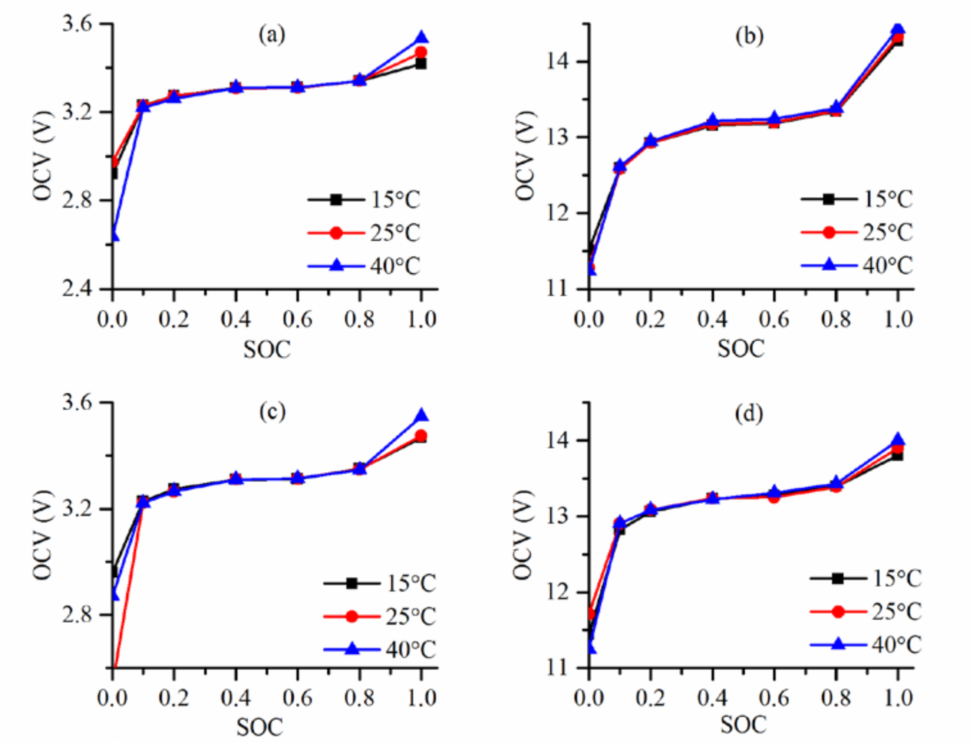

Fig.3-12 OCVs versus SOCs during battery charging at the temperatures of 15℃, 25℃ and 40℃: a) 20Ah prismatic cell, b) 40Ah 4S2P battery pack, c) 2.3Ah cylinder battery, d) 2.3Ah 4S battery pack

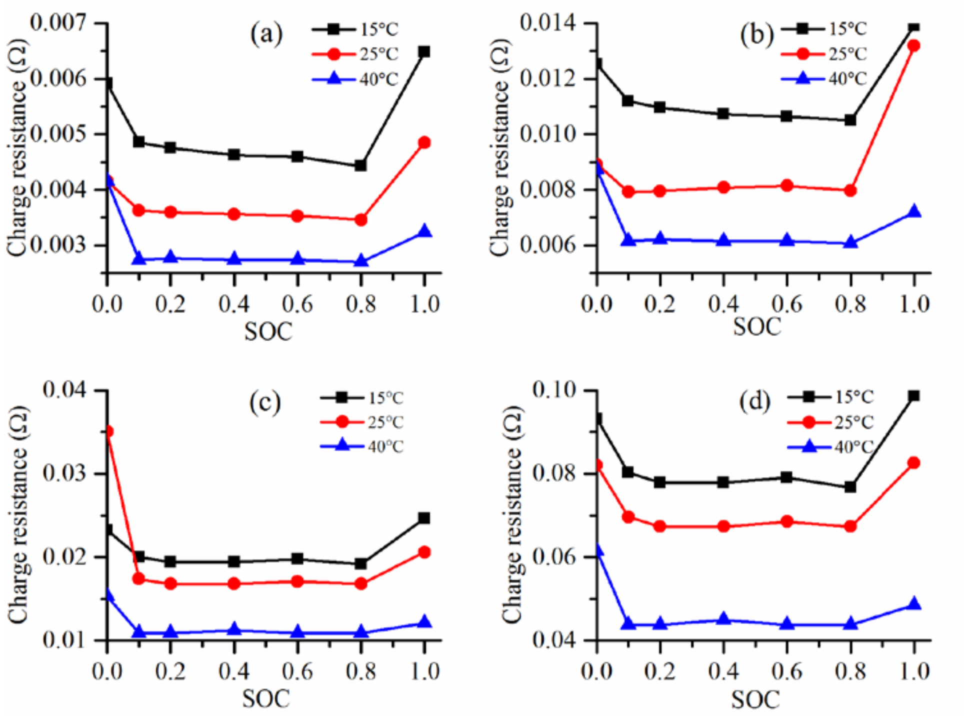

Fig. 3-13 Internal resistances versus SOCs during battery charging at the temperatures of 15℃, 25℃ and 40℃: a) 20Ah prismatic cell, b) 40Ah 4S2P battery pack, c) 2.3Ah cylinder battery, d) 2.3Ah 4S battery pack

3.4 Simulation Results

In addition to the parameters for the battery models which were determined in the previous section, the parameters of the model for the designed UMEV are shown in Table 3-3. These parameters were used in the UMEV simulation.

TABLE 3-3 UMEV VEHICLE PARAMETERS

	Parameters	**Values**
Vehicle	Vehicle mass and cargo mass (m)	3000kg
	Coefficient of aerodynamic drag Cd	0.3
	Radius of tyre (r)	0.38m
	Frontal area (A)	3 m^2
	Air density (ρ)	1.25k g/m^3
	Gravitational acceleration	$9.8m/s^2$
	Vehicle centre of gravity height (h_g)	900mm
	Wheelbase length (L)	3080mm
	Distance between front (rear) wheel axle and vehicle centre of gravity ($b = d$)	1540mm
Motor	Nominal power (P_m)	75 kW*
	Motor efficiency (η_m)	93%-98%
	Rotor inertia (I)	$0.0421kg{\cdot}m^2$
	Mass of motor	90kg
Battery	Battery pack energy (E_b)	44kWh

* Note: The switched reluctance motor is chosen in the UMEV

3.4.1 UMEV model implemented in modified ADVISOR

The simulation was conducted to determine the most suitable LiFePO4 battery system for the UMEV. The model of the UMEV developed in Section 3.2 was implemented in the modified ADVISOR. The major modifications in the ADVISOR included: 1) the front wheel drive (FWD) vehicle model was changed to the 4WD vehicle model. 2) the constant rolling resistance coefficient and constant uphill/downhill gradient were changed to variable rolling resistance coefficients and variable uphill/downhill gradients. 3) the model parameters of the existing battery were replaced by those of the two LiFePO4 batteries and two battery packs listed in Table 3-1. The following paragraph is a brief explanation of the major modifications and further details can be found in [81].

The EV model in the ADVISOR is a FWD vehicle model. For FWD vehicles, the adhesion force loads on the two front wheels. To make full use of the vehicle weight, the UMEV is designed to be a 4WD vehicle which can reach maximum vehicle-road adhesion force. Hence, the vehicle's performance and stability can be improved. The traction control and wheel/axle block in the ADVISOR were reprogrammed to implement the 4WD model.

The standard EV driving cycles were embedded in the ADVISOR associated with a constant rolling resistance coefficient. Different from conventional EV driving cycles, the UMDC has variable rolling resistance coefficients and gradients due to different types of surfaces and uphill/downhill sections in the road, as shown in Fig. 3-5. Therefore, the vehicle block, wheel/axle block and traction control block were reprogrammed to allow the input of the variable rolling resistance coefficients versus the time and speed and the input of the variable gradients versus the time and driving distance.

The Rint model was chosen to simulate the battery in ADVISOR. Its parameters were obtained from a SAFT lead-acid battery. In this study, the four battery systems made from the two LiFePO4 batteries and their corresponding battery packs were used to power the UMEV. The battery parameters extracted from the experimental data of the four battery systems in Section 3.3 were incorporated in the battery models to represent these four battery systems with a total energy of 44kWh and a total nominal voltage of 370V. Battery system A was built with the 20Ah prismatic batteries. It consists of 8 packs in series, where each pack has 14 modules in series, with each module having 6 paralleled batteries. Battery system B was built with 40Ah 4S2P battery packs. It consists of 7 packs in series, where each pack has 4 modules in series with each module having 3 paralleled battery packs. Battery system C was built with 2.3Ah cylinder batteries. It consists of 8 packs in series, where each has the 14 modules in series with each module having 52 paralleled batteries. Battery system D was built with 2.3Ah 4S1P battery packs. It consists of 7 packs in series, where each pack has 4 modules in series with each module having 52 paralleled battery packs. Table 3-4 shows the parameters of the four battery systems. In the following simulation, it is assumed that all the batteries and battery packs have the same electric characteristics, thus the model of each battery system can be easily scaled up from the model of each battery and battery pack.

TABLE 3-4 BATTERY SYSTEM PARAMETERS

Battery type	20Ah prismatic battery	40Ah 4S2P battery pack	2.3Ah cylinder battery	2.3Ah 4S1P battery pack
Battery system	A	B	C	D
Battery energy	44kWh	44kWh	44kWh	44kWh
Configuration	14S6P×8S	4S3P×7S	14S52P×8S	4S52P×7S
Number of batteries/ packs	672	84	5844	1456
Volume (L)	177	468	202	294
Weight (kg)	333	455	443	457
Price	$14784	$25200	$46752	$65520

3.4.2 Simulation results for one UMDC

The simulation of the UMEV with the four battery systems was conducted for one UMDC. The SOCs of the four battery systems are shown in Fig. 3-14. It can be seen that battery system C has the maximum residual SOC (76%), while battery system D has the minimum residual SOC (72%). After 3600s, the SOC drops more quickly than the previous period as the UMEV is driving up a slope with a gradient of 25 degrees for 10 minutes. Table 3-5 provides a summary of the residual SOCs, energy consumption, energy storage efficiency and the overall energy efficiency and driving distances of the UMEV at the end of one UMDC.

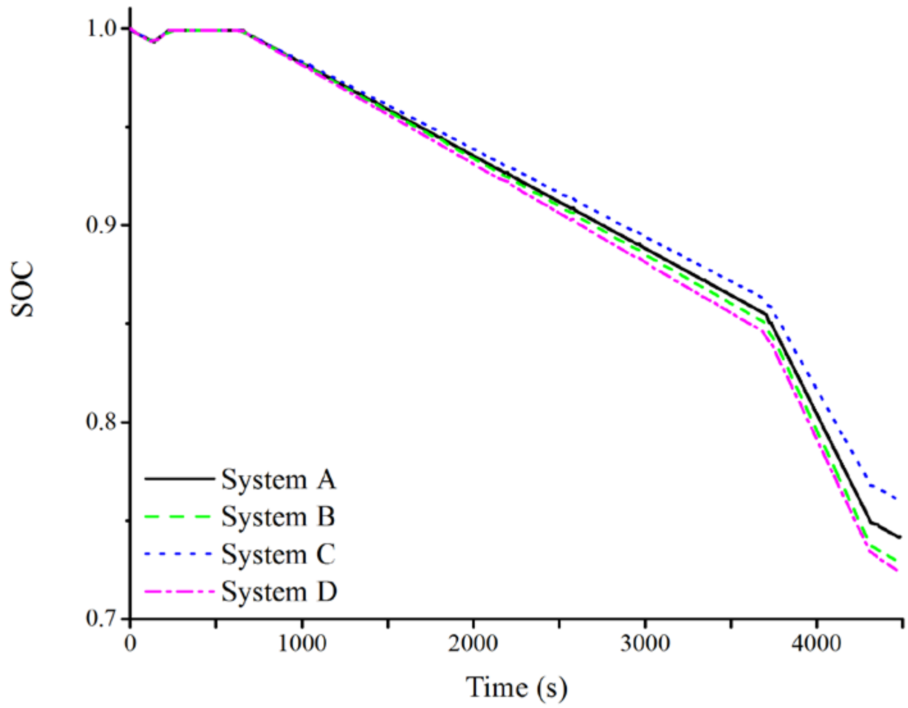

Fig. 3-14 SOCs over one UMDC

Figure 3-15 shows the average temperature of each battery system over one UMDC. It can be seen that the battery systems C and D have higher temperatures than battery systems A and B. This can be explained by the internal resistances of battery systems C and D during charging and discharging being higher than those of battery systems A and B, as shown in Figs. 3-9 and 3-13, respectively. There are dramatic temperature increases in two instances. The first is at the beginning of the UMDC when the UMEV starts to drive downhill and the regenerative braking is taking place with high energy losses in charge resistance. The second is at the time of 3400s when the UMEV starts to climb the slope with a high demand for power which can cause high energy losses in discharge resistances. There is a simple battery cooling system in ADVISOR [37]. It works as follows. When the battery system temperature reaches 30℃, the cooling fan turns on to regulate the battery system temperature. The battery system temperature depends on the balance of the heat generation from the internal resistances and the heat dissipation from the cooling system. It can be observed that there are some temperature drops over one UMDC, as shown in Fig. 3-15.

TABLE 3-5 RESIDUAL SOCS, ENERGY CONSUMPTION, EFFICIENCY, OVERALL ENERGY EFFICIENCY AND DRIVING DISTANCES OF UMEV UNDER FOUR BATTERY SYSTEMS AFTER ONE UMDC

Battery system	A	B	C	D
Residual SOC at the end of one UMDC	74%	73%	76%	72%
Energy storage efficiency	0.97	0.9	0.95	0.9
Energy Used (kJ)	41561	43015	42545	42707
Energy to overcome aerodynamics (kJ)	1008	1008	1008	1008
Energy to overcome rolling resistance (kJ)	22059	22833	22757	22846
Overall efficiency	0.555	0.554	0.559	0.559
Driving distance （km）	32.3	32.3	32.3	32.3

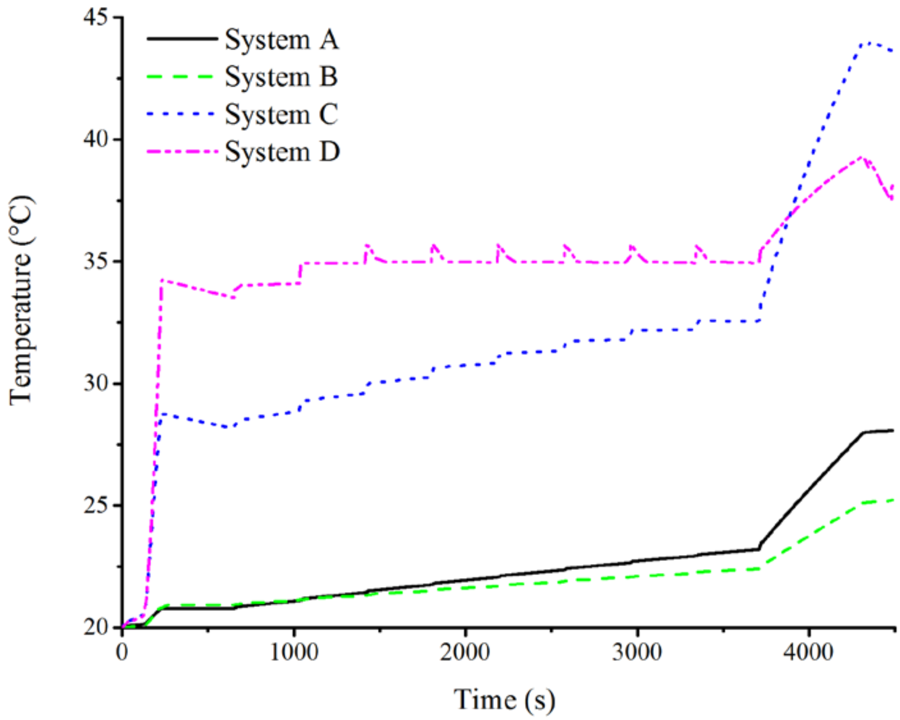

Fig. 3-15 Temperatures of battery systems over one UMDC

3.4.3 Simulation results for two UMDCs

The simulation of the UMEV was further conducted for two UMDCs. The residual SOCs and the average temperatures of the four battery systems are shown in Figs. 3-16 and 3-17, respectively. It can be seen that battery system C has the maximum residual SOC (50%) while battery system B has the minimum residual SOC (42%). Battery system D stops discharging at the beginning of the second UMDC. This is due to the fact that the average temperature of battery system D has exceeded the safe temperature threshold of 60℃ pre-set in the ADVISOR, which triggers to stop the simulation. The temperature of battery system C increases to 59℃ and then decreases as the cooling fan is turned on when the temperature exceeds 30°C. The temperatures of both battery system A and battery system B are in the comfortable range with the maximum temperature of 35℃ and 33℃ , respectively, at the end of the second UMDC. Table 3-6 provides a summary of residual SOCs, energy consumption and energy storage efficiencies and the overall energy efficiency and driving distances of the UMEV under the four battery systems after two UMDCs.

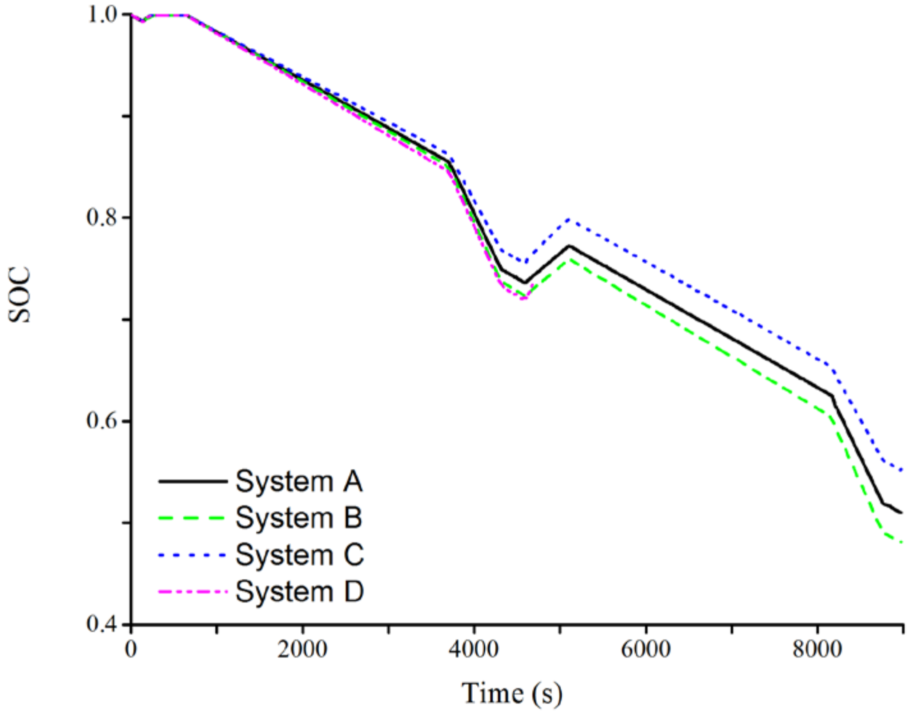

Fig. 3-16 SOCs over two UMDCs

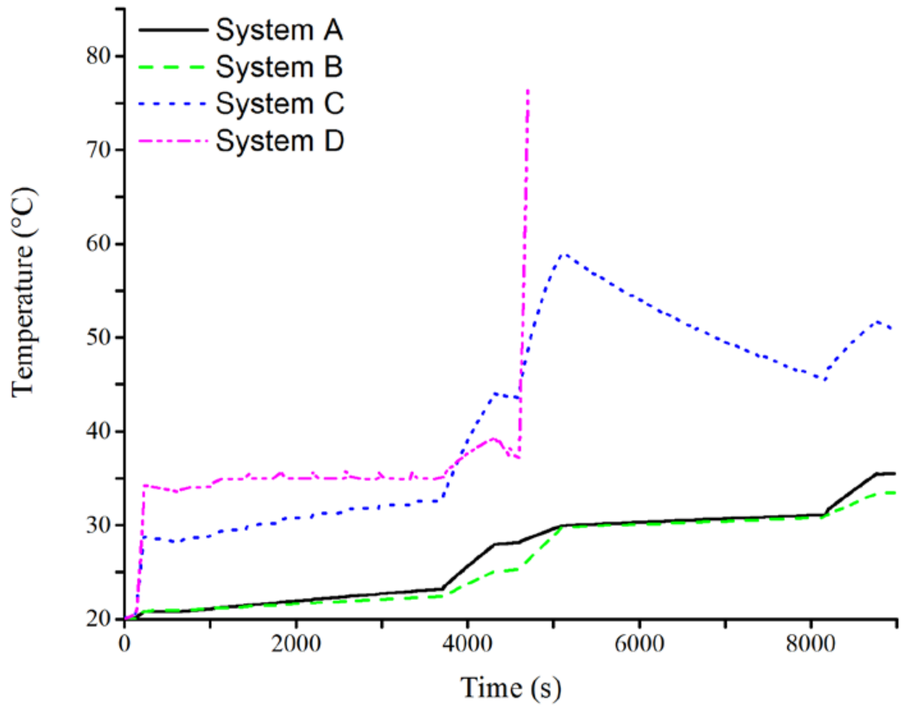

Fig. 3-17 Battery system temperatures over two UMDCs

TABLE 3-6 PARAMETERS OF BATTERY AND VEHICLE AFTER RUNNING FOR TWO UMDC CYCLES

Battery system	A	B	C	D*
Residual SOC at the end of two UMDCs	45%	42%	50%	-
Energy storage efficiency	0.98	0.9	0.95	-
Energy used (kJ)	78288	81467	80078	-
Energy to overcome aerodynamics (kJ)	2015	2015	2015	-
Energy to overcome Rolling resistance (kJ)	44123	45672	45520	-
Overall efficiency	0.589	0.585	0.594	-
Driving range （km）	64.7	64.7	64.7	34

Notes: *Simulation of the UMEV with Pack D ceased at the beginning of the second UMDC

3.4.4 Simulation results for multiple UMDCs

The simulation for multiple UMDCs was performed until the battery systems were fully discharged. The results are shown in Fig. 3-18. It can be seen that battery system C stopped discharging at the beginning of the third UMDC. This is caused by the temperature of battery system C which tends to be higher than 60 ℃, as shown in Fig. 3-19. For battery systems A and B, the simulation stopped at the time when SOC = 0. The highest temperatures, driving ranges, energy storage efficiencies and vehicle efficiencies of battery systems A and B were 53℃ and 49℃, 144.8 km and 127.3km, 98% and 90%, 65% and 60%, respectively.

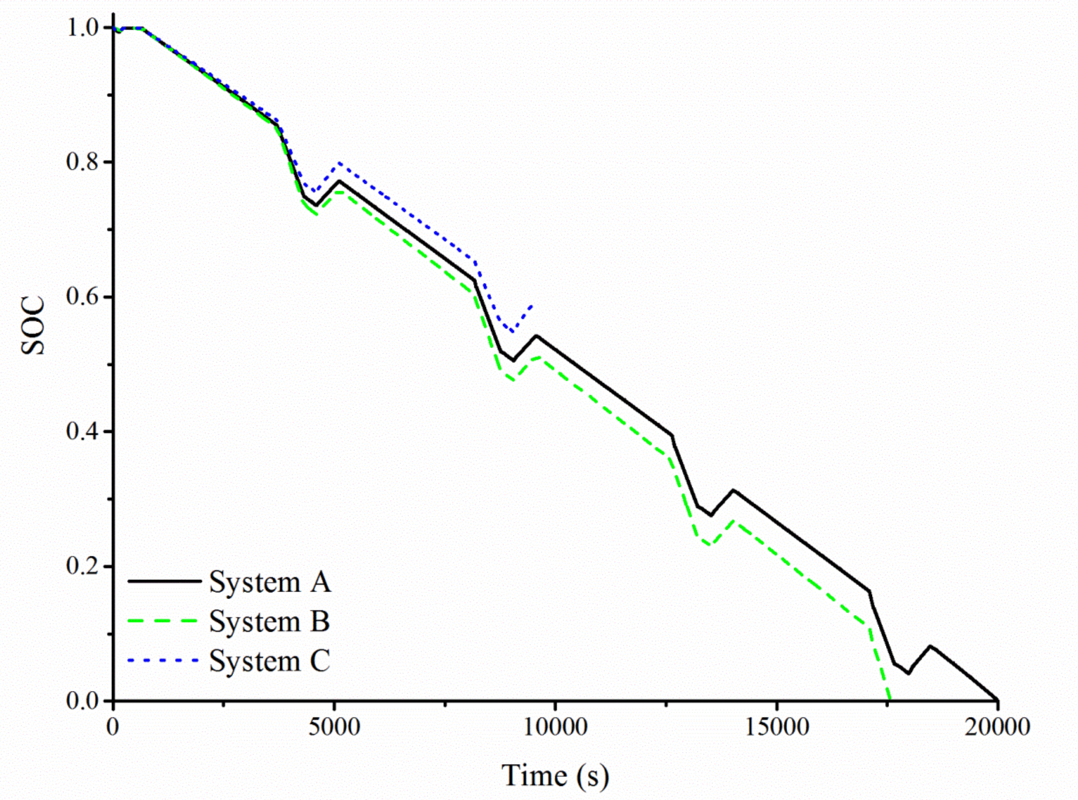

Fig. 3-18 SOCs over multiple UMDCs

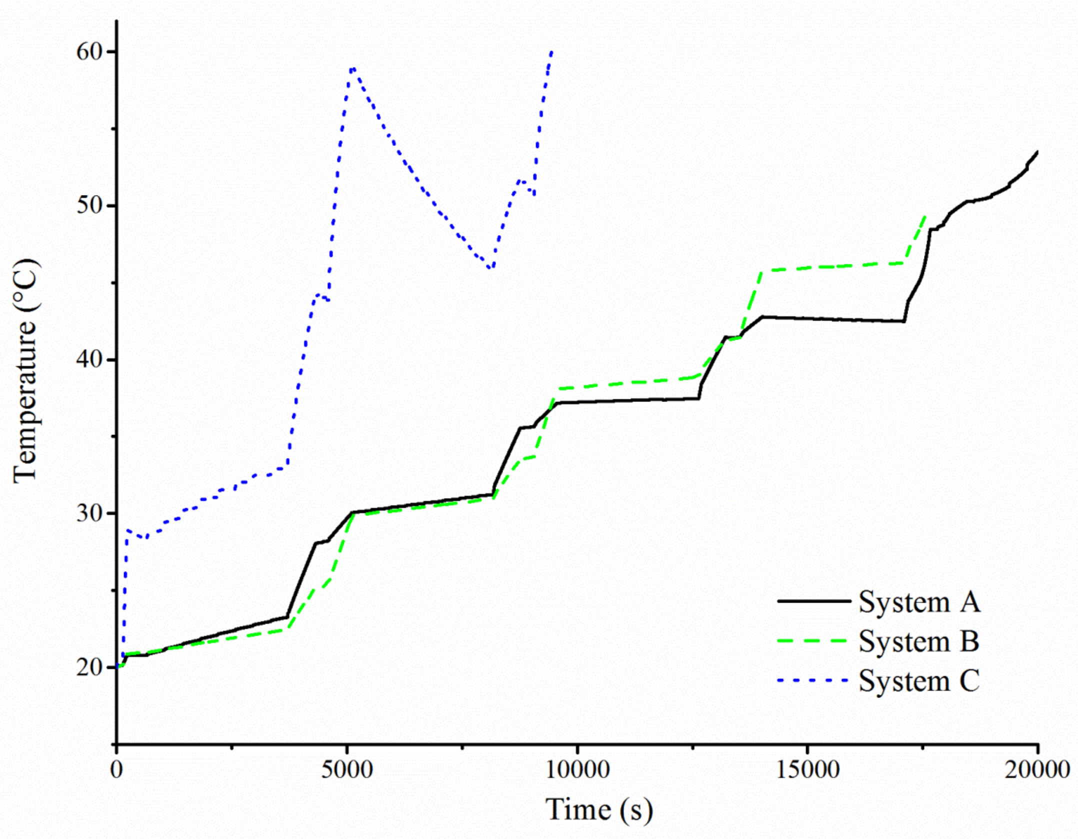

Fig. 3-19 Battery system temperatures over multiple UMDCs

3.4.5 UMDC validation test

Based on the results reported in the previous section, battery systems A and B were selected for the simulation of the UMEV under the UMDC. The current profiles corresponding to the UMDC which were produced in the modified ADVISOR had the average current of 1/3C with respect to the selected 20Ah cylinder battery in battery system A and the 40Ah 4S2P battery pack in battery system B. These profiles were used to test the battery and battery pack. It was expected that they could discharge for about three UMDCs. Figure 3-20 shows the current profiles and corresponding voltages. It can be seen that the battery and battery pack can be discharged for around three UMDCs.

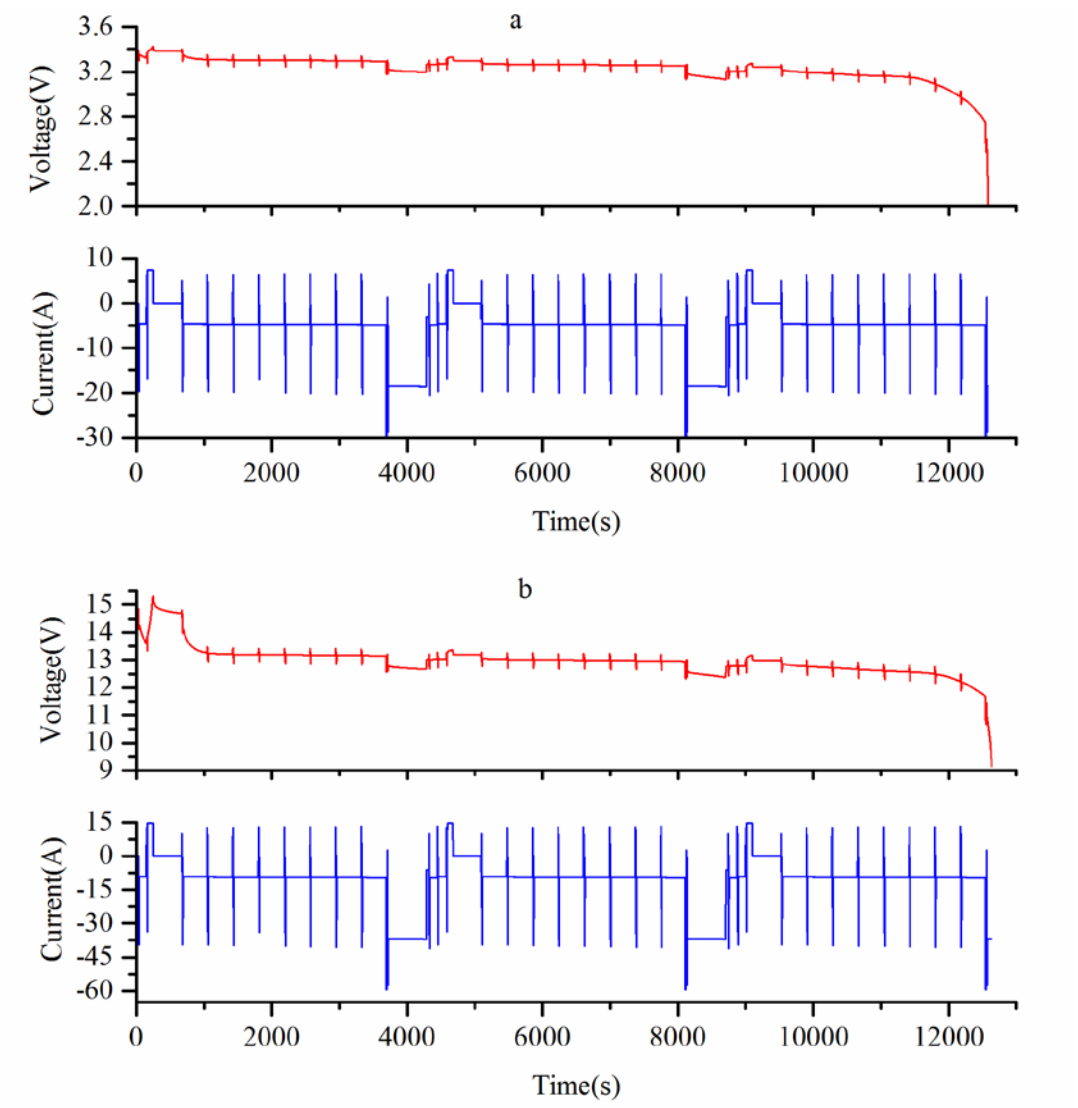

Fig. 3-20 Voltage profiles at the current profiles based on UMDC (a) 20Ah prismatic battery, (b) 40Ah 4S2P pack

3.4.6 Discussion

The simulation of the UMEV for four battery systems was performed. Battery systems C and D with a sharp temperature rise to 60℃ during operation are not sutiable for the UMEV， while battery systems A and B can release all the stored energy to power the UMEV with the temperature well below the safe temperature threshold of 60℃. To select one of them, the price, weight and driving range of these two battery systems were taken into account. According to Table 3.4, the price of battery system A is $336 per kWh, and the price of battery system B is $572 per kWh. As a result, the weight per kWh for battery system A is 7.5kg per kWh while that for battery system B is 10.3kg per kWh. The simulation results also show that the UMEV with battery system A can drive longer than that with battery system B. Therefore, battery system A is the best option for the UMEV.

3.5 Conclusion

In this chapter, a hybrid simulation approach was used to compare the four LiFePO4 battery systems for the four-wheel-drive UMEV by integrating the experimental results of these battery systems into the battery models embedded in the modified Advanced Vehicle Simulator (ADVISOR). The experimental results of these four battery systems were used to identify the internal resistances, the relationships between open circuit voltage and state of charge during charging and discharging periods and the capacities at different ambient temperatures. With the modified ADVISOR, the simulations of the UMEV were conducted at the specifically designed underground mine driving cycle with variable rolling resistance coefficients and variable uphill/downhill gradients. The results show that the battery system with the prismatic cell 20Ah is the best option for the UMEV.

CHAPTER 4 SELF-ORGANISING MAP-BASED CLASSIFICATION OF LITHIUM IRON PHOSPHATE CELLS FOR BATTERY PACKS

In this chapter, the inconsistency problems of cells are further reviewed and discussed. To alleviate problems, a self-organizing map (SOM)-based clustering method is proposed to cluster the lithium iron phosphate ($LiFePO_4$) cells. This method adopts the available capacity, internal resistance and temperature variation as the input vectors to the SOM. The SOM output clusters the cells into three categories. Cells in the same group are connected to build a sorted battery pack and randomly selected cells are connected to build an unsorted battery pack. These two packs are compared under different loads in laboratory experiments. The experimental results show that the cell consistency in the sorted pack is better than that in the unsorted pack. Therefore, the effectiveness of the proposed SOM clustering method to make sorted battery packs with consistent electrical characteristics is verified.

4.1 Introduction

Due to the progressively increasing cost of fuel and tightened control of emissions, research into and innovation of electric vehicles (EVs) has grown significantly around the world. One of the key technologies in the commercialization of EVs is batteries and their management systems [92, 93]. Recently, lithium-ion batteries have been adopted as primary power sources in EVs due to their high power and energy densities, high operating voltage, long cycle life and low self-discharge rate. Therefore, the development of lithium-ion battery management systems is very important, to ensure the safe and efficient operation of batteries [91, 94, 95]. To meet the power and energy requirements of EVs, the lithium-ion battery pack is required, which consists of hundreds and thousands of cells in parallel and series. The cells in the pack may have slightly different characteristics caused by intrinsic and extrinsic factors [43]. The former derives from the manufacturing process, such as inconsistency in the manufacturing environment and material defect. The latter derives from the application environment, such as different operational temperatures and internal resistances of each cell in the battery pack [44]. When these non-uniform cells are connected in series to build a battery pack, the cell differences lead to a reduction in the pack capacity. The reasons are explained as follows. When the pack is charging, one cell may reach the maximum charging voltage earlier than the other cells, and the charging process has to stop and the rest of the other cells are undercharged; when the pack is discharging, one cell may reach the cut-off voltage earlier than the other cells, and the discharging process has to stop and the rest of the cells are under-discharged. Therefore, the weakest cell, which is the earliest one to be fully charged or fully discharged, determines the available capacity and overall performance of the pack. Furthermore, these non-uniform cells in the pack may cause safety risks and decrease the cycle life. Two measures are normally taken to alleviate the problems of non-uniformity and imbalance of cells: one is to select cells with similar characteristics to build the battery pack and the other is to have battery balancing systems in the pack. This chapter focuses on the selection of similar cells to build the pack using a self-organizing map (SOM)-based classification method.

Different methods have been explored to select similar cells. In general, they are divided into two groups. One group is based on the observation of measured battery parameters. The electrochemical impedance spectroscopy method [96] has been applied to produce the Nyquist plots of the cells at the specific frequencies and the similarities of the plots observed to conduct cell clustering. The available capacity, internal resistance and the curves of OCVs versus SOCs have been used to cluster the cells [97]. The above methods lack systematic procedures and rely heavily on personal experience. The other group is based on machine learning approaches. A fuzzy C-mean algorithm has been applied in the analysis of voltage differences during charging/discharging for sorting cells [46]. The self-organizing map (SOM) method has been applied to group cells by capturing the features of the input vectors of the SOM, where the input vectors were the voltage and available capacity of cells, but the temperature was ignored [98]. Fang [99] also used SOM to cluster cells into three categories with high, medium and low temperature, where the temperatures at three different discharge rates were chosen as the input vectors, but the voltage and available capacity were not taken into account.

In this chapter, a self-organizing map (SOM) is proposed to cluster the cells. One contribution of our work is to adopt the newly proposed input vectors to the SOM, which are the available capacity, internal resistance and temperature variation. The output of the SOM is three clusters which categorise the cells into three groups. Another contribution is that the experimental comparison of the sorted pack with the unsorted pack under different discharging current profiles has been carefully conducted, and the sorted battery pack consists of cells which have been clustered into the same group and the unsorted battery pack is built of randomly selected cells. The results show that the cells in the sorted pack are more consistent than those in the unsorted pack, thereby verifying the effectiveness of the proposed method.

The rest of this chapter is organized as follows. In Section 4.2, the results of experiments on 12 cells with 3.3V/2.3Ah $LiFePO_4$ on the battery testing system are reported and the experimental data are obtained for clustering. In Section 4.3, the SOM method for clustering cells is presented. In Section 4.4, the pulse current discharge profiles and the current profiles based on urban dynamometer driving schedule (UDDS) for EVs are used to test the sorted and unsorted battery packs to validate the proposed method. The conclusions are given in Section4. 5.

4.2 Experiment

The sorting of cells requires numerous experimental data from the cells under investigation. A battery testing system (BTS) was built to obtain these data, as shown in Fig. 4-l. The BTS with the four independent channels can charge and discharge four cells simultaneously using programmable currents. 12 $LiFeO_4$ cells were tested under ambient temperature. The cell specification is shown in Table 4-1. The constant current/constant voltage (CCCV) charging method was adopted in this study to charge the cells with the constant current of 1C until the cell voltage reached the maximum charging voltage of 3.6V, where 1C refers to the charging current of 2.3A, namely the ratio of nominal capacity to 1 hour (2.3Ah/1h). The charging voltage was maintained at 3.6V and the charging current was reduced exponentially. When the current reached a pre-set current (e.g. 0.05C was adopted in this study), the charging process ended [90]. Having rested for 1 hour, the cells were discharged at the constant current of 1C. During the test, the voltages of the cells were collected by the voltage sensors with the sampling rate of one second. The resolution of the voltage sensor of the Arbin system is 0.1%. For each cell, 8 number of test results were used to calculate the average available capacity for clustering in the following section.

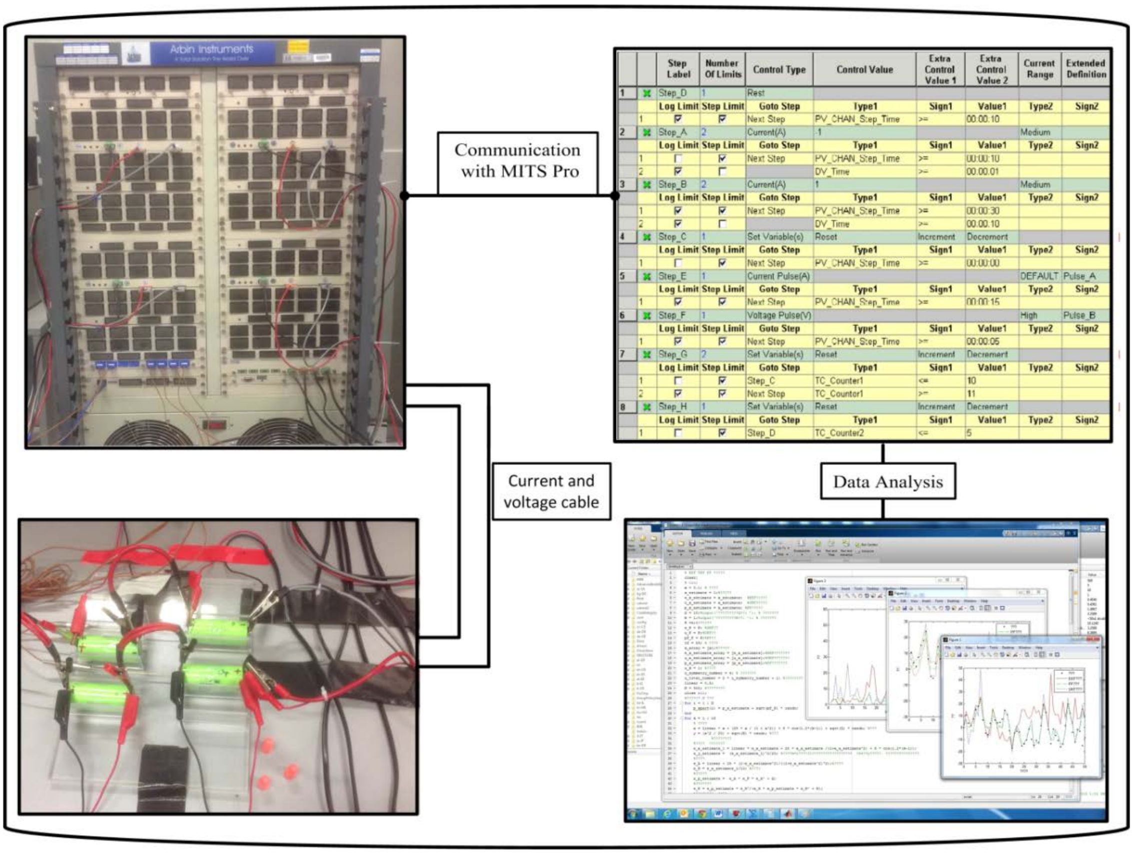

Figure 4-1.Experimental setup

TABLE 4-1 SPECIFICATION OF CELLS USED FOR TESTING

Cell type	A123 26650 cylinder type $LiFePO_4$
Nominal capacity	2.3Ah
Nominal voltage	3.3V
Cut-off voltage (upper/lower)	3.6/2.0V
Maximum continuous discharge	50A
Operating temperature	-30~55 °C

4.3 SOM-based Classification Method for Battery Sorting

A self-organizing map (SOM) is a special kind of neural network. It is a well-known unsupervised learning and data clustering method [100-102], which was initially proposed by Kohonen [103, 104]. It has proven to be an effective data clustering method in many fields [105]. The SOM contains two layers: an input layer and a competition layer with a regular two-dimensional grids of mapping units. Every unit (or neuron) i is represented by a prototype vector w_i of the same dimension as the input data vector x. The units are connected to the adjacent ones through a neighbourhood relation. The accuracy and generalization capability of the SOM is not sensitive to the number of map unit.

In this study, the available capacity, internal resistance and temperature variation of 12 cells were chosen as the input vectors x of the SOM, while the outputs of the SOM are the three clusters which classify 12 cells into three groups. The temperature varation has been introduced into the input vector of the SOM to maintain temperature consistency among the cells and further enhance battey pack performance. The distances between x and all the prototype vectors w_i were calculated [101]. The best matching unit, which is represented by b, is the map unit with the prototype closest to x:

$$\|x - w_b\| = \min\{\|x - w_i\|\} \tag{4.1}$$

After the calculation, the prototype vectors were updated. The best matching unit and its topological neighbors were moved closer to the input vector in the input space. The update rule for the prototype vector of unit i is

$$w_i(t+1) = w_i(t) + \alpha(t)[x_i - w_i(t)] \tag{4.2}$$

where $\alpha(t)$ is the adaptation coefficient. This updating procdures was repeated until all the 12 cells were clustered successfully. Figure 4-2 shows the schematic of the SOM model for cell sorting, where x_i (i=1, 2, 3) reprsents the input vectors of each cell and w_i connects to each of the input vectors to the neurons which perform clustering.

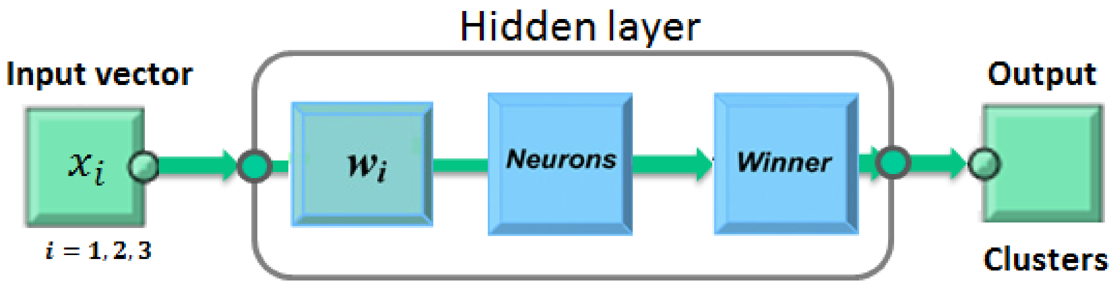

Figure 4-2.SOM model for cell sorting

To prepare for reliable experimental data to form the input vector of the SOM, each of 12 cells was tested for 8 cycles. The average of the available capacities, temperature variations and internal resistances for each cell were then calculated. Figure 4-3 shows all the average values for 12 cells. The temperature varition T_r is defined as

$$T_r = \frac{1}{8}\sum |T_h - T_{am}| \tag{4.3}$$

where T_h, T_{am} represent the highest temperature and initial environmental temperature during each discharge cycle, respectively. Three steps were used to tackle over-fitting [106]. Step 1: all values of the input vector, such as available capacity, temperature variation and internal resistance, were regularized into the range of [0, 1]. Step 2: the number of the group which can be clustered for the given 12 cells was studied. As a result, three groups have been adopted to cluster the 12 cells in this study. Step 3: the number of units in the competition layer was studied. It was found that the number of units does not affect the clustering results.

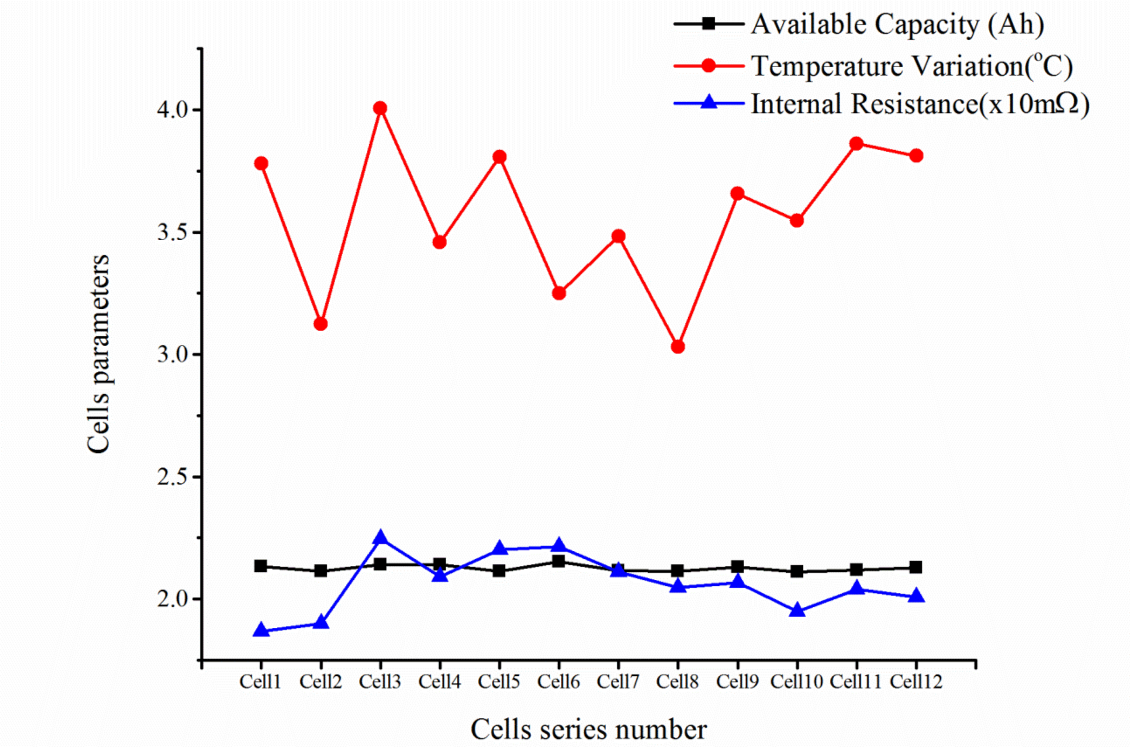

Fig.4-3. Average values of available capacity, temperature variation and internal resistance

To train the SOM, the regularized values of the input vectors are sent to the SOM model, and the neurons in the network are trained to respond to the input vector. The neuron whose prototype vector is closest to the input vector wins the competition and outputs 1 while the other neurons output 0. The number of map units used in the SOM is 108. The training results of cells 1 to 12 are demonstrated in Fig. 4-4, where x(1), x(2) and x(3) correspond to available capacity, temperature variation and internal resistance, respectively. The symbol '+' represents 12 cells and the symbol '○' indicates the neurons. It can be seen that the neuron is located on the top of cell 12, to which the other three cells 3,5 and 11 are very close. These four cells belong to the first cluster. The neuron located on the top of cell 1 represents the second cluster, including cells 1,4,7,9 and 10. The neuron located on the top of cell 8 creates the third cluster, including cells 2, 6 and 8. The outputs of the SOM model are 1, 2 and 3, as shown in Fig. 4-5.

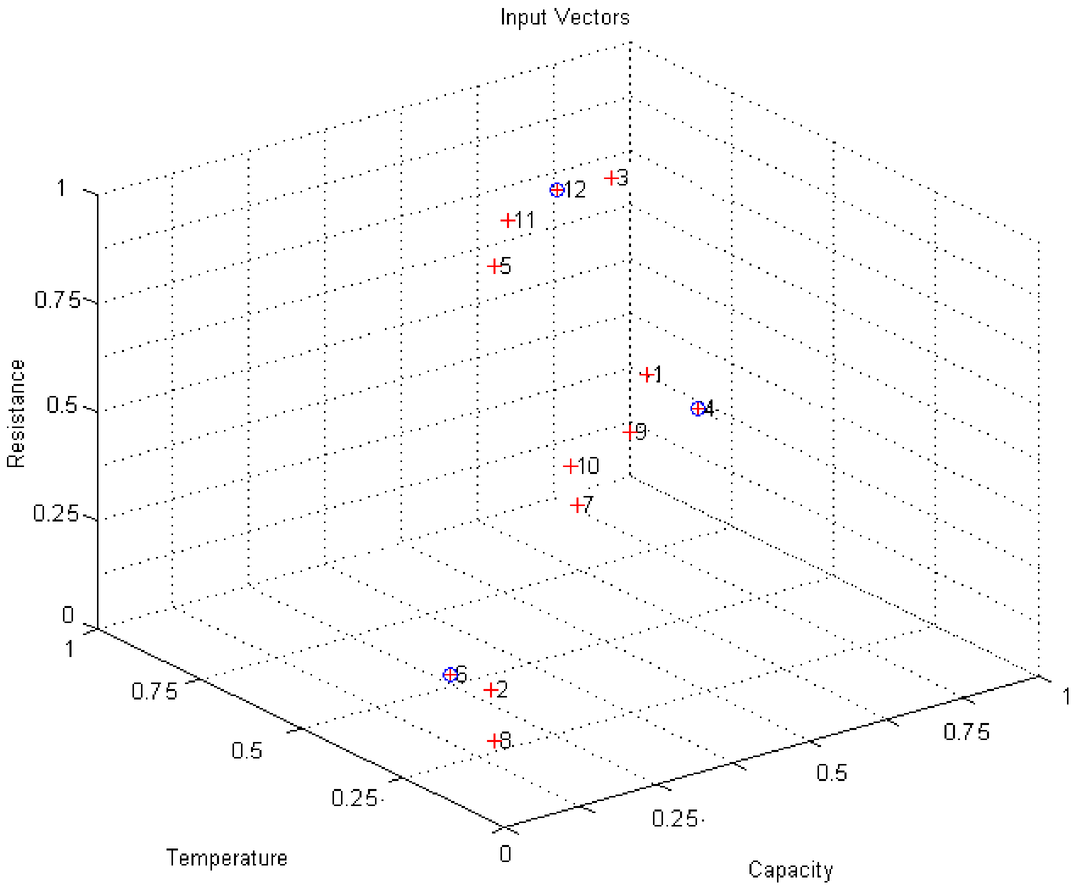

Fig.4-4. SOM training results with cells 1 to 12

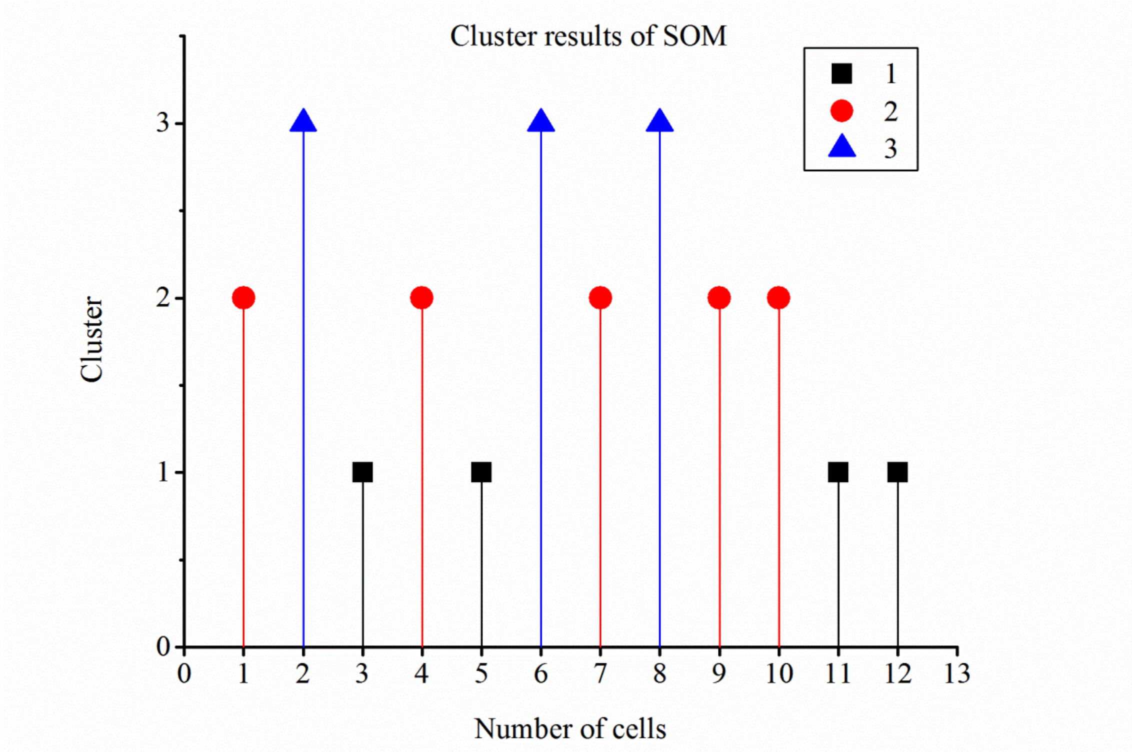

Fig.4-5. Clustering results of 12 cells

4.4 Results and Discussion

Based on the above clustering results, cells 3, 5, 11, 12 in the same cluster were connected in series to build a battery pack named the sorted battery pack. Cells 2, 3, 6, 9 were randomly chosen to connect in series to build the other battery pack named the unsorted battery pack. The basic parameters of these two battery packs are listed in Table 4-2. The pulse current discharge profiles with 1C discharge rate, constant discharge current with 2C discharge rate and the current profiles based on the UDDS for EVs were used to test these two battery packs. The following section presents the discussion of these experimental results.

TABLE 4-2 KEY SPECIFICATIONS OF BATTERY PACK

Battery pack	
Nominal capacity	2.3Ah
Nominal voltage	13.2V
Cut-off voltage (upper/lower)	14.4/8.0V
Maximum continuous discharge	30A
Operating temperature	-30~55 ^{o}C

4.4.1 Pulse current discharge test

The relationlship between the open circuit voltage (OCV) and the state of charge (SOC) is very important, because it can infer the SOC which is a crucial parameter for battery management systems. A pulse current discharge (PCD) test can obtain this relationship [91]. During the test, the fully charged battery pack was discharged at 2.2A nearly to 1C for 6 min. and rested for 1 hour to allow the terminal voltage to reach its equilibrium state, namely the OCV. Each pulse current discharge equals approximately 10% of the nominal capacity, which is equivalent to a reduction in the SOC by 10%. This discharge-rest process was repeated until the terminal voltage reached the cut-off voltage of 8.0V, which is defined as the state when the battery pack is fully discharged. As an example, Fig. 4-6 shows the profile of the PCD and the corresponding terminal voltage for the sorted battery pack.

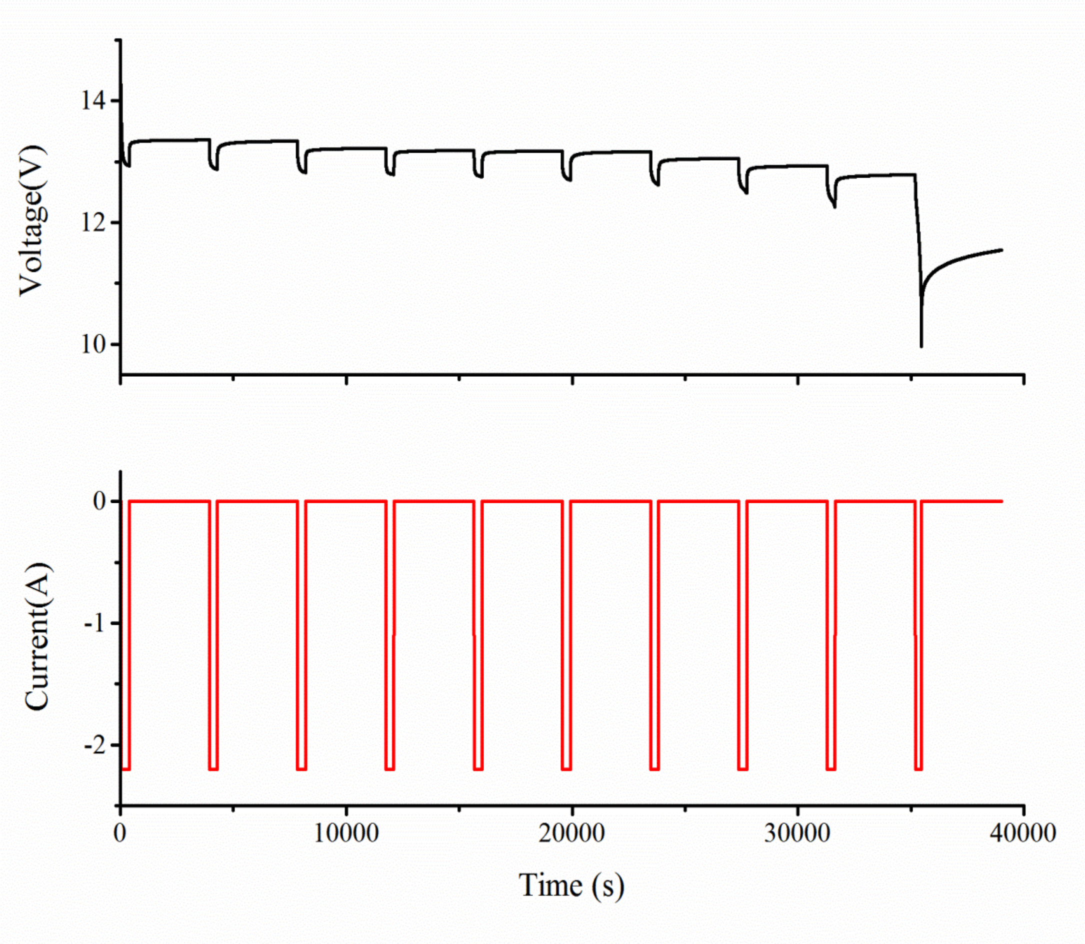

Fig.4-6. Pulse current discharge and terminal voltage for sorted battery pack

Based on the results of this PCD test, the OCV-SOC curves for each cell within the sorted pack and the unsorted pack are shown in Figs.4-7 and 4-8, respectively.

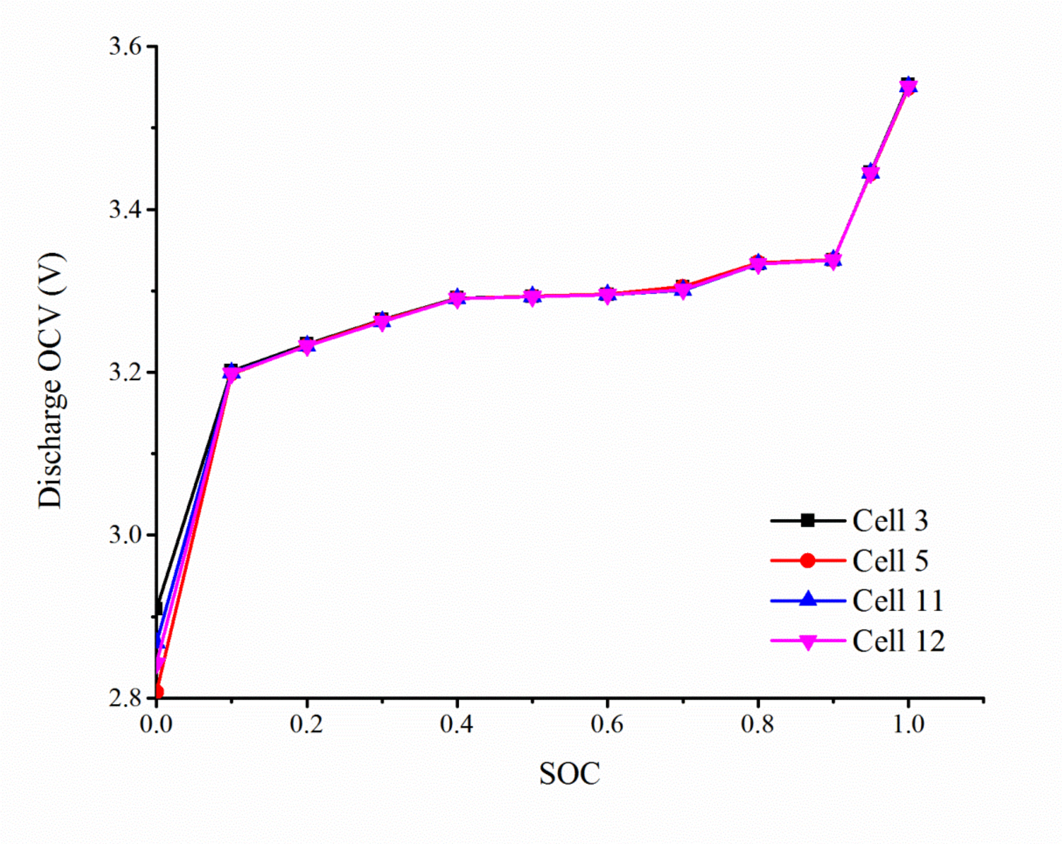

Figure 4-7. OCVs versus SOCs for cells in sorted battery pack

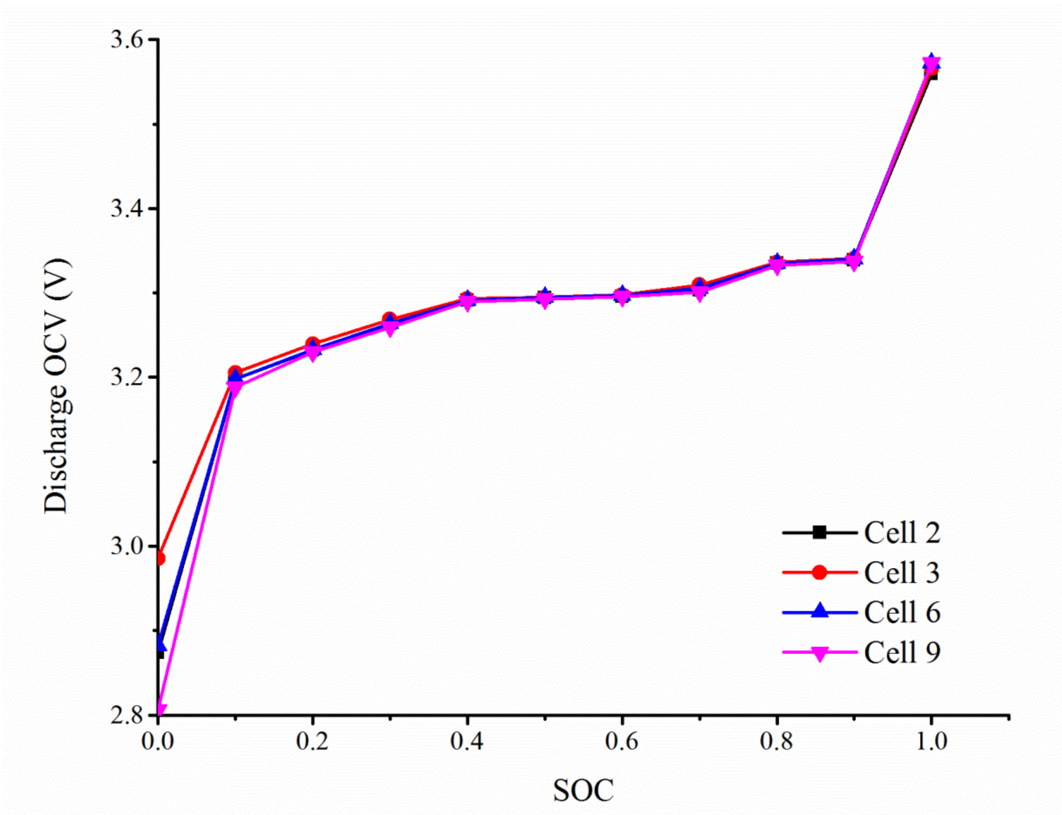

Figure 4-8. OCVs versus SOCs for cells in unsorted battery pack

Figures. 4-7 and 4-8 indicate that there is an inconsistency in the OCVs for the cells in the sorted and unsorted packs at the low range of the SOCs from 0 to 10%. In this range of SOCs, it may not create a problem for the battery pack during the charging process, since the cells in the pack have low voltages far from the maximum protection voltage. The OCVs of each cell are almost uniform at SOCs from 10% to 100% for the sorted battery pack, while the OCVs of each cell only show uniformity at the SOCs from 80% to 100% for the unsorted battery pack. The inconsistency of the cells in a wide range of SOCs (e.g. 10% to 80%) affects the performance of the unsorted battery pack in comparison with that of te sorted battery pack. Table 4-3 shows the discharge capacity of the two battery packs, and indicates that the sorted pack has more available capacity than the unsorted pack.

TABLE 4-3 AVAILABLE CAPACITIES FOR SORTED AND UNSORTED BATTERY PACKS

	Sorted battery pack	Unsorted battery pack
Discharge capacity (Ah)	2.161	2.1475

To describe the voltage inconsistency, the voltage difference between the voltage of each cell and the mean voltage of n cells in the battery pack at the same SOC is defined by

$$\Delta V_{ocvi} = \left| V_{ocvi} - \sum_{i=1}^{n} V_{ocvi} / n \right| \tag{4.4}$$

where V_{ocvi} represents the OCV at a certain SOC, and n refers to the number of cells. For example, the voltage differences of the cells in the sorted and unsorted battery packs at the SOC of 60% are shown in Table 4-4. It can be seen that the voltage differences of the cells in the sorted pack are much smaller than those in the unsorted pack. This indicates that the cells in the sorted battery pack are more consistent than the cells in the unsorted battery pack.

TABLE 4-4 VOLTAGE DIFFERENCE BETWEEN VOLTAGE OF EACH CELL AND THE MEAN VOLTAGE OF 4 CELLS IN BATTERY PACK AT SOC OF 60%

	Cell 1 (V)	Cell 2 (V)	Cell 3 (V)	Cell 4 (V)
Sorted battery pack	Cell 3	Cell 5	Cell 11	Cell 12
	0.00002	0.00042	0.00024	0.00020
Unsorted battery pack	Cell 2	Cell 3	Cell 6	Cell 9
	0.00082	0.00141	0.00045	0.00104

Another observation based on Fig. 4-7 is that the curve of the OCV-SOC is flat at the SOC range of 40% to 70%, which means when the OCV of each cell is very small the SOC of each cell is still quite large. To make this more clear, Table 4-5 provides the numerical values of the voltage/SOC difference between the voltage/SOC of each cell and the mean voltage/SOC of four cells in the sorted battery pack at the SOC of 60%/the OCV of 3.3V, where the SOC difference is calculated by

$$\Delta SOC_i = \left| SOC_i - \sum_{i=1}^{n} SOC_i / n \right| \tag{4.5}$$

TABLE 4-5 VOLTAGE/SOC DIFFERENCE BETWEEN VOLTAGE/SOC OF EACH CELL AND MEAN VOLTAGE/SOC OF 4 CELLS IN SORTED BATTERY PACK AT SOC OF 60%/OCV OF 3.3V

	Cell 3	Cell 5	Cell 11	Cell 12
Voltage (V) at 60% SOC	0.00002	0.00042	0.00024	0.00020
SOC at OCV 3.3V	1.57%	1.99%	2.03%	1.52%

It can be seen from Table 4-5 that the numerical values of the voltage differences among four cells are much smaller than those of the SOC difference. As a result, if the OCV-based method is used to conduct cell balancing, which has been widely used for most applications to date, then when the OCVs have been adjusted to the acceptable range (e.g. 0.0002V in this study), all cells in the battery pack are considered to be balanced. However, the SOC differences of four cells are still quite large and the balancing of the four cells is still required. Therefore, the cells in the battery pack should be balanced on the basis of the SOC rather than the OCV, and the SOC-based methods are more effective than the OCV-based methods in cell balancing [107].

4.4.2 Constant current discharge test

Constant current discharge testing with the high discharge rate of 2C was conducted on the two battery packs. The fully-charged two battery packs were discharged until one of the cells reached the cut-off voltage of 2V. Figures 4-9 and 4-10 show the experimental results for the cells in the sorted and unsorted battery packs. The curves highlighted by the red circles in both the sorted and unsorted packs are magnified, to demonstrate that the cell voltage differences in the sorted pack are smaller than those in the unsorted pack.

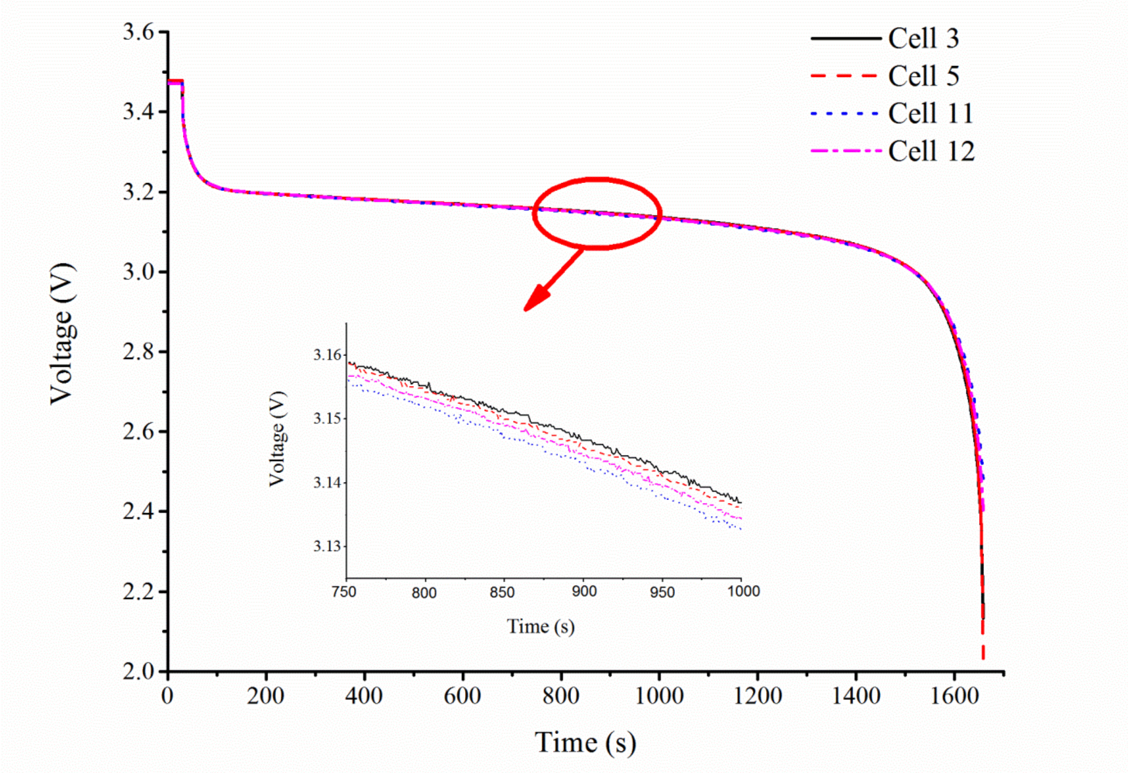

Figure 4-9. Discharge curves for cells in sorted battery pack

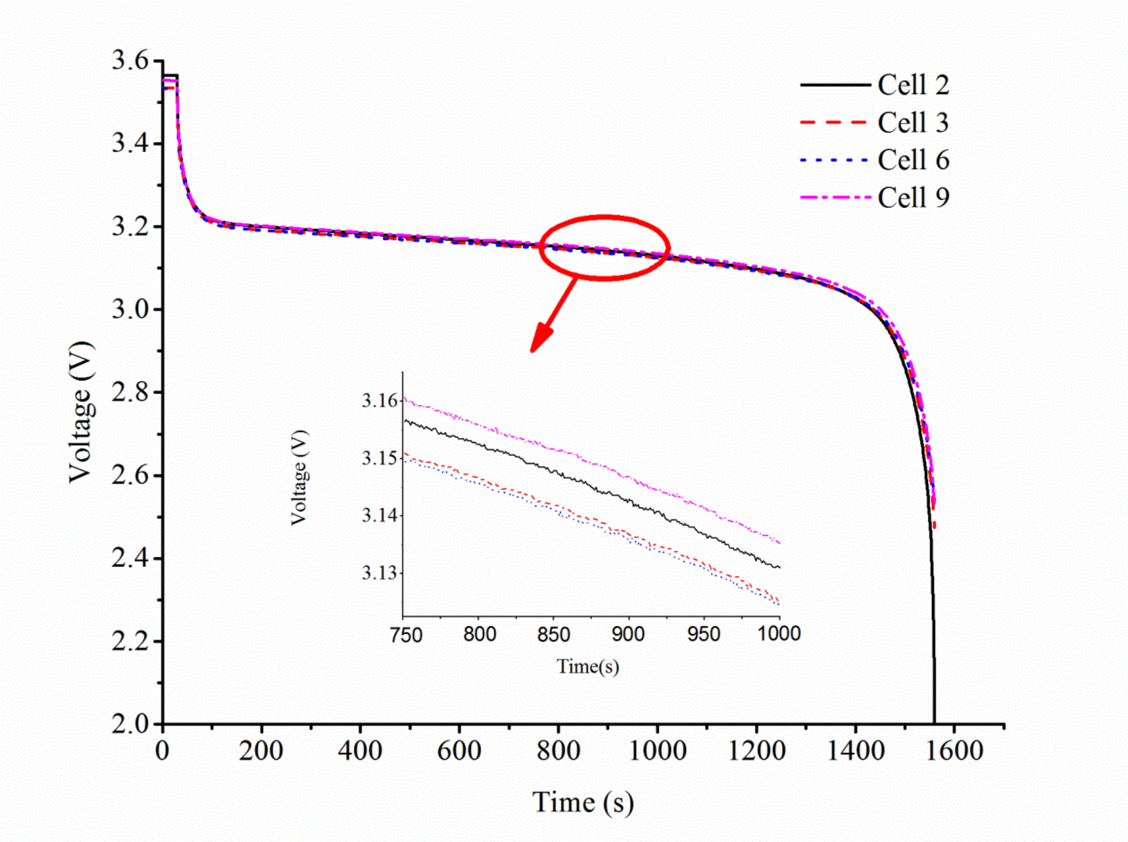

Figure 4-10.Discharge curves for cells in unsorted battery pack

To describe the temperature inconsistency, the temperature difference is defined by

$$\Delta T_i = \left| T_i - \sum_{i=1}^{n} T_i / n \right| \tag{4.6}$$

The voltage and temperature differences are shown in Fig. 4-11 and Fig. 4-12, respectively. The maximum voltage difference in the sorted pack is 0.197V, while this voltage difference in the unsorted pack is 0.583V. The maximum temperature difference in the sorted pack is 0.665 **°C,** while this temperature difference in the unsorted pack is 0.95 **°C**.

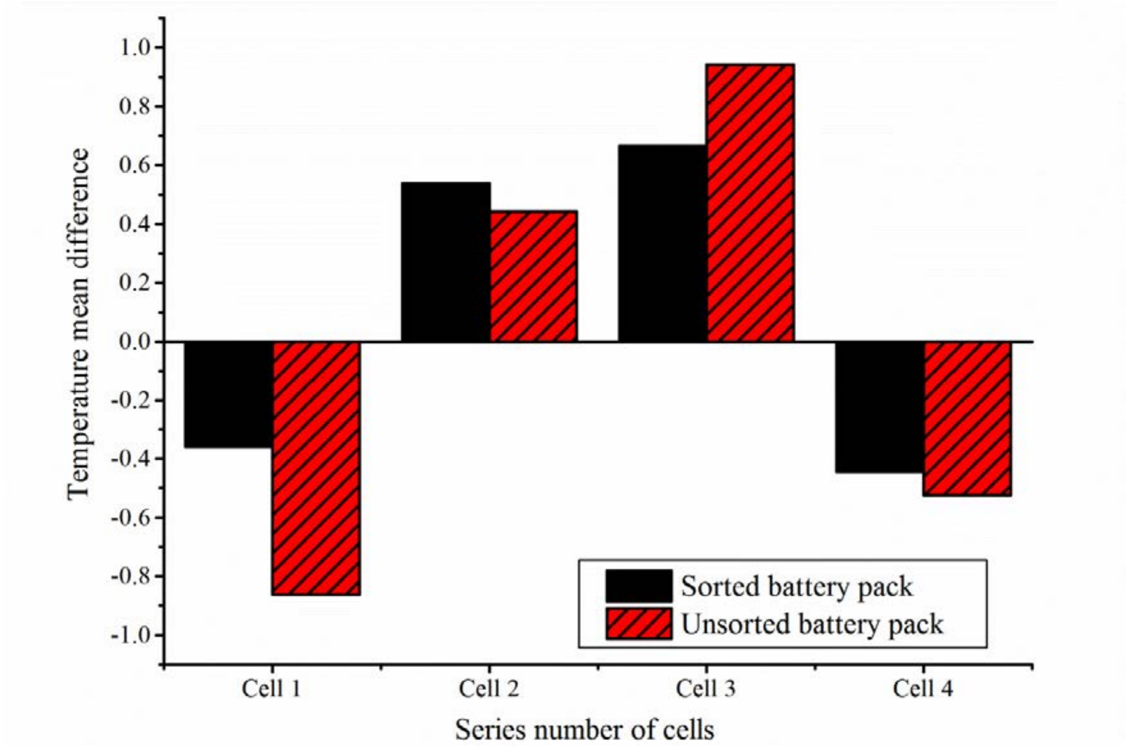

Figure 4-11.Temperature difference under 2C discharge rate

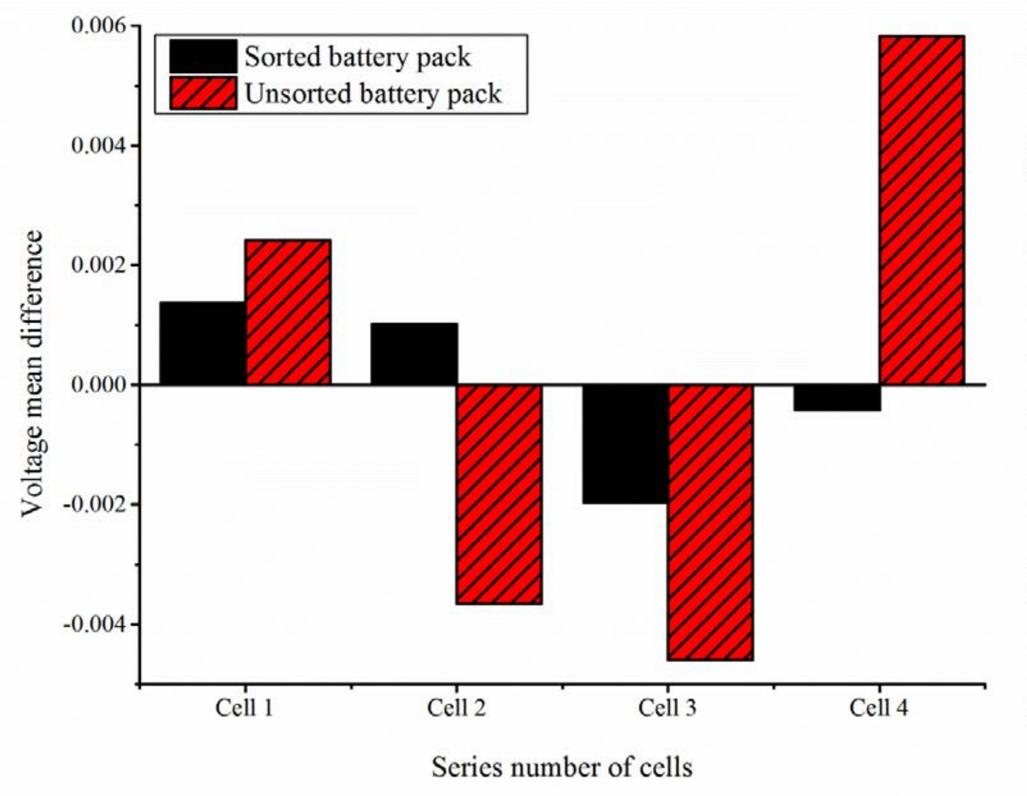

Figure 4-12.Voltage difference under 2C discharge rate

4.4.3 EV driving cycle test

The current profile based on the EV driving cycle was also used to test the two battery packs. This EV driving cycle is the urban dynamometer driving schedules (UDDSs), which has been used for several decades in the automobile industry[108]. Figure 4-13 shows the current profile of four cycles converted from the UDDS. This profile was loaded into the two battery packs under ambient temperature.

Figures 4-14 and 4-15 show the experimental results of voltage profiles for each of the cells in the sorted and unsorted packs. The voltage and temperature differences for each cell are shown in Figs 4-16 and 4-17, which indicate that the differences of the cells in the sorted pack are smaller than those of the cells in the unsorted pack. Therefore, the sorted battery pack has better voltage and temperature consistency than the unsorted battery pack.

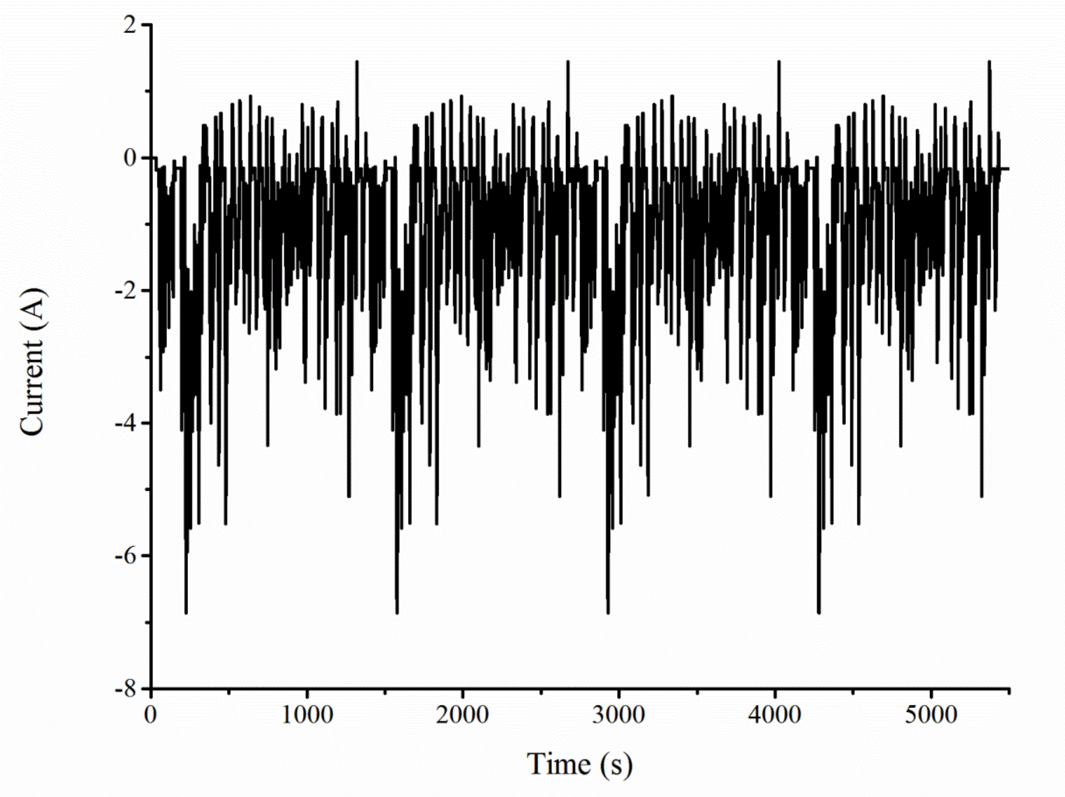

Figure 4-13. Current profile for UDDS

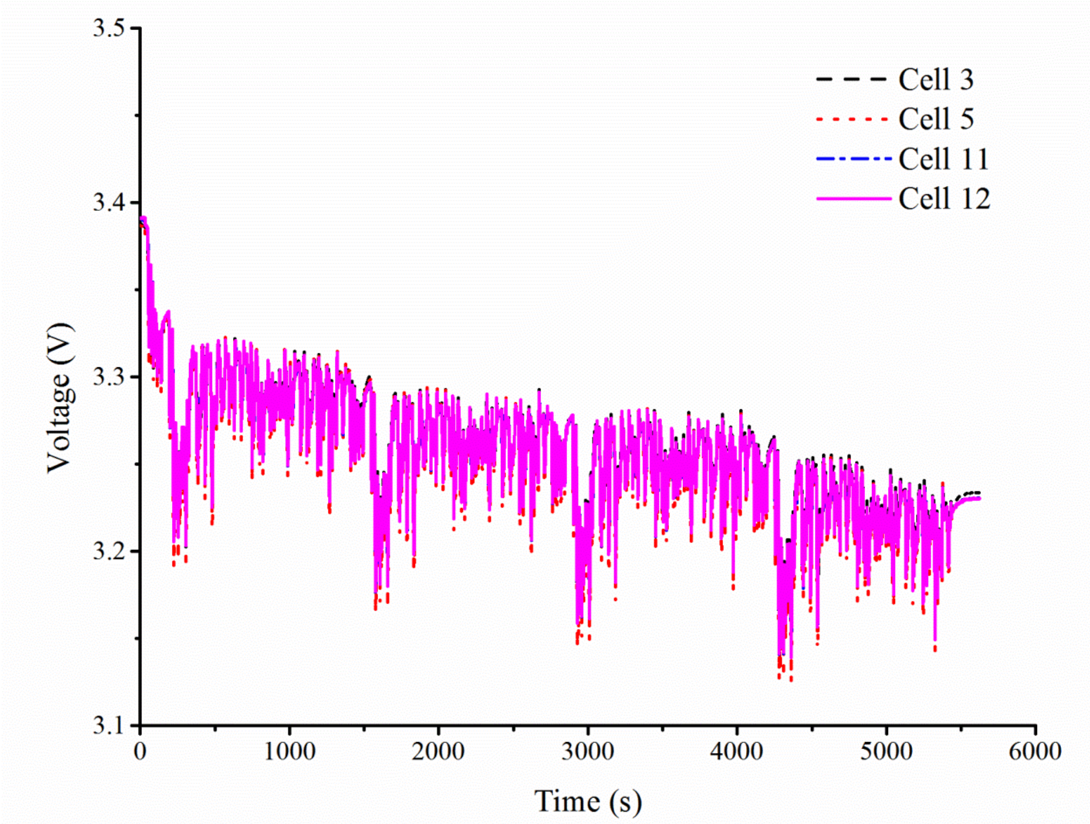

Figure 4-14. Voltage profiles of cells in sorted battery pack

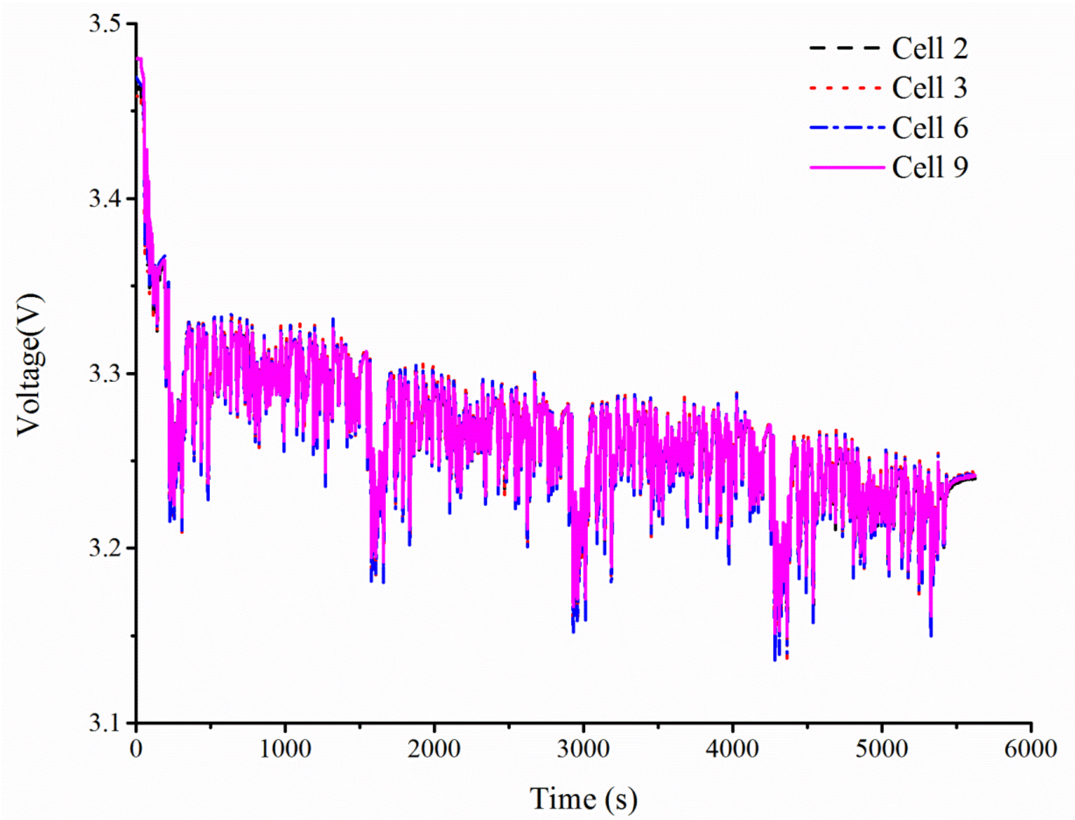

Figure 4-15. Voltage profiles of cells in unsorted battery pack

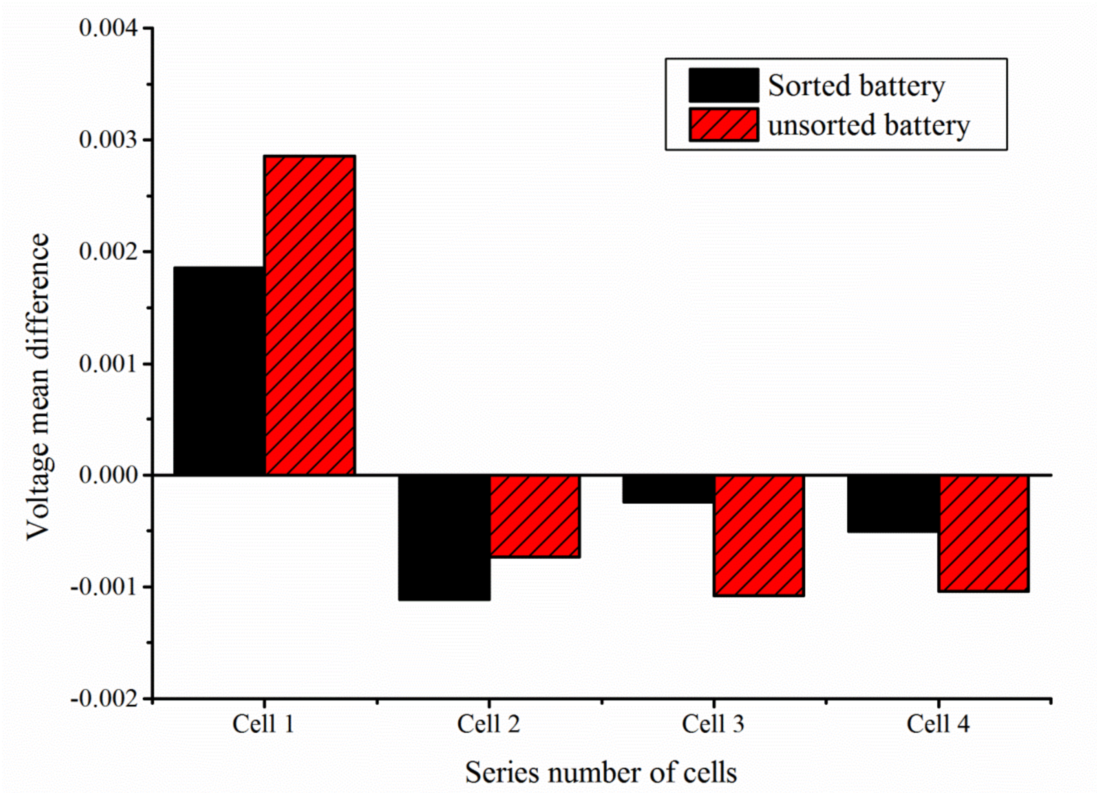

Figure 4-16. Voltage difference under current profile of UDDS

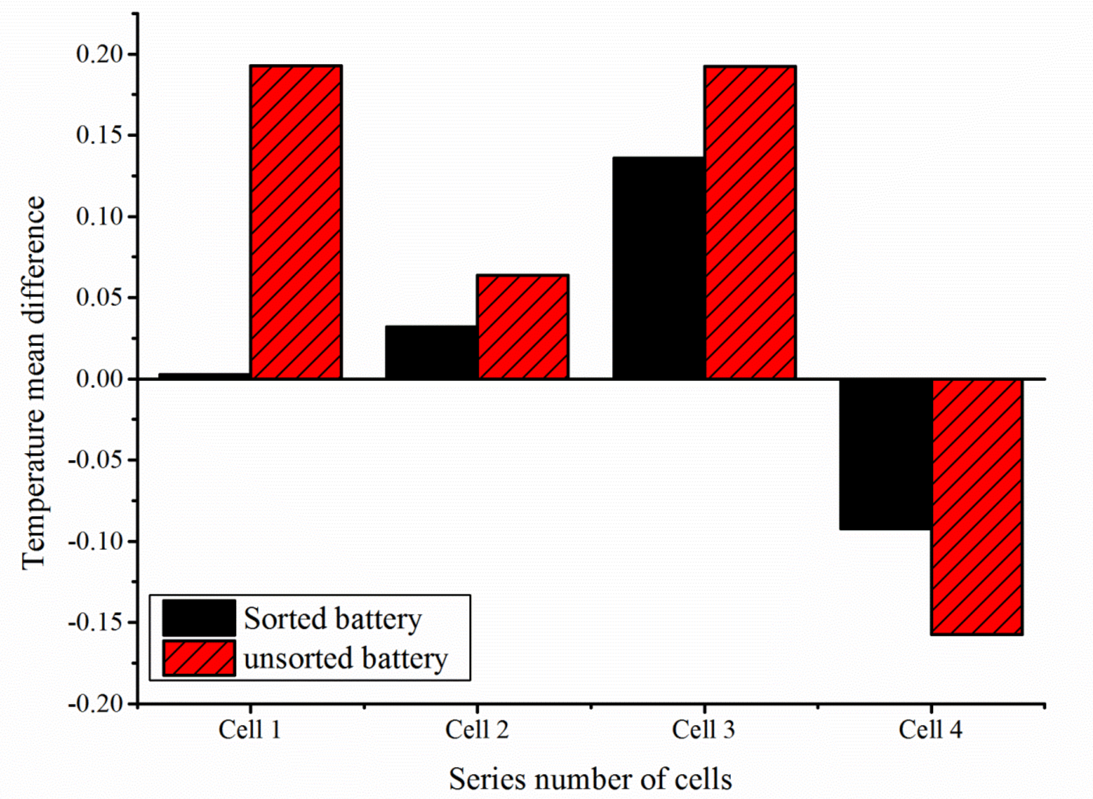

Figure 4-17. Temperature difference under current profile of UDDS

It should be noted, in Fig.4-16, the voltage difference is between the voltage of cell 2 and the average voltage of their respective battery packs. Thus, it is possible that voltage difference of cell 2 in the sorted pack is slightly greater than that of cell 2 in the unsorted pack. However, the overall voltage difference of the cells in the sorted battery pack is better than that of the cells in the unsorted battery pack under the UDDS cycle.

4.5 Conclusion

In this chapter, the neural network tool of self-organizing map has been presented to cluster 12 cells into three groups based on the available capacity, internal resistance and temperature variation of the cells. Different discharge current profiles have been used to test the sorted battery pack and the unsorted battery pack. It is found that the cells in the sorted pack have more consistent performance than the cells in the unsorted pack in terms of battery state of charge, terminal and open circuit voltages and temperature variation. In addition, the experimental results also show that state of charge-based methods for cell balancing are more effective than voltage-based methods. Future work will consider the development of the SOC estimation method for sorted and unsorted battery packs and a cell balancing technique based on battery SOC rather than battery terminal voltage.

CHAPTER 5 BATTERY PACK STATE-OF-CHARGE ESTIMATION WITH H INFINITY OBSERVER

In this chapter, a H-infinity observer (HIO) for SOC estimation is proposed for series-connected battery packs in UMEVs. In the proposed method, an average virtual cell (AVC) model is defined and the SOC of the AVC model is estimated to represent the pack SOC when all terminal voltage differences (TVDs) between each individual cell in the pack and the AVC are within a pre-set voltage threshold. To ensure that all the TVDs are within the threshhold, lithium iron phosphate cells are clustered into the group with similar characteristics and the cells in the same group are used to build the sorted battery pack. The experimental results on pulse current discharge and current profiles based on both urban dynamometer driving schedules (UDDSs) and an underground mine driving cycle (UMDC) on the sorted battery pack are reported to verify the effectiveness of the proposed HIO for pack SOC estimation for UMEVs.

5.1 Introduction

With the progressively tightening emission controls in underground mines, the electrification of personnel carrier vehicles for underground mines has attracted increasing attention, as electric vehicles (EVs) provide the significant advantages of low noise and zero emissions over diesel engine vehicles [2]. EVs currently use lithium-ion batteries as their main power source due to their high energy and power density, long cycle life and low self-discharge rate [29]. To meet the voltage and current requirements of EVs, hundreds and thousands of lithium-ion battery cells are required to be connected in series and parallel to build a battery pack. In such battery packs, state of charge (SOC) estimation is crucial to maintain the performance of the battery pack and ensure the safe operation of EVs. This is very challenging due to the inconsistencies of the cells in the pack.

A number of SOC estimation methods have been proposed, and each method has merits in certain aspects. Generally, SOC estimation methods for a single cell can be categorized into three types. One of the most applicable types is an ampere-hour counting method which integrates the current over time, based on the current measurement [50, 109]. It is the simplest SOC estimation method. The second type of SOC estimation methods is to apply machine learning techniques, such as artificial neural networks, fuzzy logic and the support vector machine [74, 75, 110]. They can be applied to any types of batteries without the requirement of battery models. The third type is model-based SOC estimation methods, such as the Kalman filter, sliding mode observer, and H-infinity observer [54, 55, 62, 65, 91]. Model-based SOC estimation methods are the most popular, due to the merits of the closed-loop, online and available feed-back of the dynamic estimation error.

Studies of battery pack SOC estimation taking cell inconsistencies into account have been carried out recently. Plett [111] introduced a method named “bar-delta filtering” to estimate pack SOC by utilizing the similarity of the cell characteristics in the pack and the average pack SOC. Liu et al. [112] propose a minimum voltage (V-min) model which uses the minimal voltage of cell in the pack as the pack voltage to estimate pack SOC using the extended Kalman filter (EKF). Roscher et al. [14] incorporate the measured and derived impedance data to estimate the pack SOC. Dai et al. [113] apply the EKF to estimate cell SOCs in the pack based on the differences between the average pack SOC and the SOC differences among the cells in the pack. Kim et al. [45] propose an improved EKF to estimate the pack SOC, where a systematic cell filtering approach is used to choose cells with similar electro-chemical characteristics to build a sorted battery pack. Xiong et al. [114] adopt a similar cell filtering approach to that in [17] to build a sorted battery pack and apply the adaptive EKF to improve the accuracy of pack SOC estimation. Later, Xiong et al. [115] integrate an online bias correction technique and the adaptive EKF to estimate the cell SOC and pack SOC. Zhong et al. [116] introduce the concept that the pack SOC depends on the SOCs of the first over-discharged cell and the first over-charged cell in the pack, as these two cells limit the available capacity of the pack. The unscented particle filter is then used to estimate the SOCs of those two cells. Hua et al. [117] apply the nonlinear predictive filter to estimate the SOC for the weakest cell in the pack and use this weakest cell SOC to represent the pack SOC.

In this chapter, a systematic cell sorting approach based on a self-organizing map (SOM) is used to cluster the cells into groups with similar characteristics and the cells in the same group are connected in series to build a sorted battery pack. Based on the sorted battery pack, an H-infinity observer (HIO) is proposed to estimate the pack SOC using an average virtual cell (AVC) model. Compared with the other pack SOC estimation methods, HIO for pack SOC estimation has no requirement of the assumption about the noise while minimizing the worst statistical case estimation error to achieve high accuracy. Pack SOC estimation using the AVC model can save computation time and provide fast SOC estimation for each individual cell in the pack.

This chapter is organized as follows. In Section 5.2, a model-based SOC estimation method is proposed with the explanation of the HIO for battery pack SOC estimation. Section 5.3 demonstrates the cell test, the SOM sorting approach and battery parameter identification. Section 5.4 evaluates the effectiveness of the HIO for battery pack SOC estimation, followed by the conclusion.

5.2 Battery Modeling and HIO for SOC Estimation

5.2.1 Battery modelling

The SOC describes the ratio of the remaining capacity to the nominal capacity of a battery with its value between 0 to 100%. It can be expressed by

$$s_t = s_0 - \frac{1}{Q}\int_{t_0}^{t} \eta I(\tau)d\tau \tag{5.1}$$

where s_0 denotes the initial SOC, Q represents the battery nominal capacity, η is the coulombic efficiency and is normally taken as one for discharge, and $I(\tau)$ is the instantaneous current (assuming the discharge to be positive). The time derivative of the SOC s_t gives

$$\dot{s}_t = -\frac{\eta}{Q} I(\tau) \tag{5.2}$$

Of all the battery equivalent circuit models (BECMs), the Thevenin model is widely accepted to describe the dynamic characteristics of a lithium-ion battery, and is adopted in this study, as shown in Fig. 5-1. According to the Kirchhoff voltage law, the electrical behaviours of the battery in terms of this model can be expressed as

$$V_t = V_o - V_p - IR_i \tag{5.3}$$

$$\dot{V}_p = -\frac{1}{C_p R_p} V_p + \frac{I}{C_p} \tag{5.4}$$

where V_o represents the open circuit voltage (OCV) which is directly related to the SOC, I is the load current, V_t is the terminal voltage of the battery, R_i denotes the internal ohmic resistance, R_p is the polarization resistance and C_p is the polarization capacitance to describe the transient dynamic voltage response during charging and discharging, and V_p is the polarization voltage across the C_p.

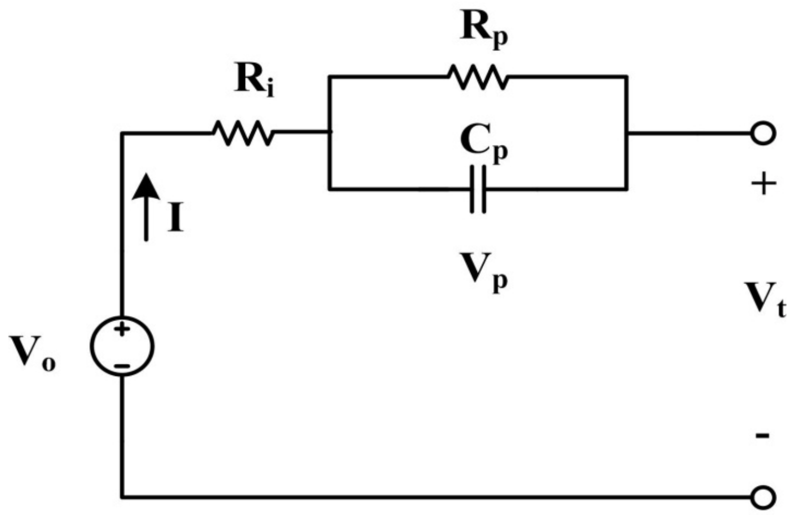

Fig. 5-1 Battery equivalent circuit model

If the state variables of the battery system are defined as $x=[V_p \quad s_t]^T$ which need to be estimated, the input and output of the battery system are defined as $u=I$ and $y=V_t$, respectively, then Eqs.5.2 and 5.4 can be combined into the state space Eq. 5.5, and Eq. 5.3 can be written as the system output Eq. 5.6, as shown below:

$$\dot{x}=Ax+Bu+F\psi \tag{5.5}$$

$$y=Cx+Du+E(t)+G\psi \tag{5.6}$$

where $\psi=[\omega \quad \nu \quad \zeta]^T$ denotes the noise vector of the system, and the system matrices are shown as follows:

$$A=\begin{bmatrix} -\frac{1}{R_pC_p} & 0 \\ 0 & 0 \end{bmatrix} \quad , \quad B=\begin{bmatrix} \frac{1}{C_p} & \frac{-\eta}{Q} \end{bmatrix}^T \quad , \quad C=\begin{bmatrix} -1 & 0 \end{bmatrix} \quad , \quad D=-R_i \quad , \quad E(t)=V_{oc}(s_t)$$

$$F=\begin{bmatrix} 1 & 0 & 0 \\ 0 & 1 & 0 \end{bmatrix}, \; G=[0 \quad 0 \quad 1] \; .$$

5.2.2 H infinity observer technique for SOC estimation

H-infinity observer (HIO) has been used to solve the state estimation problems in linear and nonlinear systems. Compared with the KF, the HIO requires no prior knowledge of noise statistics. It can minimize the effect of the worst possible disturbances on the estimation errors and hence it is more robust against model uncertainty [118].

Based on Eqs.5.5 and 5.6, the HIO can be expressed as

$$\dot{\hat{x}} = A\hat{x} + Bu + K(y - \hat{y}) \tag{5.7}$$

$$\hat{y} = C\hat{x} + Du + E(t) \tag{5.8}$$

where K is the observer gain, and $\hat{x}$, $\hat{y}$ are the estimation values of x and y, respectively. The estimation errors of the state and output are defined as

$$e_x = x - \hat{x} \qquad e_y = y - \hat{y} \tag{5.9}$$

Eq. 5.9 leads to the error dynamics

$$\dot{e}_x = (A - KC)e_x + (F - KG)\psi \tag{5.10}$$

$$e_y = Ce_x + F\psi \tag{5.11}$$

The aim of the HIO design for the system represented by Eqs.5.5 and 5.6 is as follows: for a given attenuation level $\gamma > 0$, find the observers of Eqs.5.7 and 5.8 such that the corresponding error dynamics (Eqs.5.10 and 5.11) are asymptotically stable and satisfy the following inequality under the zero initial conditions:

$$\|e_x\| < \gamma \|\psi\| \tag{5.12}$$

The linear matrix inequality (LMI) approach in the MATLAB Toolbox [119] can easily be used to solve Eq. 5.12 to obtain the attenuation term γ.

According to the robust control theory, the system is stable if there exists a positive definite matrix $P = P^T > 0$ and a matrix X with a proper dimension such that the following inequality is satisfied:

$$\begin{bmatrix} A^T P - C^T X^T + PA - XC + I & PF - XG \\ (PF - XG)^T & -\gamma^2 I \end{bmatrix} < 0 \tag{5.13}$$

where P and X can be solved by using the function $\min cx$ solver and the $feasp$ solver in the LMI MATLAB Toolbox, then observer gain can be computed by $K = P^{-1}X$.

5.2.3 Battery pack SOC and cell individual SOC estimation

Battery packs in EVs normally consist of hundreds of cells connected in series. Their diversities lead to the differences of the terminal voltage in each cell in the pack. Based on the relationship of the terminal voltage and the SOC of each cell, the average virtual cell (AVC) model is defined and the SOC of the AVC model is estimated to represent the pack SOC. The terminal voltage of the AVC $\overline{V_{tn}}$ is

$$\overline{V_{tn}} = V_t / n \tag{5.14}$$

where n denotes the number of cells connected in series in the pack. The terminal voltage difference (TVD) between the *ith* cell in the pack and the AVC is defined as

$$\Delta V_i = V_{it} - \overline{V_{tn}} \tag{5.15}$$

Depending on the value of the TVD, the SOC estimation of the pack and each cell will be carried out in the following two ways:

- when the TVDs $\|\Delta V_i\|$ of all cells in the pack are less than the pre-set voltage threshold, which is normally for the sorted battery pack, the terminal voltage of the AVC $\overline{V_{tn}}$ is used to estimate the pack SOC based on the HIO, and this pack

SOC also represents the SOC of each individual cell in the pack. This will significantly save computation time.

- When the TVD $\|\Delta V_i\|$ of one cell in the pack (e.g, the *k*th cell) is larger than the pre-set threshold, the SOC estimation can be divided into two steps. The first step is to estimate the SOC for that cell individually using the terminal voltage V_{kt} of that cell. The second step is to calculate the terminal voltage of the AVC for the battery pack not including the *k*th cell using the equation $\overline{V_{t(n-1)}} = (V_t - V_{kt}) / (n-1)$, this terminal voltage $\overline{V_{t(n-1)}}$ is then used to estimate the SOC of the battery pack not including the *k*th cell. Similarly, if the TVDs $\|\Delta V_i\|$ of the *l*th and *m*th cells are larger than the pre-set threshold, the SOCs of the *l*th and *m*th cells will be estimated individually, then the pack SOC not including the *l*th and *m*th cells can be estimated in the same manner as the pack not including the *k*th cell. The above two steps can be repetitively applied to the pack SOC and the SOCs of the cells the TVDs $\|\Delta V_i\|$ of which are larger than the pre-set threshold. The TVDs of the cells in the sorted battery pack gradually become larger and exceed the pre-set threshold, since the cells in the pack are exposed to different operational environments (e.g. temperature) and ageing speeds with the increase of charging and discharging cycles.

5.3 Experiment and Parameter Identification

5.3.1 Experiment set-up

An experimental bench was established to validate the proposed HIO for pack SOC estimation. As shown in Fig. 4-1, the test bench consisted of (1) the Arbin2000 battery test, (2) an ESPEC temperature chamber, (3) a PC with Arbin Mits Pro software installed. The $LiFePO_4$ battery cells, which are widely used in EVs, were selected for testing in this study. The cell has a nominal capacity of 2.3Ah and a nominal voltage of 3.3V. Based on the proposed method, the experimental data were used to firstly cluster the cells for building the sorted battery pack, then identify the parameters of the battery models and finally to verify the effectiveness of the proposed HIO for the pack SOC estimation.

5.3.2 Battery sorting approach

The battery sorting approach based on a self-organizing map (SOM) was used to cluster 12 $LiFePO_4$ battery cells to build a battery pack. Its details are explained in our previous research work [120] and Chapter 4. In this sorting approach, the available capacity, internal resistance and temperature variation of 12 cells are chosen as the input vectors of the SOM, while the outputs of the SOM are three clusters which classify 12 cells into three groups. Four cells in one of the groups with similar characteristics are selected to connect in series to build a battery pack which is named the sorted battery pack in the following sections.

5.3.3 Parameter identification

To obtain the BECM parameters in Fig. 1, the pulse current discharge (PCD) test was conducted on the sorted battery pack at room temperature. In the PCD test, the sorted battery pack in the fully charged state (SOC=100%) is discharged at 1C for 6 minutes and then rested for 1 hour to allow the terminal voltage to reach its equilibrium state where the terminal voltage is considered as the open circuit voltage (OCV). Each PCD at 1C discharge for 6 minutes is equivalent to approximately 10% of the nominal capacity which equals the 10% SOC reduction. This process is repeated until the terminal voltage reaches the cut-off voltage when the battery pack is fully discharged (SOC=0%). Figure 5-2 shows the discharge current profile and the corresponding terminal voltage. Figure 5-3 shows the OCV versus the SOC of the sorted battery pack under the PCD test, where the OCV versus the SOC is obtained by using the ampere-hour counting method based on experimental data. Ten sets of transient responses in the terminal voltage correspond to ten sets of the PCDs. Therefore, ten sets of the BECM parameters for different SOCs and their relative mean square errors (RMSEs) between the BECM and the experimental data are shown in Table 5-1.

Using the MATLAB LMI toolbox, the inequality Eq. 5.12 can be solved, the minimum attenuation level of γ is 0.905. By selecting $\gamma = 1.55$, the estimation process is more robust. Then，the matrix P and X can be obtained as

$P = \begin{bmatrix} 3.76 & -1.62 \\ -1.62 & 3.76 \end{bmatrix}$ $X = \begin{bmatrix} 0.5921 \\ 2.1337 \end{bmatrix}$ and the observer gain $K = P^{-1}X = \begin{bmatrix} 0.4936 \\ 0.7801 \end{bmatrix}$.

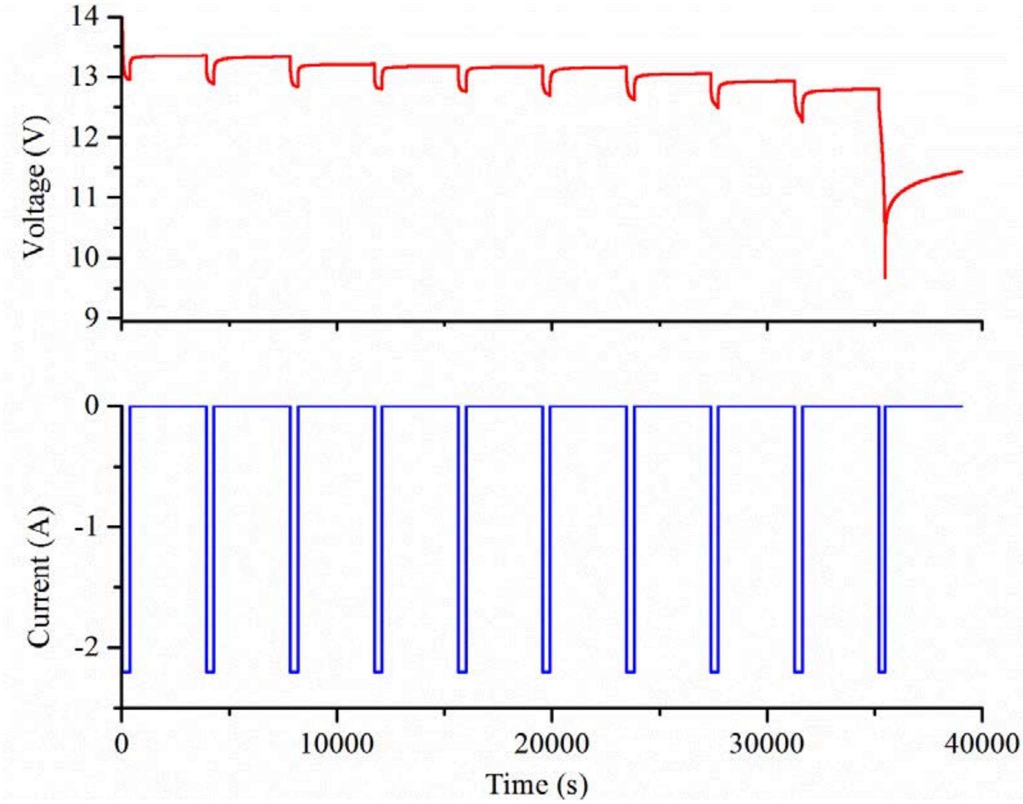

Fig.5-2 Terminal voltage and current of sorted battery pack under PCD test

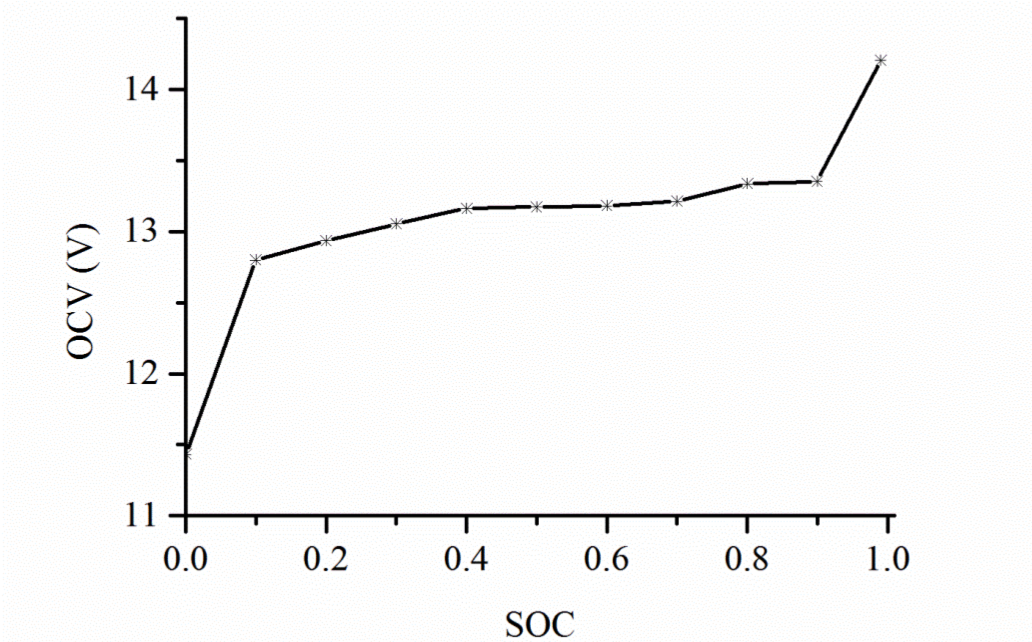

Fig.5-3 Experimental OCV-SOC relationship of LiFePO4 battery pack

TABLE 5-1. BATTERY PACK CIRCUIT PARAMETERS AT DIFFERENT SOCS

SOC	V_o (V)	C_p (F)	R_p (Ω)	R_o (Ω)	RMSE
10%	12.800	219.349	0.095	0.105	0.003067
20%	12.935	257.800	0.059	0.103	0.004241
30%	13.054	292.562	0.054	0.102	0.003171
40%	13.164	307.096	0.046	0.101	0.002833
50%	13.173	324.776	0.045	0.101	0.003081
60%	13.182	342.232	0.044	0.100	0.004304
70%	13.213	305.248	0.040	0.100	0.003553
80%	13.337	294.075	0.045	0.100	0.003552
90%	13.354	274.893	0.040	0.099	0.004981
100%	14.206	47.713	0.214	0.119	0.018300

5.4 Verification and Analysis

Three experiments were conducted to validate the proposed HIO for pack SOC estimation: the PCD test, the UDDS test and the UMDC test. The UDDS test is a typical dynamic driving cycle which was adopted to evaluate the effectiveness of the SOC estimation in EVs. The UMDC was specially constructed for this study to evaluate SOC estimation in underground mining electric vehicles (UMEVs) [81].

5.4.1 PCD test validation

Figure 5-4 and Figure 5-5 show the comparison between the estimated and true terminal voltages and pack SOCs under the PCD test and their estimation errors, where the true terminal voltage is the measured voltage value and the true SOC is calculated by the ampere-hour counting method.

It can be seen from Fig.5-5(a) that the SOC estimation only has a slight difference from the true SOC. These results are obtained when the SOC is purposely set to the wrong initial SOC of 82 percent, where the true initial SOC is 100 percent for the fully charged battery pack. This indicates that the HIO can estimate the pack SOC accurately, regardless of initial SOCs. The estimated SOC can track the true SOC and the errors most of the time are maintained within 3%, as shown in Fig.5-5(b). The terminal voltage errors between the estimated and experimental values are only within 5% for most of the time, except at the initial state and the end of discharge, as shown in Fig.5-4(b).

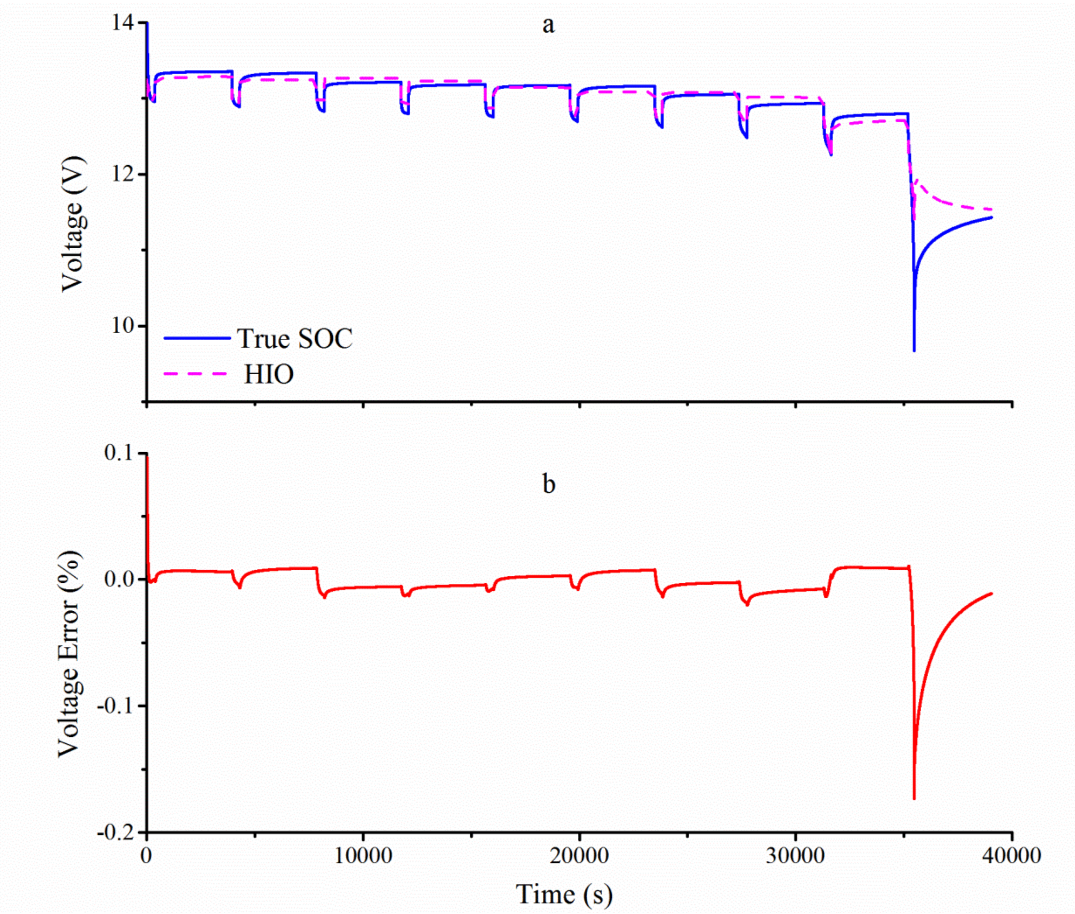

Fig.5-4 Comparison of terminal voltages estimated from HIO with those obtained from experiments and their errors for sorted battery pack under PCD test (a).HIO estimated pack voltage (b). Estimated voltage error

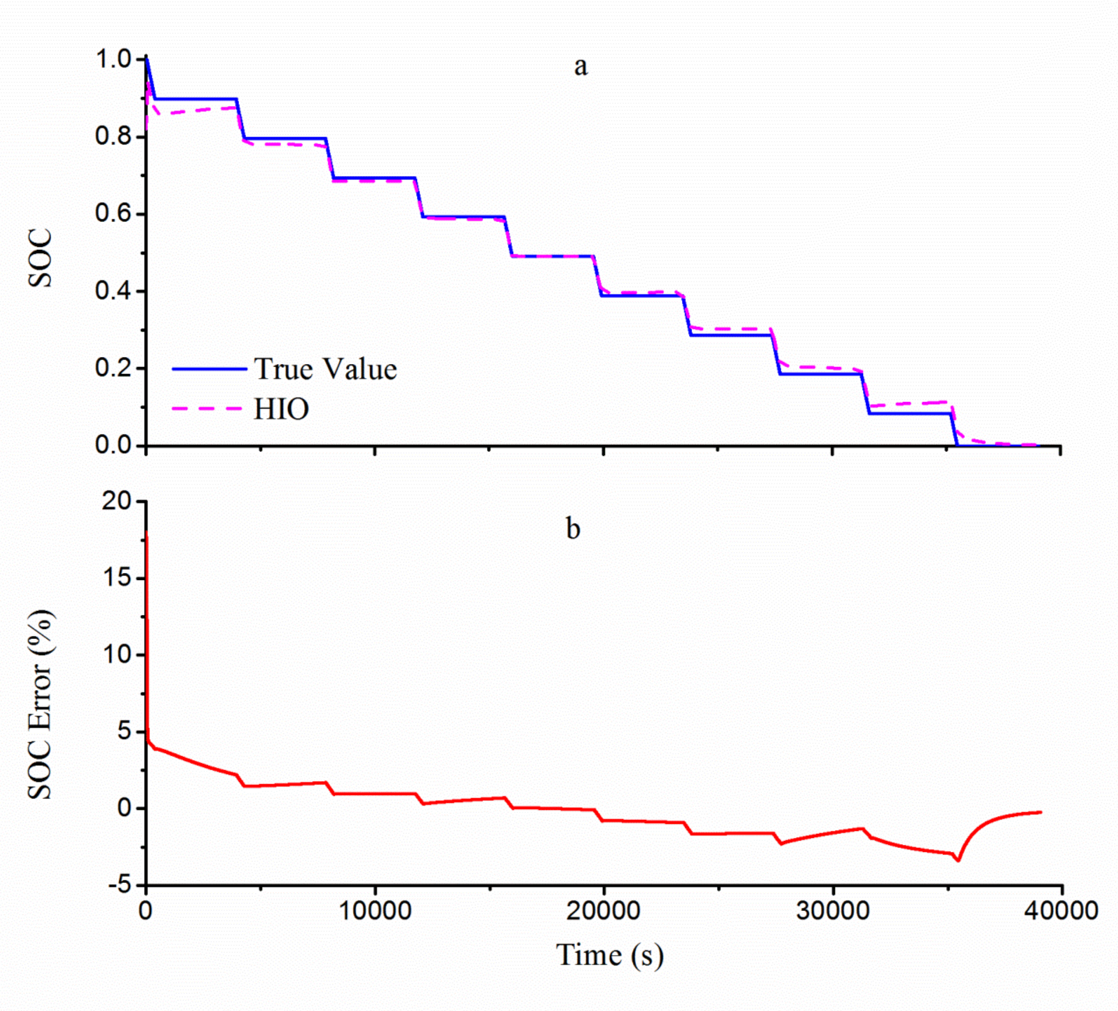

Fig.5-5. Comparison of SOCs estimated from HIO with those obtained from experiments and their errors for sorted battery pack under PCD test (a). HIO estimated pack SOC (b). SOC error

5.4.2 UDDS test validation

In Chapter 4 the UDDS cycle was used to do the validation. Figure 4-13 shows the current profile of four cycles converted from the UDDS using the EV simulation progam [80]. In this chapter, UDDS continues to be used to do the validation.

Figure 5-6 shows the comparison between the estimated and true terminal voltages and pack SOCs under the UDDS test and their estimation errors, where the current profile based on the UDDS is obtained using the EV simulation progam [80]. Due to the regenerative characteristic in the UDDS, the estimated voltage is a little bit larger than the true value which can be seen from Fig.5-6 (a). It can be seen from Fig. 5-7 (a) that the estimated pack SOC can track the true pack SOC with the maximum SOC error below 5%, as shown in Fig. 5-7(b) for the entire discharge period.

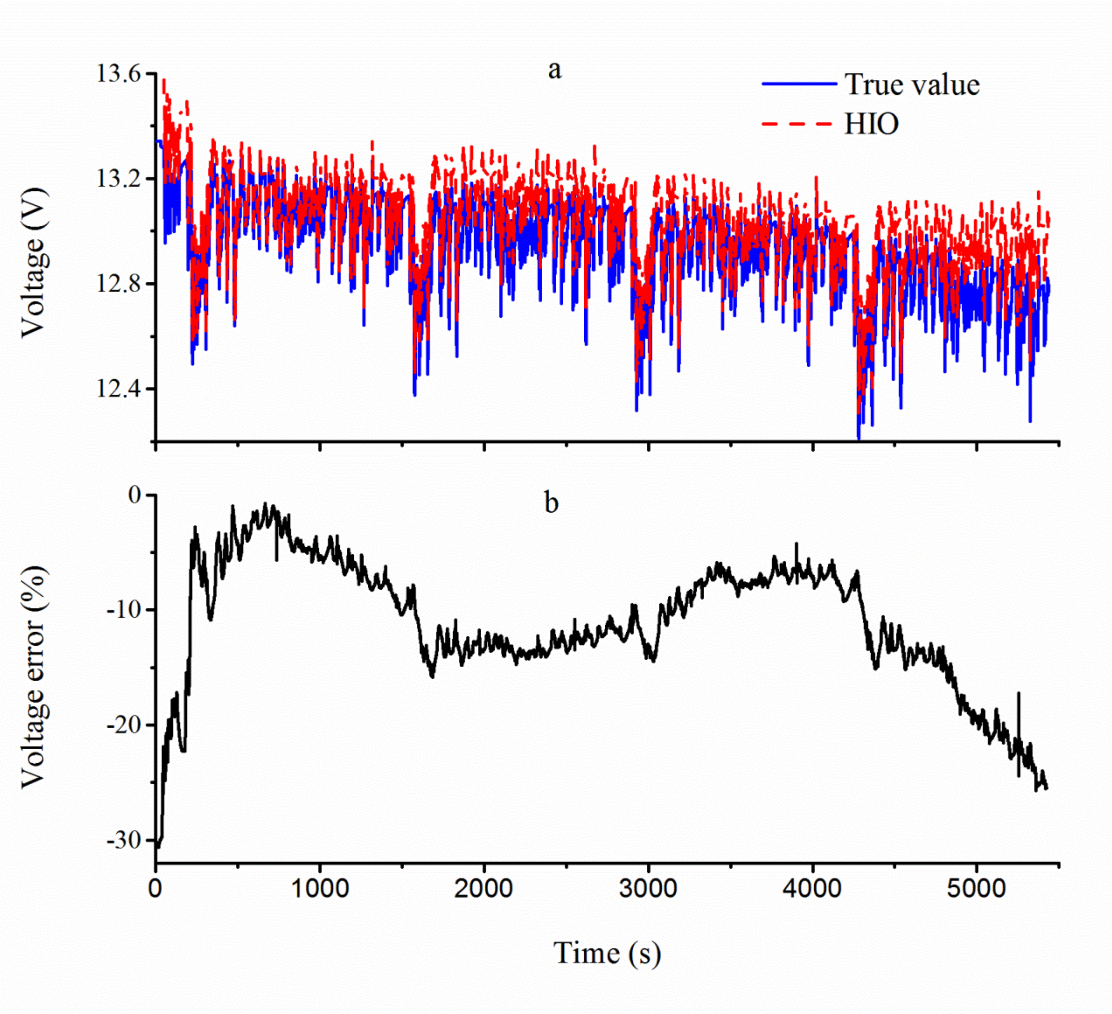

Fig.5-6. Comparison of terminal voltages estimated from HIO with those obtained from experiments and their errors for sorted battery pack under UDDS test (a). HIO estimated terminal voltage (b). Estimated voltage error

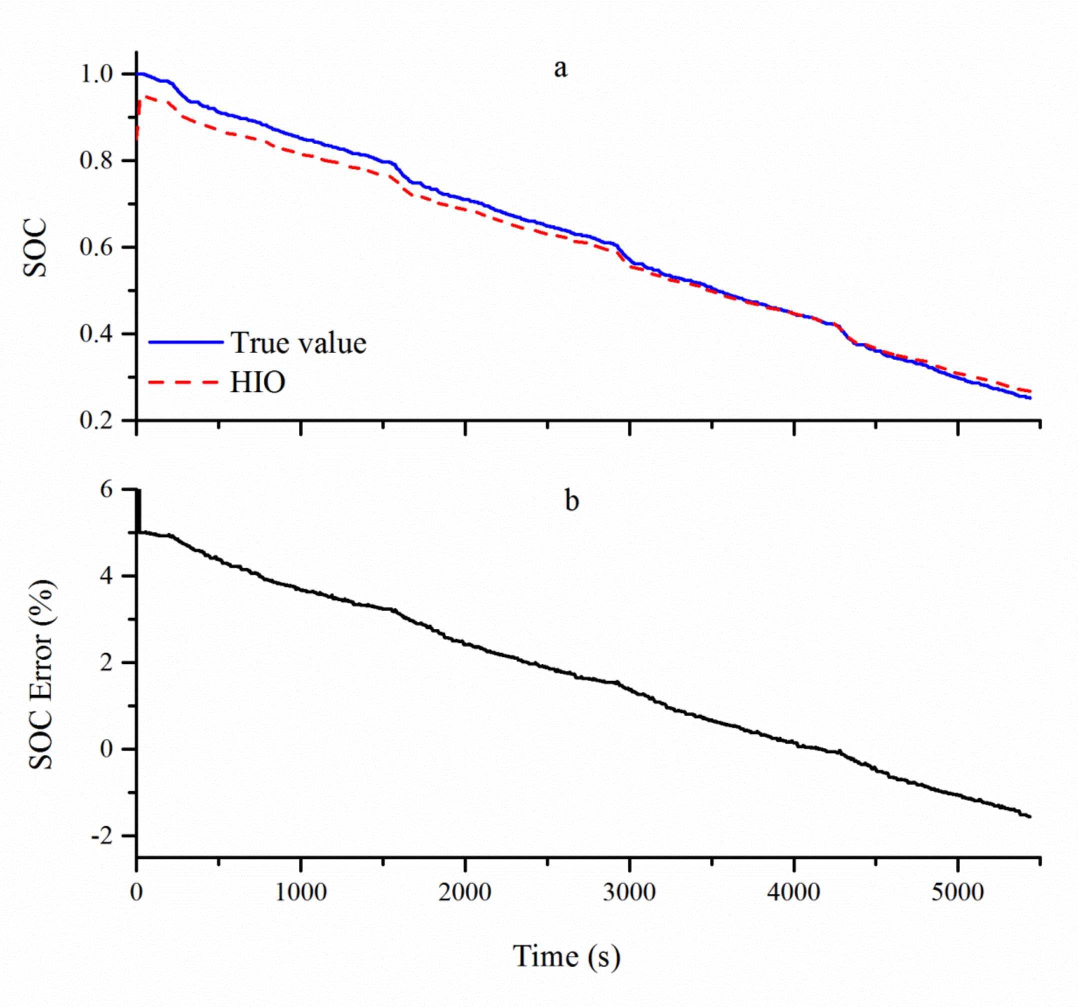

Fig. 5-7 Comparison of SOCs estimated from HIO with those obtained from experiments and their errors for sorted battery pack under UDDS test (a).HIO estimated pack SOC (b).estimated SOC error

As mentioned previously, when the TVDs $\|\Delta V_i\|$ of all cells are less than the pre-set threshold, the SOC of the AVC model can be used to represent the pack SOC. Figure 5-8 shows the comparison of the estimated SOC of a cell (e.g. cell one in the pack) and the SOC of the AVC with the true pack SOC under the UDDS test. Due to the convergence speed of HIO, the SOC error at high SOC value is little bit larger than that of low SOC value. However, the estimated SOCs of both cell one and the AVCs are very close to the true pack SOC with the error less than 5%, which is indicated by the small SOC differences between the AVC and cell one. As shown in Fig. 5-8(b), these SOC differences are limited to 2% in the entire discharge period. Therefore, the SOC of the AVC can represent the SOC of cell one in the pack.

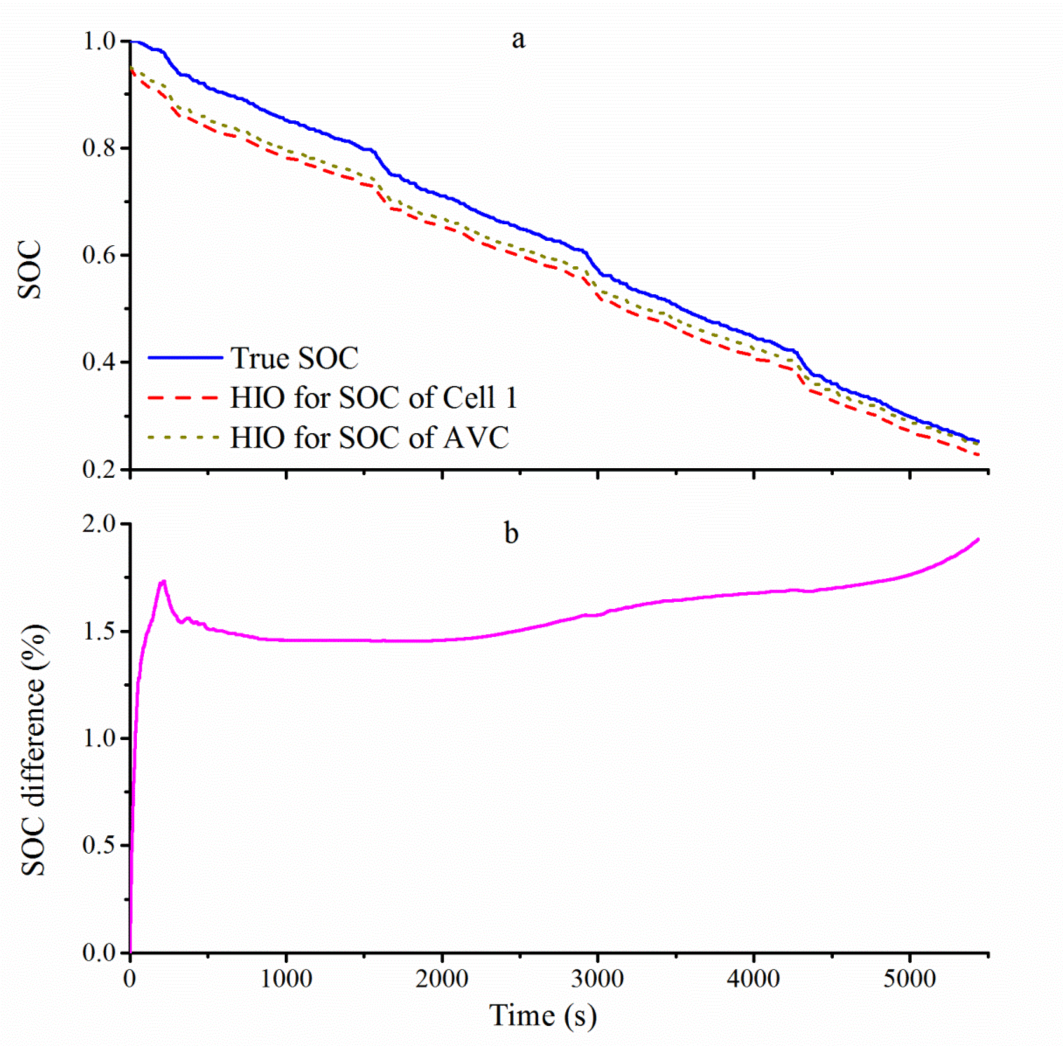

Fig.5-8 Comparisons SOC of AVC with the SOC of cell one and true SOC (a) & SOC difference (b)

Figure 5-9 and Figure 5-10 show the comparison between the estimated and true terminal voltage and SOC of each cell under the UDDS test. It can be seen from Fig. 5-9(a) that the terminal voltage of each cell responds to the corresponding current and has a similar trend. Their terminal voltage differences are all within 10%, as shown in Fig.5-9(b). In Fig.5-10(a), it can be observed that the estimated SOC of each cell can track the true SOC with their maximum SOC differences between each cell and the AVC below 5%, as shown in Fig.5-10(b).

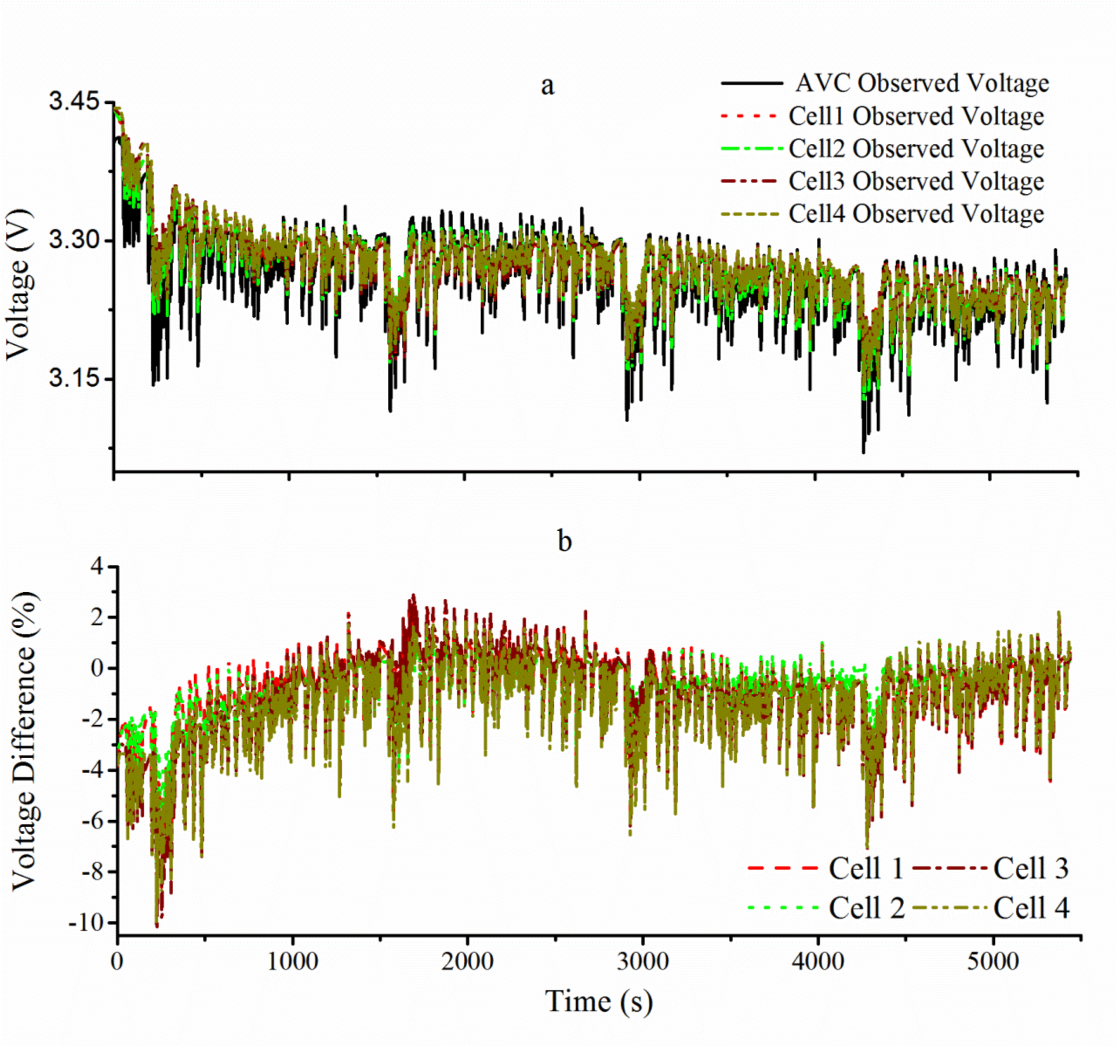

Fig.5-9 Comparison of terminal voltages estimated from HIOs with those obtained from experiments for each of four cells and their differences for sorted battery pack under UDDS test (a). Observed voltage (b).voltage difference

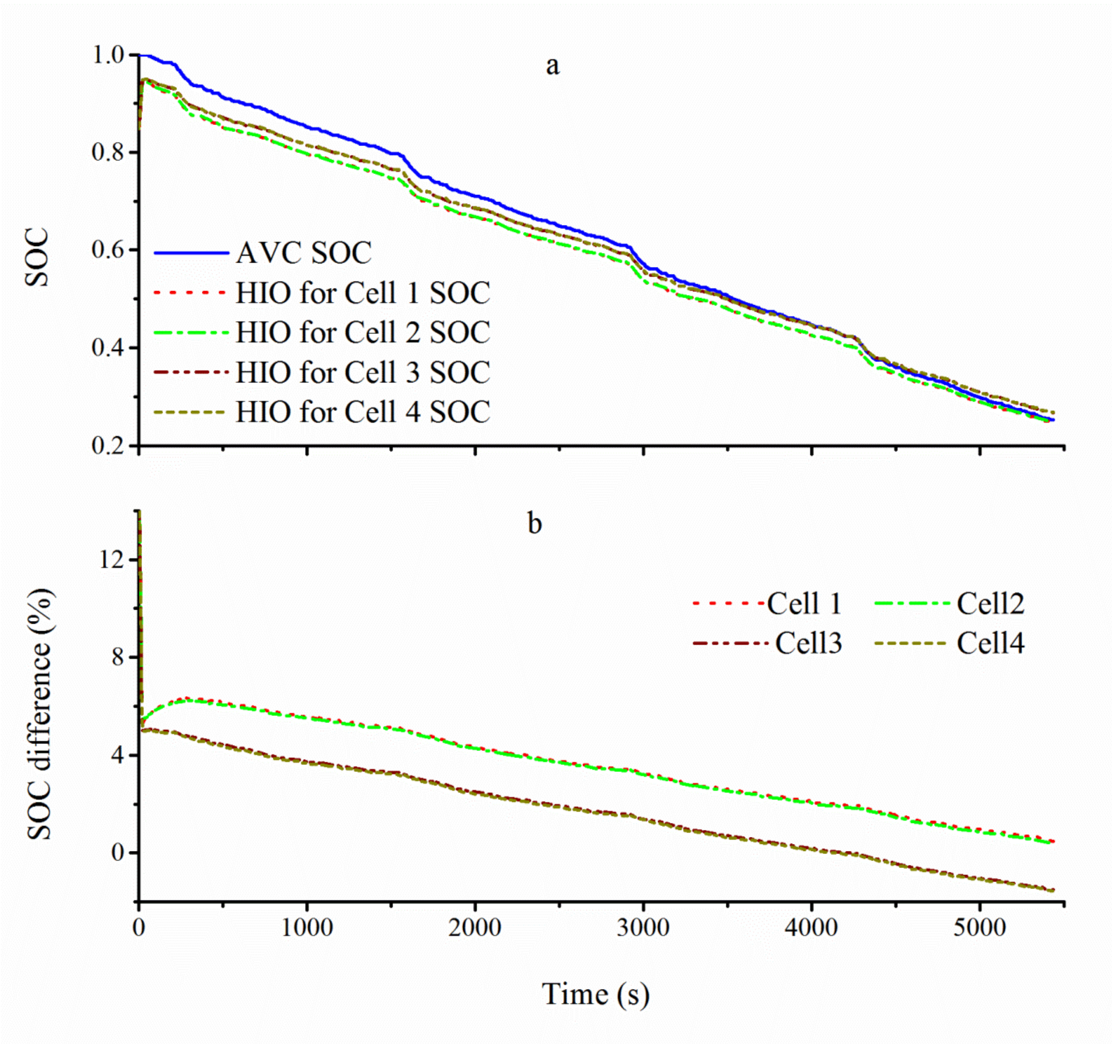

Fig.5-10 Comparison of SOC estimated from HIOs with those obtained from experiments for each of four cells and their differences for sorted battery pack under UDDS test (a).HIO for cell SOC (b).SOC error

5.4.3 UMDC test validation

The underground mine road consists of variable rolling resistance coefficients and variable uphill/downhill gradients. The driving cycle in underground mines is different from the existing standard driving cycles. Based on the data collected from Australian mines, a single return trip of the UMEV to the mine workface is proposed, taking into account the most severe conditions of the pit and drift in Australian mines [81]. The underground mine driving cycle (UMDC) is constructed as a single return trip from the workshop to the workface and then return to the workshop. The speed versus time for the UMEV are converted to the current profile based on the UMDC using the EV simulation program [80], where different road gradients and rolling resistance coefficients along the road are taken into account. This obtained current profile was used to test the sorted battery pack for the verification of the proposed HIO for SOC estimation under the UMDC. Figure 5-11 shows the battery pack current and voltage profiles under the UMDC drive cycle test.

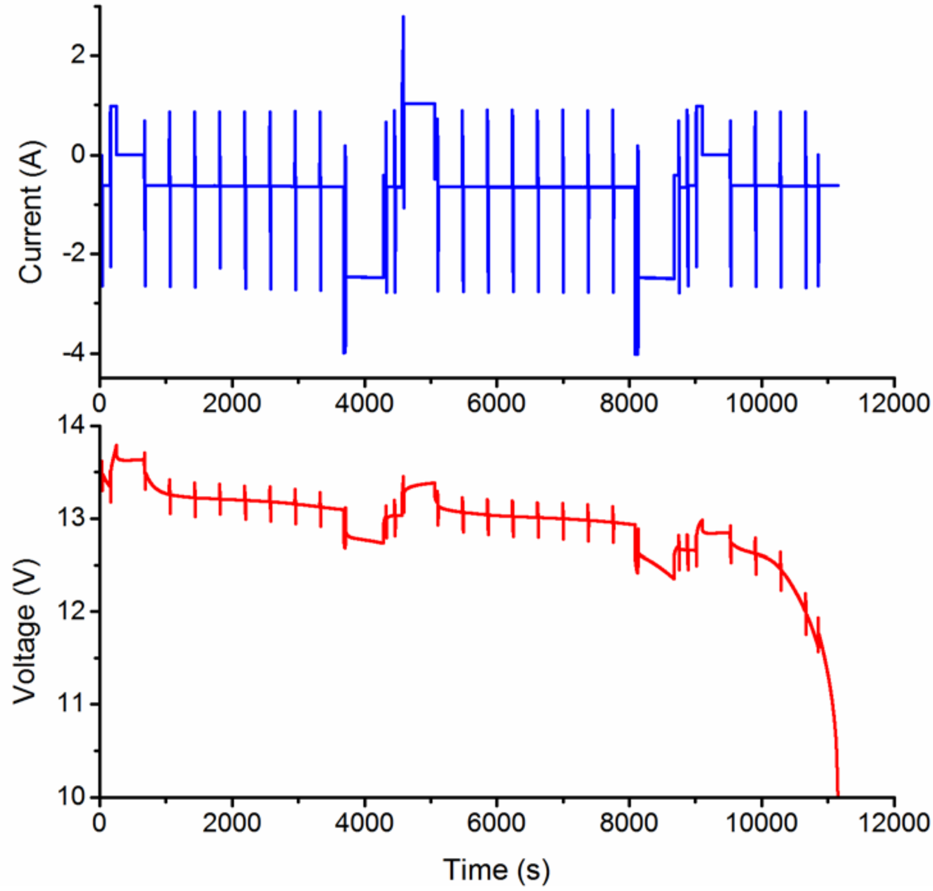

Fig.5-11 Battery pack current and voltage profile under UMDC cycle test

Figure 5-12 and Figure 5-13 show the estimated terminal voltages and SOCs for each cell and AVC under the current profile based on the UMDC and their differences. It can be seen from Fig.5-12(a) that the estimated terminal voltage of each cell is in good agreement with that of the AVC under the current profile based on the UMDC test.

Their terminal voltage differences are within 10%, except for the last 10% SOC discharge time.

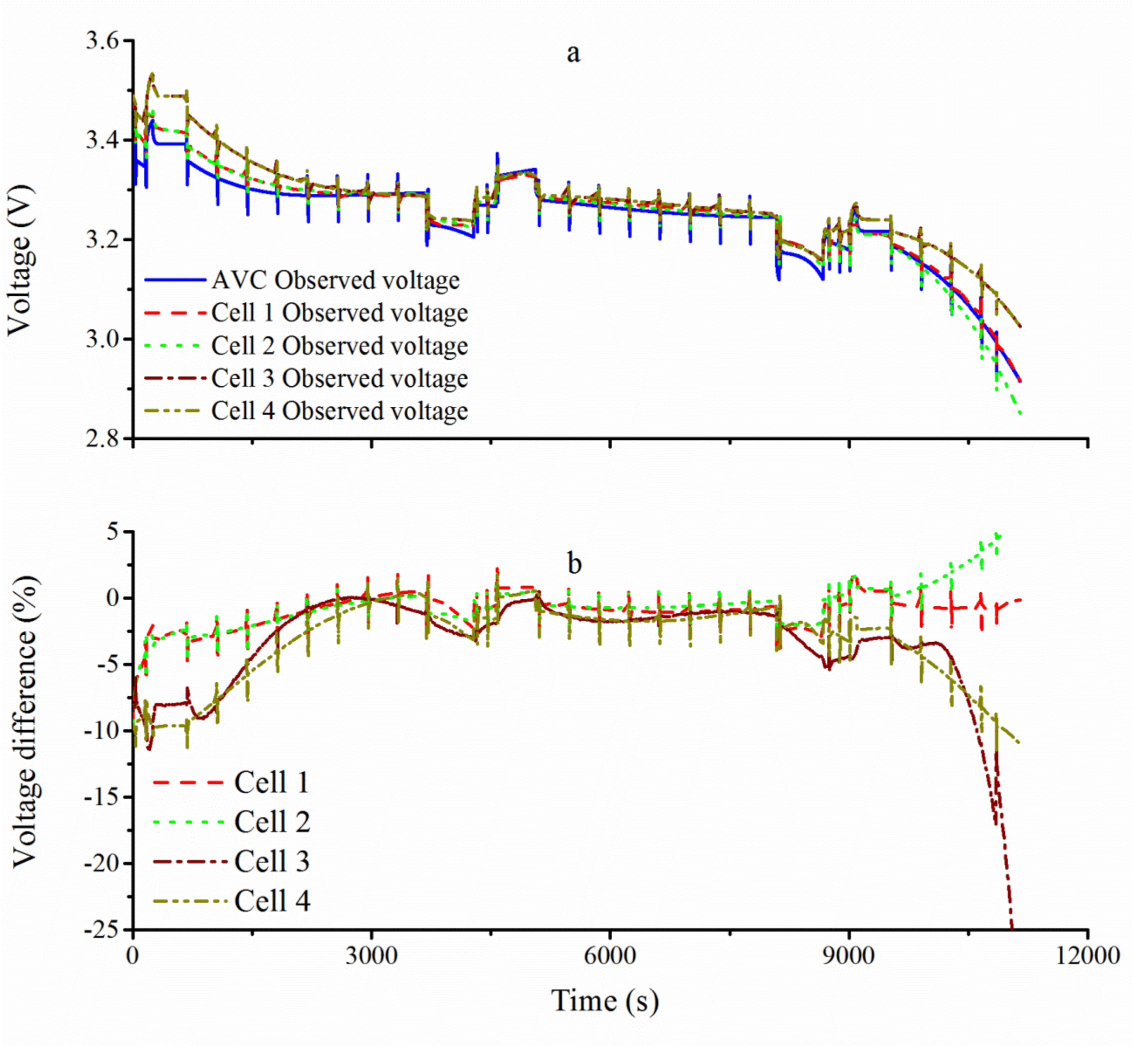

Fig.5-12 Battery pack cell voltage variation and voltage difference under UMDC cycle test (a).Observed voltage (b).Voltage difference

It can also be seen from Fig. 5-13(a) that the estimated SOC of each cell can track the SOC of the AVC, as indicated by their small SOC differences between each cell and the AVC less than 5%, as shown in Fig. 5-13(b).

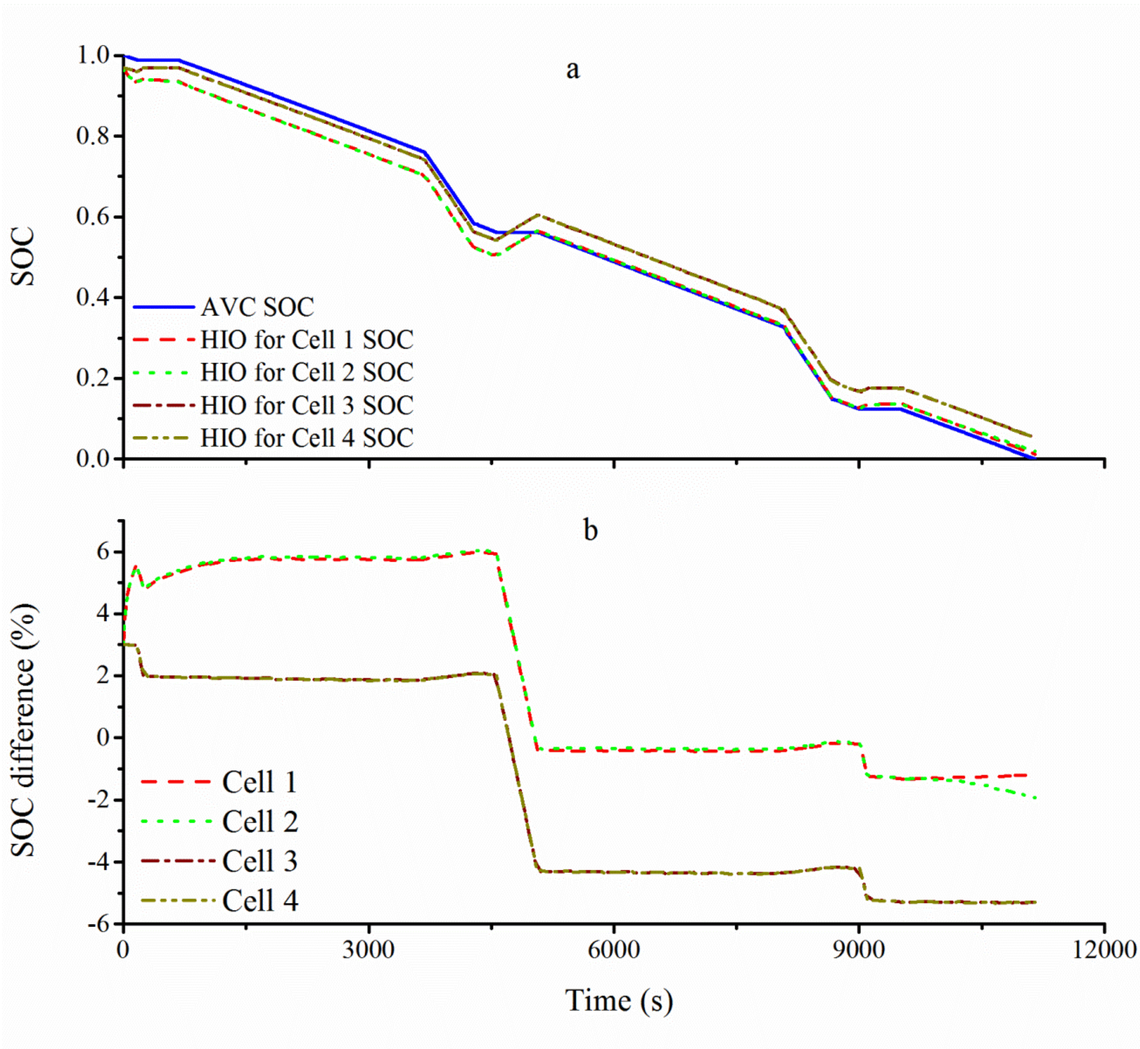

Fig.5-13 Battery pack SOC estimation and error under UMDC cycle test (a). HIO for cell SOC (b).SOC difference

5.4.4 Discussion

Based on the above three validation tests, the performance of the proposed HIO for pack SOC estimation has been effectively verified in the sorted battery pack, where the TVDs between each cell and the AVC is less than the pre-set voltage threshold. The results show that the SOC of the AVC can be used to represent the pack SOC and the SOC of each cell in the pack.

5.5 Conclusion

This chapter has presented the H-infinity observer (HIO) for pack SOC estimation in underground mine electric vehicles (UMEVs). Lithium iron phosphate battery cells have been selected to conduct the experiments in this study. They were first sorted into groups with similar characteristics and then the sorted cells were connected in series to build the battery pack. Based on the sorted battery pack, the average virtual cell (AVC) model is defined and the SOC of the AVC is estimated to represent the pack SOC. The experimental results of the sorted battery pack under pulse current discharge and current profiles based on UDDS and UMDC were used to verify the performance of the proposed HIO for the pack SOC estimation. The results show that the proposed approach has robust tracking capability of the pack SOC under the operational conditions of the UMEV.

CHAPTER 6 CONCLUSIONS

In this chapter, the contributions of the current work are highlighted and summarized. In addition, some research topics are proposed for future research.

6.1 Summary of Contributions

The battery management system (BMS) for EVs is a very broad and complex topic. In the present thesis, the BMS for underground mine electric vehicles (UMEVs) has been investigated. Given the special road conditions and the heavy weight of UMEVs, battery selection is important for the UMEV battery system, and the hybrid simulation method has been used for battery selection in this study. To alleviate the inconsistency of the cells in the battery pack, a new battery sorting method is proposed to cluster the cells into groups to make battery packs for UMEVs. The most important part of the BMS is the state of charge (SOC) estimation of the battery pack. A new pack SOC estimation approach based on H infinity observer is proposed using the average virtual cell (AVC) model.

The key contributions of the thesis are summarized as follows.

In **Chapter 3**, a hybrid simulation method is proposed for the selection of battery systems for UMEVs. The dynamic model of a four wheel drive UMEV has been developed by modifying the existing EV model in the ADVISOR platform. The experimental results of the four battery systems were integrated with the battery model used in the UMEV to compare and evaluate battery performance in the UMEV. A specifically designed driving cycle with diverse rolling resistance coefficients and variable uphill/downhill gradients for underground mines has been adopted as the load for the UMEV. The simulation of the UMEV was performed under the underground mine driving cycle. The results show that the best option for UMEVs is the battery system which is made of A123 20Ah $LiFePO_4$ batteries.

In **Chapter 4**, a self-organizing map (SOM)-based cell clustering method is proposed to cluster the cells to alleviate the inconsistency of the cells in the battery pack. The experimental results of 12 $LiFePO_4$ cells were analysed to extract the parameters of the available capacity, internal resistance and temperature variation. These parameters were adopted as the input vectors for the SOM, and the output of the SOM clusters the cells into three groups. The cells in the same group were chosen to build a sorted battery pack which was then compared with the unsorted battery pack. The consistency of the sorted battery pack was tested and evaluated, and the results show that it provides better performance than the unsorted battery pack, thereby verifying the effectiveness of the proposed method for cell clustering.

In **Chapter 5,** an H infinity observer-based SOC estimation method for battery packs is proposed based on the adoption of the concept of an average voltage cell (AVC) model. The terminal voltage of the AVC was used to estimate the pack SOC in the estimation process. The differences of the terminal voltage of each cell in the pack and the AVC were set as the terminal voltage differences (TVDs) and these TVDs are less than the pre-set value with the proposed cell clustering method in this study. When the TVD of one cell is more than the pre-set value, this cell's SOC is estimated based on its own terminal voltage. The performance of the proposed approach for the pack SOC estimation was verified under the UDDS and the specifically designed underground mine driving cycle. The results show that the proposed method has robust tracking capability for the pack SOC estimation in the operating conditions of UMEVs.

6.2 Future Research

The following topics related to the battery management system are proposed for future research.

6.2.1 Battery thermal management

Battery temperature affects the availability of battery discharge power, energy and charge acceptance during energy recovery from regenerative braking. Temperature also affects the life of the battery [121, 122]. Therefore, batteries should ideally operate within a certain temperature range that is optimum for performance and life. The desirable operating temperature range of the $LiFePO_4$ battery is 20°C to 45°C [123, 124]. In addition to considering the temperature of a battery pack, uneven temperature distribution in a pack should also be considered [124, 125]. Temperature variations from cell to cell in a pack could lead to different charge/discharge behaviours for each cell. This, in turn, could lead to electrically unbalanced cells/packs, and reduced battery pack performance. The unbalance and inconsistence of cells will cause safety issues and affect the cycle life of the battery pack. Equalization for battery pack is necessary to prevent the enlargement of the inconsistence in cell capacity and temperature and can be used to ensure the lifetime of the battery pack to be extended [126-131]. And the goal of a thermal management system is to deliver a battery pack at an optimum average temperature with even temperature distribution.

6.2.2 Battery state of health estimation

The battery state of health (SOH) reflects the general condition of a battery and its ability to deliver the specified performance compared with a new battery [132, 133]. With the increasing number of cycles, the inconsistence of each battery in the pack can cause the reduction in the battery pack capacity and the SOH of the battery pack will be reduced [134]. However, if the SOM is used to sort the cells into a group based on the experimental data of the aging cells, this SOM will be still effective. The battery SOH condition can be determined by the capacity, internal resistance, power density, self-discharge rate and other battery parameters. It can be obtained by comparing the parameters at the current states with those of a new or healthy battery. For example, in the case of battery capacity, it is not easy to estimate battery capacity online because the battery needs to be fully charged and fully discharged when carrying out capacity estimation.

The SOH estimation methods currently available include the durability model-based estimation method and the battery model-based parameter identification method [135-140]. Similar to SOC estimation, EV battery pack SOH estimation is quite challenging due to the number of cells connected in the pack which may produce inconsistent behaviours.

6.2.3 Fault diagnosis in battery packs

Fault diagnosis has been applied in vehicles and other industrial applications for many years. Compared with other mechanical and electrical systems, EVs are much more complex due to electrochemical characteristics of lithium ion battery systems and hysteresis and inconsistency among the cells in the battery pack. As a result, fault diagnosis for battery systems in EVs is challenging [141]. Since battery faults affect the performance and life of EVs, early fault diagnosis of battery systems can reduce losses, minimize maintenance fees and ensure vehicle performance, safety and reliability [142]. Therefore, fault diagnosis is one of the technologies necessary to ensure the safety of battery packs.

Faults in battery systems are mainly related to the following parameters: voltage, current, temperature during battery charging and discharging [141]. Faults can occur due to over-voltage or under-voltage, over-current or short circuits and abnormal temperature [143]. Analysis of the durability, reliability and failure mode of lithium ion batteries is crucial to guarantee cell quality and the safety of the battery pack. Fault diagnosis functionality should be included in the BMS and provide early alarms of unhealthy cells in the battery pack.

REFERENCES

[1] C. C. Chan, "An overview of electric vehicle technology," Proceedings of the IEEE, vol. 81, pp. 1202-1213, 1993.

[2] C. C. Chan, "The past, present and future of electric vehicle development," in Proceedings of the IEEE 1999 International Conference on Power Electronics and Drive Systems, vol.1, pp. 11-13, 1999.

[3] M. DeLuchi, Q. Wang, and D. Sperling, "Electric vehicles: Performance, life-cycle costs, emissions, and recharging requirements," Transportation Research Part A: General, vol. 23, pp. 255-278, 1989.

[4] D. Xu, L. Wang, and J. Yang, "Research on li-ion battery management system," in 2010 International Conference on Electrical and Control Engineering (ICECE) , pp. 4106-4109, 2010.

[5] L. Lu, X. Han, J. Li, J. Hua, and M. Ouyang, "A review on the key issues for lithium-ion battery management in electric vehicles," Journal of Power Sources, vol. 226, pp. 272-288, 2013.

[6] A. c. G. Mary Bellis. (6th May). The Early Years, Electric cars from 1830 to 1930. Available: http://inventors.about.com/

[7] C.C. Chan, Modern electric vehicle technology, 2001.

[8] S. H. Robin Cowan. (1996, 6th May). Escaping Lock-in: the Case of the Electric Vehicle Available: http://www.cgl.uwaterloo.ca/~racowan/escape.html

[9] L. Situ, "Electric Vehicle development: The past, present and future," in PESA 2009 3rd International Conference on Power Electronics Systems and Applications, pp. 1-3, 2009.

[10] D. L. B. Arnold R. Miller, "Advanced underground vehicle power and control fuellcell mine locomotive," Proceeding of the 2002 U.S. DOE Hydrogen Program Review, pp. 5-9, 2002.

[11] W. G. Oetringhaus, "Railless vehicle underground mining," United States Patent, 1985.

[12] M. A. Reyes and T. Novak, "Injury surveillance and safety considerations for large-format, lead-acid batteries used in mining applications," in IEEE Industry Applications Society Annual Meeting, pp. 1-7, 2014.

[13] Mining.com. (2012, March 13). Electric underground vechile revolutionizes the mining industry. Available: http://www.mining.com/electric-underground-vehicle-revolutionizes-the-mining-industry/

[14] M. A. Roscher, O. S. Bohlen, and D. U. Sauer, "Reliable state estimation of multicell lithium-ion battery systems," IEEE Transactions on Energy Conversion, vol. 26, pp. 737-743, 2011.

[15] D. D. Berndt, Maintenance-free batteries : lead-acid, nickel/cadmium, nickel/hydride : a handbook of battery technology, 1997.

[16] (2016, 25/04). GE fairchild battery powered load haul dump. Available: http://www.getransportation.com/mining/ge-fairchild-battery-powered-load-haul-dump

[17] (25/04). MAC-12 AC 96V electric transporter. Available: http://www.damascuscorp.com/vehicles/mac12.aspx

[18] S. A. H. K.E. Aifantis, and R.V. Kumar, "High energy density lithium batteries, materials, engineering, applications," Germany: Wiley-VCH publisher, 2010.

[19] D. Berndt, Maintenance-free batteries : lead-acid, nickel/cadmium, nickel/hydride : a handbook of battery technology, Taunton, Somerset, England : New York: Research Studies Press ; John Wiley, 1993.

[20] D. G. Enos, "Chapter 3 - Lead-acid batteries for medium- and large-scale energy storage A2 - Menictas, Chris," in Advances in Batteries for Medium and Large-Scale Energy Storage, M. Skyllas-Kazacos and T. M. Lim, Eds., Woodhead Publishing, pp. 57-71, 2015.

[21] X. Zhang and C. Mi, Vehicle power management: modeling, control and optimization. London: Springer London, 2011.

[22] D. A. J. Rand and P. T. Moseley, "Chapter 13 - Energy storage with lead–acid batteries," in Electrochemical Energy Storage for Renewable Sources and Grid Balancing, ed Amsterdam: Elsevier, pp. 201-222, 2015.

[23] J. Garche, P. T. Moseley, and E. Karden, "5 - Lead–acid batteries for hybrid electric vehicles and battery electric vehicles," in Advances in Battery Technologies for Electric Vehicles, ed: Woodhead Publishing, pp. 75-101, 2015.

[24] M. Fetcenko, J. Koch, and M. Zelinsky, "6 - Nickel–metal hydride and nickel–zinc batteries for hybrid electric vehicles and battery electric vehicles A2 - Scrosati, Bruno," in Advances in Battery Technologies for Electric Vehicles, J. Garche and W. Tillmetz, Eds., ed: Woodhead Publishing, pp. 103-126, 2015.

[25] K. T. Chau, Y. S. Wong, and C. C. Chan, "An overview of energy sources for electric vehicles," Energy Conversion and Management, vol. 40, pp. 1021-1039, 1999.

[26] W. H. Zhu, Y. Zhu, and B. J. Tatarchuk, "Self-discharge characteristics and performance degradation of Ni-MH batteries for storage applications," International Journal of Hydrogen Energy, vol. 39, pp. 19789-19798, 2014.

[27] W.X. Shen, T. Tu Vo, and A. Kapoor, "Charging algorithms of lithium-ion batteries: An overview," in 2012 7th IEEE Conference on Industrial Electronics and Applications (ICIEA), pp. 1567-1572, 2012.

[28] H. S. Ryu, H. J. Ahn, K. W. Kim, J. H. Ahn, K. K. Cho, and T. H. Nam, "Self-discharge characteristics of lithium/sulfur batteries using TEGDME liquid electrolyte," *Electrochimica Acta*, vol. 52, pp. 1563-1566, 2006.

[29] X. Chen, W. X. Shen, T. Tu Vo, Z. Cao, A. Kapoor, "An overview of lithium-ion batteries for electric vehicles," presented at the The 10th International Power and Energy Conference (IPEC 2012), pp. 230-235, 2012.

[30] I. Buchmann. (10th Dec). *Battery university-Types of lithium-ion*. Available: http://batteryuniversity.com/learn/article/types_of_lithium_ion

[31] H. J. Bergveld, "Battery management systems design by modelling," Eindhoven Philips Research Laboratories, 2001.

[32] B. Lawson. (10th Jan). *Battery management systems (BMS)*. Available: http://www.mpoweruk.com/bms.htm

[33] B. Kras, B. Polnik, and R. Konsek, "Suspended battery drivetrain as an example of advanced control and safety system of li-ion battery pack technology in mining industry," in 2013 World Electric Vehicle Symposium and Exhibition (EVS27), pp. 1-8, 2013.

[34] M. Redelbach, E. D. Özdemir, and H. E. Friedrich, "Optimizing battery sizes of plug-in hybrid and extended range electric vehicles for different user types," Energy Policy, vol. 73, pp. 158-168, 2014.

[35] B. Wahono, W. B. Santoso, A. Nur, and Amin, "Analysis of range extender electric vehicle performance using vehicle simulator," Energy Procedia, vol. 68, pp. 409-418, 2015.

[36] C.-S. N. Shiau, C. Samaras, R. Hauffe, and J. J. Michalek, "Impact of battery weight and charging patterns on the economic and environmental benefits of plug-in hybrid vehicles," Energy Policy, vol. 37, pp. 2653-2663, 2009.

[37] V. H. Johnson, "Battery performance models in ADVISOR," Journal of Power Sources, vol. 110, pp. 321-329, 2002.

[38] K. J. Kelly, " Modelling tools for predicting the impact of rolling resistance on energy usage and fuel effieciency for realistic driving cycles," presented at the International Tire Exhibition and Conference, 2002.

[39] D. W. Gao, C. Mi, and A. Emadi, " Modeling and simulation of electric and hybrid vehicles," Proceedings of the IEEE, vol. 95, pp. 729-745, 2007.

[40] B. D. G. Z. Aymeric Rousseau, Justin Kern, John Anderson, Mike Duoba, "Honda insight validation using PSAT", SAE Technical Paper 2001-01-2538, 2001

[41] F. Milano, "An open source power system analysis toolbox," in IEEE Transactions on Power Systems, vol. 20, no. 3, pp. 1199-1206, 2005..

[42] Y. S. W. a. C. C. C. K. T. Chau, "EVSIM — A PC-based simulation tool for an electric vehicle technology course," International Journal of Electrical Engineering Education, vol. 04, pp.167-179, 2000

[43] J. Wang, Z. Sun, X. Wei, and H. Dai, "Lifespan uniformity for the battery pack in the automotive application," Automotive Safety and Energy, vol. Vol. 2 No. 3, pp.223-228, 2011.

[44] F. Wen, C. Lin, J. Jiang, and Z. Wang, "A new evaluation method to the sonsistency of lithium-ion batteries in electric vehicles," in 2012 Asia-Pacific Power and Energy Engineering Conference (APPEEC), pp. 1-4, 2012

[45] J. Kim and B. H. Cho, "Screening process-based modeling of the multi-cell battery string in series and parallel connections for high accuracy state-of-charge estimation," Energy, vol. 57, pp. 581-599, 2013.

[46] L. Guo and G. W. Liu, "Research of lithium-ion battery sorting method based on fuzzy C-means algorithm," Advanced Materials Research, pp.983-988 , 2011.

[47] B. Lawson. (10th Jan). State of charge (SOC) determination. Available: http://www.mpoweruk.com/soc.htm

[48] I. Snihir, W. Rey, E. Verbitskiy, A. Belfadhel-Ayeb, and P. H. L. Notten, "Battery open-circuit voltage estimation by a method of statistical analysis," Journal of Power Sources, vol. 159, pp. 1484-1487, 2006.

[49] M. A. Roscher and D. U. Sauer, "Dynamic electric behavior and open-circuit-voltage modeling of LiFePO4-based lithium ion secondary batteries," Journal of Power Sources, vol. 196, pp. 331-336, 2011.

[50] K. S. Ng, C.-S. Moo, Y.-P. Chen, and Y.-C. Hsieh, "Enhanced coulomb counting method for estimating state-of-charge and state-of-health of lithium-ion batteries," *Applied Energy*, vol. 86, pp. 1506-1511, 2009.

[51] H. He, R. Xiong, and J. Fan, "Evaluation of lithium-ion battery equivalent circuit models for state of charge estimation by an experimental approach," Energies, vol. 4, pp. 582-598, 2011.

[52] G. L. Plett, "Extended Kalman filtering for battery management systems of LiPB-based HEV battery packs: Part 1. Background," Journal of Power Sources, vol. 134, pp. 252-261, 2004.

[53] G. L. Plett, "Extended Kalman filtering for battery management systems of LiPB-based HEV battery packs: Part 2. Modeling and identification," Journal of Power Sources, vol. 134, pp. 262-276, 2004.

[54] G. L. Plett, "Extended Kalman filtering for battery management systems of LiPB-based HEV battery packs: Part 3. State and parameter estimation," Journal of Power Sources, vol. 134, pp. 277-292, 2004.

[55] G. L. Plett, "Sigma-point Kalman filtering for battery management systems of LiPB-based HEV battery packs: Part 1: Introduction and state estimation," Journal of Power Sources, vol. 161, pp. 1356-1368, 2006.

[56] G. L. Plett, "Sigma-point Kalman filtering for battery management systems of LiPB-based HEV battery packs: Part 2: Simultaneous state and parameter estimation," Journal of Power Sources, vol. 161, pp. 1369-1384, 2006.

[57] H. He, R. Xiong, X. Zhang, F. Sun, and J. Fan, "State-of-charge estimation of the lithium-ion battery using an adaptive extended Kalman filter based on an improved Thevenin model," IEEE Transactions on Vehicular Technology, vol. 60, pp. 1461-1469, 2011.

[58] J. Wang, J. Guo, and L. Ding, "An adaptive Kalman filtering based State of Charge combined estimator for electric vehicle battery pack," Energy Conversion and Management, vol. 50, pp. 3182-3186, 2009.

[59] S. Sepasi, R. Ghorbani, and B. Y. Liaw, "Improved extended Kalman filter for state of charge estimation of battery pack," Journal of Power Sources, vol. 255, pp. 368-376, 2014.

[60] F. Sun, X. Hu, Y. Zou, and S. Li, "Adaptive unscented Kalman filtering for state of charge estimation of a lithium-ion battery for electric vehicles," Energy, vol. 36, pp. 3531-3540, 2011.

[61] R. Xiong, X. Gong, C. C. Mi, and F. Sun, "A robust state-of-charge estimator for multiple types of lithium-ion batteries using adaptive extended Kalman filter," Journal of Power Sources, vol. 243, pp. 805-816, 2013.

[62] R. Xiong, H. He, F. Sun, and K. Zhao, "Evaluation on state of charge estimation of batteries with adaptive extended Kalman filter by experiment approach," IEEE Transactions on Vehicular Technology, vol. 62, pp. 108-117, 2013

[63] S. S. Haykin, Kalman Filtering & Neural Networks. New York: John Wiley & Sons, Inc. Engineering, 2001.

[64] X. Chen, W. X. Shen, M. Dai, Z. Cao, J. Jin, and A. Kapoor, "Robust adaptive sliding mode observer using RBF neural network for lithium-ion battery state of charge estimation in electric vehicles," IEEE Transactions on Vehicular Technology, vol 65. , pp. 1936-1947, 2015.

[65] X. Chen, W. X. Shen, Z. Cao, and A. Kapoor, "A novel approach for state of charge estimation based on adaptive switching gain sliding mode observer in electric vehicles," Journal of Power Sources, vol. 246, pp. 667-678, 2014.

[66] N. Koirala, F. He, and W.X. Shen, "Comparison of two battery equivalent circuit models for state of charge estimation in electric vehicles," in 2015 IEEE 10th Conference on Industrial Electronics and Applications (ICIEA), pp. 17-22, 2015.

[67] C. Unterrieder, R. Priewasser, S. Marsili, and M. Huemer, "Battery state estimation using mixed Kalman/H-infinity, adaptive Luenberger and sliding mode observer," in 2013 IEEE Vehicle Power and Propulsion Conference (VPPC), pp. 1-6, 2013.

[68] N. Abolhassani Monfared, N. Gharib, H. Moqtaderi, M. Hejabi, M. Amiri, F. Torabi, *et al.*, "Prediction of state-of-charge effects on lead-acid battery characteristics using neural network parameter modifier," Journal of Power Sources, vol. 158, pp. 932-935, 2006.

[69] W. X. Shen, "State of available capacity estimation for lead-acid batteries in electric vehicles using neural network," Energy Conversion and Management, vol. 48, pp. 433-442, 2007.

[70] T. Weigert, Q. Tian, and K. Lian, "State-of-charge prediction of batteries and battery–supercapacitor hybrids using artificial neural networks," Journal of Power Sources, vol. 196, pp. 4061-4066, 2011.

[71] C. Hametner and S. Jakubek, "State of charge estimation for Lithium Ion cells: Design of experiments, nonlinear identification and fuzzy observer design," Journal of Power Sources, vol. 238, pp. 413-421, 2013.

[72] M. Charkhgard and M. Farrokhi, "State-of-charge estimation for lithium-ion batteries ssing neural networks and EKF," IEEE Transactions on Industrial Electronics, vol. 57, pp. 4178-4187, 2010.

[73] J. N. Hu, J. J. Hu, H. B. Lin, X. P. Li, C. L. Jiang, X. H. Qiu*, et al.*, "State-of-charge estimation for battery management system using optimized support vector machine for regression," Journal of Power Sources, vol. 269, pp. 682-693, 2014.

[74] T. Hansen and C. J. Wang, "Support vector based battery state of charge estimator," Journal of Power Sources, vol. 141, pp. 351-358, 2005.

[75] W. X. Shen, C. C. Chan, E. W. C. Lo, and K. T. Chau, "A new battery available capacity indicator for electric vehicles using neural network," Energy Conversion and Management, vol. 43, pp. 817-826, 2002.

[76] J. P. Aditya and M. Ferdowsi, "Comparison of NiMH and Li-ion batteries in automotive applications," in IEEE Vehicle Power and Propulsion Conference, pp. 1-6, 2008.

[77] L. Antti., "Evaluation of energy storage system requirements for hybrid mining loader," in *IEEE Vehicle Power and Propulsion Conference (VPPC)*, pp. 1-6, 2011.

[78] K. B. Wipke, M. R. Cuddy, and S. D. Burch, "ADVISOR 2.1: a user-friendly advanced powertrain simulation using a combined backward/forward approach," IEEE Transactions on Vehicular Technology, vol. 48, pp. 1751-1761, 1999.

[79] A. C. Baisden and A. Emadi, "ADVISOR-based model of a battery and an ultra-capacitor energy source for hybrid electric vehicles," IEEE Transactions on Vehicular Technology, vol. 53, pp. 199-205, 2004.

[80] R. C. Kroeze and P. T. Krein, "Electrical battery model for use in dynamic electric vehicle simulations," in IEEE Power Electronics Specialists Conference, pp. 1336-1342, 2008.

[81] F. He, X. Cui, W. X. Shen, A. Kapoor, D. Honnery, and D. Dayawansa, "Modelling of electric vehicles for underground mining personnel transport," in *8th IEEE Conference on Industrial Electronics and Applications (ICIEA)*, pp. 870-875, 2013.

[82] J. Larminie and J. Lowry: ‘Electric vehicle technology explained’, Wiley, 2003.

[83] T. D. Gillespie. (1992). Fundamentals of vehicle dynamics. Available: https://books.google.com.au/books?id=L6xd0nx5KbwC

[84] W. W. Marr, W. J. Walsh, and P. C. Symons, "Modeling battery performance in electric vehicle applications," Energy Conversion and Management, vol. 33, pp. 843-847, 1992.

[85] H. He, R. Xiong, H. Guo, and S. Li, "Comparison study on the battery models used for the energy management of batteries in electric vehicles," Energy Conversion and Management, vol. 64, pp. 113-121, 2012.

[86] M. Einhorn, F. V. Conte, C. Kral, and J. Fleig, "Comparison, selection, and parameterization of electrical battery models for automotive applications," IEEE Transactions on Power Electronics, vol. 28, pp. 1429-1437, 2013.

[87] Y. Xing, W. He, M. Pecht, and K. L. Tsui, "State of charge estimation of lithium-ion batteries using the open-circuit voltage at various ambient temperatures," Applied Energy, vol. 113, pp. 106-115, 2014.

[88] Masiero, G., Ogasavara, M.H., Jussani, A.C., and Risso, M.L.: ‘Electric vehicles in China: BYD strategies and government subsidies’, RAI Revista de Administração e Inovação, 13, (1), pp. 3-11,2016.

[89] Z. Ma, J. Jiang, W. Shi, W. Zhang, and C. C. Mi, "Investigation of path dependence in commercial lithium-ion cells for pure electric bus applications: Aging mechanism identification," Journal of Power Sources, vol. 274, pp. 29-40, 2015.

[90] W. X. Shen, T. T. Vo, and A. Kapoor, "Charging algorithms of lithium-ion batteries: An overview," in *7th IEEE Conference on Industrial Electronics and Applications (ICIEA)*, pp. 1567-1572, 2012.

[91] X. Chen, W. X. Shen, Z. Cao, and A. Kapoor, "Adaptive gain sliding mode observer for state of charge estimation based on combined battery equivalent circuit model," *Computers & Chemical Engineering*, vol. 64, pp. 114-123, 2014.

[92] T.-K. Lee;, Y. Kim;, D. M. Rizzo;, and Z. S. Filipi, "Battery power management in heavy-duty HEVs based on the estimated critical surface charge," International Journal of Vehicle Design, vol.61, No.1/2/3/4, pp.108-127, 2013.

[93] X. Hu, R. Xiong, and B. Egardt, "Model-based dynamic power assessment of lithium-ion batteries considering different operating conditions," IEEE Transactions on Industrial Informatics, vol. 10, pp. 1948-1959, 2014.

[94] Y. Zou, X. Hu, H. Ma, and S. E. Li, "Combined state of charge and state of health estimation over lithium-ion battery cell cycle lifespan for electric vehicles," Journal of Power Sources, vol. 273, pp. 793-803, 2015.

[95] M. Muratori;, M. Canova;, and Y. Guezennec, "A spatially-reduced dynamic model for the thermal characterisation of Li-ion battery cells," International Journal of Vehicle Design, vol. 58, No.2/3/4, , pp.134-158, 2012.

[96] H. Wang, K. Dong, G. Li, and F. Wu, "Research on the consistency of the power battery based on multi-points impedance spectrum," in 2010 International Forum on Strategic Technology (IFOST), pp. 1-4, 2010.

[97] J. Kim, J. Shin, C. Chun, and B. H. Cho, "Stable configuration of a Li-Ion series battery pack based on a screening process for improved voltage/SOC balancing," IEEE Transactions on Power Electronics, vol. 27, pp. 411-424, 2012.

[98] R. Paolo, F. Leonardo, M. Adriano, C. Matteo, L. Sauro, F. Luca, *et al.*, "Selection of lithium cells for EV battery pack using self-organizing map," Automotive Safety and Energy, vol. 2 No.2, p. 8, 2011.

[99] K. Fang, S. Chen, D. Mu, B. Wu, and F. Wu, "Investigation of nickel–metal hydride battery sorting based on charging thermal behavior," Journal of Power Sources, vol. 224, pp. 120-124, 2013.

[100] F. Trentini, M. Hagenbuchner, A. Sperduti, and F. Scarselli, "A Self-Organising Map Approach for Clustering of XML Documents," in 2006 IJCNN International Joint Conference on Neural Networks, pp. 1805-1812, 2006.

[101] J. Vesanto and E. Alhoniemi, "Clustering of the self-organizing map," IEEE Transactions on Neural Networks, vol. 11, pp. 586-600, 2000.

[102] X. Zhang, J. Chen, and J. Dong, "Color clustering using self-organizing maps," in 2007 ICWAPR International Conference on Wavelet Analysis and Pattern Recognition, pp. 986-989, 2007.

[103] T. Kohonen, "The self-organizing map," Proceedings of the IEEE, vol. 78, pp. 1464-1480, 1990.

[104] T. Kohonen, E. Oja, O. Simula, A. Visa, and J. Kangas, "Engineering applications of the self-organizing map," Proceedings of the IEEE, vol. 84, pp. 1358-1384, 1996.

[105] S. S. Haykin, Neural networks and learning machines, Prentice Hall, 2009.

[106] U. Seiddert and L. C. Jain, Self-organizing neural networks : recent advances and applications. New York : Physica-Verlag, 2001.

[107] J. Xu, S. Li, C. Mi, Z. Chen, and B. Cao, "SOC based battery cell balancing with a novel topology and reduced component count," Energies, vol. 6, pp. 2726-2740, 2013.

[108] G. Hunt. USABC electric vehicle battery test procedures manual [Online]. Available: http://www.uscar.org/guest/article_view.php?articles_id=86

[109] H. Blanke, O. Bohlen, S. Buller, R. W. D. Doncker, B. Fricke, A. Hammouche, et al., "Impedance measurements on lead-acid batteries for state-of-charge, state-of-health and cranking capability prognosis in electric and hybrid electric vehicles," Journal of Power Sources, vol. 144, pp. 418-425, 2005.

[110] W. X. Shen, C. C. Chan, E. W. C. Lo, and K. T. Chau, "Adaptive neuro-fuzzy modeling of battery residual capacity for electric vehicles," IEEE Transactions on Industrial Electronics, vol. 49, pp. 677-684, 2002.

[111] G. L. Plett, " Efficient battery pack state estimation using bar-delta filtering," presented at The International Battery, Hybrid and Fuel Cell Electric Vehicle Symposium (EVS24), Stavanger, Norway, 2009.

[112] X. Liu, Y. He, and Z. Chen, "State-of-charge estimation for power Li-ion battery pack using Vmin-EKF," in 2010 2nd International Conference on Software Engineering and Data Mining (SEDM) , pp. 27-31, 2010.

[113] H. Dai, X. Wei, Z. Sun, J. Wang, and W. Gu, "Online cell SOC estimation of Li-ion battery packs using a dual time-scale Kalman filtering for EV applications," Applied Energy, vol. 95, pp. 227-237, 2012.

[114] R. Xiong, F. Sun, X. Gong, and H. He, "Adaptive state of charge estimator for lithium-ion cells series battery pack in electric vehicles," Journal of Power Sources, vol. 242, pp. 699-713, 2013.

[115] F. Sun, R. Xiong, and H. He, "A systematic state-of-charge estimation framework for multi-cell battery pack in electric vehicles using bias correction technique," Applied Energy, vol. 162, pp. 1399-1409, 2016.

[116] L. Zhong, C. Zhang, Y. He, and Z. Chen, "A method for the estimation of the battery pack state of charge based on in-pack cells uniformity analysis," Applied Energy, vol. 113, pp. 558-564, 2014.

[117] Y. Hua, A. Cordoba-Arenas, N. Warner, and G. Rizzoni, "A multi time-scale state-of-charge and state-of-health estimation framework using nonlinear predictive filter for lithium-ion battery pack with passive balance control," Journal of Power Sources, vol. 280, pp. 293-312, 2015.

[118] D. Simon, "Optimal state estimation Kalman, H infinity and nonlinear approaches," N.J. Hoboken: Wiley-Interscience, 2006.

[119] H. Li and M. Fu, "A linear matrix inequality approach to robust H infinity filtering," IEEE Transactions on Signal Processing, vol. 45, pp. 2338-2350, 1997.

[120] F. He, W. X. Shen, Q. Song, A. Kapoor, D. Honnery, and D. Dayawansa, "Self-organising map based classification of LiFePO4 cells for battery pack in EVs," International Journal of Vehicle Design, vol. 69, pp. 151-167, 2015.

[121] M. Debert, G. Colin, G. Bloch, and Y. Chamaillard, "An observer looks at the cell temperature in automotive battery packs," Control Engineering Practice, vol. 21, pp. 1035-1042, 2013.

[122] Z. Rao and S. Wang, "A review of power battery thermal energy management," Renewable and Sustainable Energy Reviews, vol. 15, pp. 4554-4571, 2011.

[123] A. Marongiu, T. Pavanarit, and D. U. Sauer, "Influence of current and temperature variation on a $LiFePO_4$ battery total capacity," in 2013 World Electric Vehicle Symposium and Exhibition (EVS27) , pp. 1-11, 2013.

[124] N. Yang, X. Zhang, B. Shang, and G. Li, "Unbalanced discharging and aging due to temperature differences among the cells in a lithium-ion battery pack with parallel combination," Journal of Power Sources, vol. 306, pp. 733-741, 2016.

[125] B. Wu, V. Yufit, M. Marinescu, G. J. Offer, R. F. Martinez-Botas, and N. P. Brandon, "Coupled thermal–electrochemical modelling of uneven heat generation in lithium-ion battery packs," Journal of Power Sources, vol. 243, pp. 544-554, 2013.

[126] F. Baronti, R. Roncella, and R. Saletti, "Performance comparison of active balancing techniques for lithium-ion batteries," Journal of Power Sources, vol. 267, pp. 603-609, 2014.

[127] J. Gallardo-Lozano, E. Romero-Cadaval, M. I. Milanes-Montero, and M. A. Guerrero-Martinez, "Battery equalization active methods," Journal of Power Sources, vol. 246, pp. 934-949, 2014.

[128] W. Han, L. Zhang, and Y. Han, "Computationally efficient methods for state of charge approximation and performance measure calculation in series-connected battery equalization systems," Journal of Power Sources, vol. 286, pp. 145-158, 2015.

[129] Y. Wang, C. Zhang, Z. Chen, J. Xie, and X. Zhang, "A novel active equalization method for lithium-ion batteries in electric vehicles," Applied Energy, vol. 145, pp. 36-42, 2015.

[130] Y. Zheng, M. Ouyang, L. Lu, J. Li, X. Han, and L. Xu, "On-line equalization for lithium-ion battery packs based on charging cell voltages: Part 2. Fuzzy logic equalization," Journal of Power Sources, vol. 247, pp. 460-466, 2014.

[131] Y. Zheng, M. Ouyang, L. Lu, J. Li, X. Han, and L. Xu, "On-line equalization for lithium-ion battery packs based on charging cell voltages: Part 1. Equalization based on remaining charging capacity estimation," Journal of Power Sources, vol. 247, pp. 676-686, 2014.

[132] H. Dai, X. Wei, and Z. Sun, "A new SOH prediction concept for the power lithium-ion battery used on HEVs," in *2009* VPPC IEEE Vehicle Power and Propulsion Conference, pp. 1649-1653, 2009.

[133] K. M. Tsang and W. L. Chan, "State of health detection for Lithium ion batteries in photovoltaic system," Energy Conversion and Management, vol. 65, pp. 7-12, 2013.

[134] L. Lu, X. Han, J. Li, J. Hua, and M. Ouyang, "A review on the key issues for lithium-ion battery management in electric vehicles," Journal of Power Sources, vol. 226, pp. 272-288, 2013.

[135] D. Andre, C. Appel, T. Soczka-Guth, and D. U. Sauer, "Advanced mathematical methods of SOC and SOH estimation for lithium-ion batteries," Journal of Power Sources, vol. 224, pp. 20-27, 2013.

[136] I. Baghdadi, O. Briat, P. Gyan, and J. M. Vinassa, "State of health assessment for lithium batteries based on voltage–time relaxation measure," Electrochimica Acta, vol. 194, pp. 461-472, 2016.

[137] Z. Guo, X. Qiu, G. Hou, B. Y. Liaw, and C. Zhang, "State of health estimation for lithium ion batteries based on charging curves," Journal of Power Sources, vol. 249, pp. 457-462, 2014.

[138] C. Lin, A. Tang, and W. Wang, "A Review of SOH Estimation Methods in Lithium-ion Batteries for Electric Vehicle Applications," Energy Procedia, vol. 75, pp. 1920-1925, 2015.

[139] S. Torai, M. Nakagomi, S. Yoshitake, S. Yamaguchi, and N. Oyama, "State-of-health estimation of LiFePO4/graphite batteries based on a model using differential capacity," Journal of Power Sources, vol. 306, pp. 62-69, 2016.

[140] Y. Zou, X. Hu, H. Ma, and S. E. Li, "Combined state of charge and state of health estimation over lithium-ion battery cell cycle lifespan for electric vehicles," Journal of Power Sources, vol. 273, pp. 793-803, 2015.

[141] C. Wu, C. Zhu, Y. Ge, and Y. Zhao, "A review on fault mechanism and diagnosis approach for Li-Ion batteries," Journal of Nanomaterials, vol.2015, pp.1-9, 2015.

[142] A. Barré, B. Deguilhem, S. Grolleau, M. Gérard, F. Suard, and D. Riu, "A review on lithium-ion battery ageing mechanisms and estimations for automotive applications," Journal of Power Sources, vol. 241, pp. 680-689, 2013.

[143] Y. Zheng, X. Han, L. Lu, J. Li, and M. Ouyang, "Lithium ion battery pack power fade fault identification based on Shannon entropy in electric vehicles," Journal of Power Sources, vol. 223, pp. 136-146, 2013.

LIST OF PUBLICATIONS

1. **Fengxian He**, Xiudong Cui, W. X. Shen, A. Kapoor, Damon Honnery, Daya Dayawansa , "Modelling of Electric Vehicles for Underground Mining Personnel Transport "in Proceedings of the 2013 8th IEEE Conference on Industrial Electronics and Applications (ICIEA 2013), Australia, 19-21 June, 2013, pp. 870-875.
2. **Fengxian He**, W. X. Shen, Qiang Song, A. Kapoor, Damon Honnery, Daya Dayawansa, "Clustering LiFePO4 cells for battery pack based on neural network in EVs", in Proceedings of the 2014 IEEE Conference and Expo on Transportation Electrification Asia-Pacific (ITEC Asia-Pacific), Beijing, Aug. 31 -Sept. 3, 2014, pp. 1-5.
3. **Fengxian He**, W. X. Shen, Qiang Song, A. Kapoor, Damon Honnery, Daya Dayawansa, "Self-organising map based classification of LiFePO4 cells for battery pack in EVs", International Journal of Vehicle Design, vol.69, pp.151-167. 2015.
4. Narayani Koirala, **Fengxian He** and W. X. Shen, "Comparison of two battery equivalent circuit models for state of charge estimation in electric vehicles", in Proceeding of 2015 IEEE 10th Conference on Industrial Electronics and Applications (ICIEA), 15-17 June, 2015, pp.17-22.
5. **Fengxian He**, W. X. Shen, A. Kapoor, Damon Honnery, Daya Dayawansa, "H infinity observer based state of charge estimation for battery packs in electric vehicles", Accepted by 2016 IEEE 11th Conference on Industrial Electronics and Applications (ICIEA).
6. **Fengxian He**, W. X. Shen, Xiudong Cui, A. Kapoor, Damon Honnery, Daya Dayawansa, "Quantitative comparison for selection of $LiFePO_4$ battery system in

underground mine electric vehicles", submitted to IEEE Transactions on Transportation Electrification, March, 2016.

7. **Fengxian He**, W. X. Shen, A. Kapoor, Damon Honnery, Daya Dayawansa, "State of charge estimation for battery packs using H infinity observer in underground mine electric vehicles", submitted to SAE International Journal of Passage car, Electronic & Electric System, May 2016.

8. **Fengxian He**, W. X. Shen，Daya Dayawansa, Damon Honnery, Rahul Rao, Travis Leenaerts: 'Battery Management System for a Compact Electric Personnel Transport Vehicle for Underground Coal Mines', Final report for ARC Linkage Project (LP110200302), 28 pages, March, 2016.